POLITECNICO
MILANO 1863

SCHOOL OF INDUSTRIAL AND INFORMATION ENGINEERING

Master of Science in Mechanical Engineering

Full vehicle modelling with Simulink-GasDyn coupling for WLTP driving cycle simulations

Supervisor

Prof. Gianluca D'ERRICO

Co-Supervisor

Dott. Andrea Massimo MARINONI

Candidate

Nicolò CITTERIO – 927332

Abstract

This master thesis has as objective the development of a co-simulation model between two softwares: GasDyn and Simulink. The first one will be used to model and simulate the phenomena related to an internal combustion engine, and will be coupled with Simulink, which will be responsible of simulating the longitudinal dynamics of a vehicle.

In particular, the object of this case of study is the Renault Captur, a medium crossover city car sold by the French manufacturer, which is equipped with the HR10DDTg2 engine, an inline three cylinder , 1000cc turbocharged engine.

The main objectives taken on in this work will be:

- Validation of the Renault engine model developed previously in the GasDyn environment, by comparing it with the experimental results given by the manufacturer.
- Construction and development of a longitudinal dynamics vehicle model in the Simulink environment, to reproduce faithfully the behaviour of the vehicle object of the study.
- Comparison between a baseline and two alternative engine management strategies in the optic of fuel consumption and pollutant emissions reduction in a European legislation homologation cycle.

In a preliminary phase, the data outputted by the GasDyn engine model will be compared with the experimental engine dyno bench results given by Renault in

terms of engine performance related quantities (BMEP, Torque, Power, BSFC) and in terms of engine pollutant emissions (NOx, CO, HC, CO2).

Successively, a vehicle model replicating the longitudinal dynamics of a car placed on a rolling dyno will be formulated, implementing each different subsystem related to a car in the Simulink environment (car body, wheels, brakes, tires, gearbox, driver controller, etc.), and testing in base driving cycles for the truthfulness of the model.

Finally, three different engine strategies (Baseline, Start & Stop, Deactivated Cylinder) will be compared by simulating a WLTP driving cycle, analysing the results both from the vehicle dynamics point of view and from the internal combustion engine point of view.

Table of Contents

Abstract 3

List of Figures 9

List of Tables 13

Chapter 1 Introduction 15

Chapter 2 State of the Art 21

Chapter 3 GasDyn software and engine model 39
3.1 GasDyn software 39
3.2 Conservation equations 40
3.2.1 Mass conservation equation 41
3.2.2 Energy conservation equation 41
3.2.3 Momentum conservation equation 42
3.2.4 Conservative form of equations 43
3.2.5 Numerical method solution 46
3.3 Engine model object of the study 48
3.3.1 Stationary engine model 49
3.3.2 Stationary, transient operation and co-simulation 52

Chapter 4 Simulink software and vehicle model 54
4.1 Simulink software 54
4.2 Longitudinal vehicle dynamics 56
4.2.1 Car body 56
4.2.2 Front and rear wheel 59
4.2.3 Gearbox 65
4.2.4 GasDyn S-Function 69
4.2.5 Control logics 70

Chapter 5 WLTP Cycle Simulation 79
5.1 Base Engine WLTP cycle 79

5.2 Vehicle dynamics 80
5.2.1 Vehicle velocity 80
5.2.2 Torque request 84
5.2.3 Engine operating points 85
5.2.4 Engine air-to-fuel ratio 88
5.3 Fuel consumption and pollutant emissions 89
5.3.1 Fuel consumption 89
5.3.2 CO2 emissions 91
5.3.3 CO, HC, and NOx Emissions 92
5.4 Engine temperatures 100
5.4.1 Turbine temperatures 101
5.4.2 Catalyst temperatures 102
5.4.3 Intake side temperatures 104
5.5 Wastegate valve control 108

Chapter 6 Alternative engine strategies 111
6.1 Simulink model modifications 112
6.2 Driving quantities comparison 113
6.3 Fuel consumption and pollutants comparison 116
6.4 Engine temperatures comparison 122

Chapter 7 Conclusions 126

Chapter 8 Bibliography 129

List of Figures

Figure 1.1 Internal Combustion Engines are subject to a strong virtualization procedure in the last decade to reduce pollutant emissions. 17
Figure 1.2 Comparison between NEDC cycle and the more recent WLTP, in the table the main differences are summarized. 19
Figure 2.1 Different motorizations available nowadays on the medium city car market. 21
Figure 2.2 Bubble chart describing the different electrification levels on vehicles, depending on their power and electric energy use. 23
Figure 2.3 On the left, the Fiat TwinAir engine, on the right, the Ford EcoBoost 125. We can see how they are visibly very compact. 25
Figure 2.4 Schematization of a turbocharged engine. 26
Figure 2.5 Comparison between a NA engine map and a TC one. 27
Figure 2.6 Comparison in torque request fulfilment between a NA engine (green line) and a turbocharged one (blue line). 29
Figure 2.7 Turbine equipped with wastegate valve. 30
Figure 2.8 Schematization of Variable Geometry Turbine guide flaps. 31
Figure 2.9 The new eTurboCharger developed by Garrett. 32
Figure 2.10 Effect of a correct spark advance (1), an excessive one (2) inducing knocking, and a too retarded spark (3), not developing a good amount of in-chamber pressure... 33
Figure 2.11 Example of valve timing chart, with indicated Exhaust valve opening and closing (EVO, EVC) and Intake valve opening and closing (IVO, IVC). 34
Figure 2.12 Operation of a typical first-generation variable valve timing system..... 35
Figure 2.13 Schematization of Honda's VTEC technology, where a pin moved by oil pressure puts into operation the high-performance cam lobe. 36
Figure 2.14 Different valve variable actuation strategies depending on the area of the engine map. 37
Figure 3.1 Control volume schematization adopted to write conservation laws..... 40
Figure 3.2 Mesh in a duct used to compute 1D numerical solutions 46
Figure 3.3 Example of a complex pipe made of several sub-elements connected together. The pipe is treated as a continuous duct by the numerical method. 47
Figure 3.4 Overview of the engine object of this study modelled in the GasDyn environment 48
Figure 3.5 Comparison between experimental and simulated BMEP. 50
Figure 3.6 Comparison between experimental and simulated BSFC. 51

Figure 3.7 Comparison between experimental and simulated pollutant emissions. 52
Figure 4.1 Overview of the Simulink full vehicle simulation model 55
Figure 4.2 Forces scheme of a car body, used to formulate the dynamical equilibrium equations 56
Figure 4.3 Carbody block in Simulink, having on the left the input signals and on the right the outputted quantities. 58
Figure 4.4 Carbody block parameters, set to reproduce the characteristics of the vehicle object of the study. 59
Figure 4.5 Force schematization of a car wheel 59
Figure 4.6 Disk brake schematization, on the right the image to compute the mean effective braking radius 61
Figure 4.7 Schematization of a drum brake, with the external drum on which two shoes insist, pushed by a hydraulic piston. 62
Figure 4.8 Typical tire behaviour in terms of longitudinal force as a function of longitudinal slip. 63
Figure 4.9 Simulink tire block settings of the Pacejka magic formula coefficients 63
Figure 4.10 Front wheel, rear wheel, and brake distributor block in Simulink 64
Figure 4.11 Technical data regarding front and rear braking systems, along with dynamical quantities regarding the wheels. 65
Figure 4.12 Visual representation of the elasticity given by a gearbox to an engine. 66
Figure 4.13 Mechanical model of two coupled gear wheels 66
Figure 4.14 Schematization of a gearbox and differential for a front wheel drive car 67
Figure 4.15 Gearbox Simulink block 68
Figure 4.16 General layout of the modelled gearbox, on the left the different selectable gear ratios, on the right logical blocks to model the clutch engagement and disengagement. 69
Figure 4.17 GasDyn S-Function block and interpreter to extract data coming from the cosimulation software 70
Figure 4.18 Longitudinal driver block, responsible of controlling brake and throttle pedals based on the velocity error 70
Figure 4.19 Driving cycle block, which outputs the reference speed to be followed by the vehicle. 71
Figure 4.20 Final coefficients for the driver PI controller 72
Figure 4.21 Variable subsystem in Simulink, giving the possibility to select the gearshift control logic to be adopted 73
Figure 4.22 The final gearshift sequence as per European Committee Norm. 74
Figure 4.23 Engine control unit blocks, responsible of controlling the engine and its strategies 75
Figure 4.24 Engine torque map adopted for the torque request controller 76
Figure 4.25 Start & Stop controller block layout 77

Figure 5.1 Comparison between the reference cycle speed (red) and the actual vehicle speed (blue) 80
Figure 5.2 First driving sub-cycle detail. 81
Figure 5.3 Second driving sub-cycle detail. 82
Figure 5.4 Third driving sub-cycle detail. 82
Figure 5.5 Fourth driving sub-cycle detail. 83
Figure 5.6 Torque requested by Simulink compared to the torque erogated by the GasDyn engine model 84
Figure 5.7 A more detailed view of the previous graph 85
Figure 5.8 First sub-cycle operative points cloud 86
Figure 5.9 Second sub-cycle operative points cloud 86
Figure 5.10 Third sub-cycle operative points cloud 87
Figure 5.11 Fourth sub-cycle operative points cloud 87
Figure 5.12 Engine fuel map compared to the effective AFR ratio during the driving cycle. 88
Figure 5.13 Cumulated fuel consumption trend, with the average consumption divided for the four sub-cycles 90
Figure 5.14 Instantaneous CO2 emissions in g/s compared to fuel consumption 91
Figure 5.15 Detailed view of CO2 and fuel consumption comparison 91
Figure 5.16 Cumulated CO emissions 93
Figure 5.17 Overview on the instantaneous CO emissions, compared to the instantaneous air-to-fuel ratio 93
Figure 5.18 Zoom on the comparison between CO emissions and AFR 94
Figure 5.19 On the left, the emission of pollutants as a function of equivalence ratio, on the right the TWC conversion efficiency as a function of equivalence ratio. 95
Figure 5.20 Cumulated HC emissions 96
Figure 5.21 Instantaneous HC emissions compared with instantaneous AFR. 97
Figure 5.22 Detailed view of HC emissions versus AFR 97
Figure 5.23 Cumulated NOx emissions. 98
Figure 5.24 Overview on instantaneous NOx emissions and engine AFR 98
Figure 5.25 Detailed view of NOx emissions compared to engine AFR 99
Figure 5.26 Temperatures before the turbine inlet of flow, wall and the reading a thermocouple would produce. 101
Figure 5.27 Temperatures after the turbine outlet of flow, walls and the reading a thermocouple would produce. 101
Figure 5.28 Temperatures before entering the catalyst of flow, walls and the reading a thermocouple would produce. 102
Figure 5.29 Temperatures after exiting the catalyst of flow, walls and the reading a thermocouple would produce. 103
Figure 5.30 Temperatures before the compressor intake of wall, flow and thermocouple reading. 104

Figure 5.31 Temperatures after the compressor intake of wall, flow and thermocouple reading. 105
Figure 5.32 Flow temperature difference across the compressor. 106
Figure 5.33 Temperature difference in the flow between entrance and exit from the intercooler. 107
Figure 5.34 Full overview of the wastegate valve behaviour 108
Figure 5.35 Detailed view during an idling phase of the engine 109
Figure 5.36 Detailed view of an acceleration phase of the vehicle. 110
Figure 6.1 Start & Stop control unit logic 112
Figure 6.2 Brake torque output comparison between base model and deactivated cylinder model. 113
Figure 6.3 Detail of the boost pressure, compared between base model and deactivated cylinder model. 114
Figure 6.4 Detail of the throttle opening, compared between base model and deactivated cylinder model. 115
Figure 6.5 Cumulated fuel consumption plot, comparing the three engine models. 116
Figure 6.6 A detailed view of the fuel consumption during a stop in the cycle. 117
Figure 6.7 Comparison between CO2 emissions of the three engines. 118
Figure 6.8 Comparison between HC emissions of the three engines. 119
Figure 6.9 Comparison between NOx emissions of the three engines. 119
Figure 6.10 Comparison between CO emissions of the three engines. 120
Figure 6.11 Wall temperatures compared between the three models. 122
Figure 6.12 A more detailed view of the wall temperatures. 122
Figure 6.13 Flow temperatures before entering the turbine inlet. 123
Figure 6.14 A more detailed view of the flow temperatures. 124
Figure 6.15 Thermocouple readings of a virtual thermocouple placed at the catalyst entrance. 125

List of Tables

Table 1 Engine characteristics summary..... 49
Table 2 Gear ratios characterizing the Renault Captur gearbox..... 68
Table 3 Summary of the differences in terms of engine emissions and consumption between the three proposed engine strategies. 121

Chapter 1 Introduction

In the last decade, the importance of virtual simulation has grown exponentially and has taken a fundamental role in the preliminary design and development phase of any industrial product, as it allows companies to reduce drastically the number of prototypes and experiments needed to obtain a component which suits the engineering requirements it must meet. In particular, focusing on the OEM industry, the tendency of the last years has been pushing toward a reduced environmental impact of engine emissions. Thanks to the introduction of virtual preliminary simulation, companies have been able to assess a priori if an under-development model will be able to comply with the current European legislations, limiting thus the experimental prototype campaign duration and investment for the company [1].

The widespread of this approach has been possible thanks also to the continuous and exponential improvement of computer technology, both from a software and from a hardware point of view, reaching also in laptops a consistent level of computational power to solve virtual simulation problems. In terms of vehicle simulation, softwares are now able to compute fully the dynamics of a vehicle by solving linear and non-linear equations which regulate the movement of a vehicle, for example the interaction between road and tyres or the delivery of power through a transmission. Instead in terms of engine simulation softwares are able to predict and model a very widespread number of phenomena, starting from the combustion and the pollutants formation inside the combustion chamber, following with all the fluid dynamic quantities inside the intake and exhaust ducts, the chemical

phenomena occurring inside the three-way catalyst and the thermodynamics of the entire engine.

Virtual simulation in the modern-day engineering world always passes through a validation procedure, in which the computed results are reproduced experimentally, and the time history of different quantities is recorded and successively compared with the simulated ones. This allows to tune at best the virtual model accordingly, and once the model is considered as valid it can be used to vary the operating conditions in order to understand the variation of output and make it meet with the engineering requirements previously defined.

This aspect of virtual simulation is probably the most important and interesting, because it gives the possibility to the designer to vary the features of the project both in order to comply with some set limits, or to begin an optimal approach study.

The dark side of virtual simulation is, as previously said, the computational expense it requires, because the more a model is precise and refined, the higher the time required to solve it by a machine is, thus a trade-off between time and precision is always present in a simulation study. The great advantage of these virtual models is that, already with a limited experimental campaign and refinement of the models, they are able to reproduce faithfully the physical phenomena object of the study, giving a consistent advantage in terms of comprehension of the physical underlying model to the designer.

This virtual model development and tuning will be described in the following chapters, in which a coupling model between Gasdyn, in charge of the simulations related to the internal combustion engine, and Simulink, carrying out the computations from a vehicle dynamics point of view. With the term coupling approach it is usually intended when a virtual simulation model is built using more than one software; this enhances ulteriorly the power of the simulation, because different phenomena can be modelled and computed in a very specific and tuned software environment, as in this case where Gasdyn is more focused in solving

mono-dimensional fluid dynamics and thermodynamics equations while Simulink solves the mechanical dynamics equations, and only the strictly necessary information is passed between one software and the other.

Figure 1.1 Internal Combustion Engines are subject to a strong virtualization procedure in the last decade to reduce pollutant emissions.

Moreover, in the Simulink environment it is possible to formulate complex control logics, which are typical of modern-day vehicles ECUs to reduce pollutant emissions and fuel consumption, for example the Start&Stop logic or the Cylinder-On-Demand one, implementing them in the model and simulating advantages and disadvantages of each different solution.

In this simulation environment it has also been possible to implement a PI controller which is able to reproduce the behaviour of a human driver acting on the throttle and brake pedals while following a reference velocity history, thus reproducing the typical experimental conditions of homologation cycles.

European legislation has introduced in the last years the so called “EuroX” legislations [2], in which different test procedures are described and car manufacturers must carry out in order to have the approval for commercialization of a certain car model. In particular, the latest testing procedure described is the WLTP testing cycle, which is a reference speed that a testing driver must follow on a rolling dyno test bench, while different parameters of the vehicle are recorded and tested. In particular, exhaust fumes are collected and diluted following precise procedures and successively compared to the current legislation limits [3].

The WLTP cycle replaced different pre-existing test cycles, which were at the time already outdated, in particular in Europe it substituted the New European Driving Cycle (NEDC), which was composed by four repeated urban driving cycles plus an extra-urban part. This is because the old test did not retrace the actual driving styles of modern vehicles, even if most of them have a high-speed part. In order to be more representative of the modern driving styles and rhythms, compared to NEDC cycle, the WLTP cycle is longer both temporally and spatially, the mean velocity and the maximum one are higher in value, and it has stronger accelerations and decelerations. Furthermore, the WLTP considers the different characteristics: they are divided in different categories and some aspects, as the maximum speed, are calibrated accordingly. The two homologation cycles just presented are shown in the figure below, while the following table summarizes the main differences between them [4].

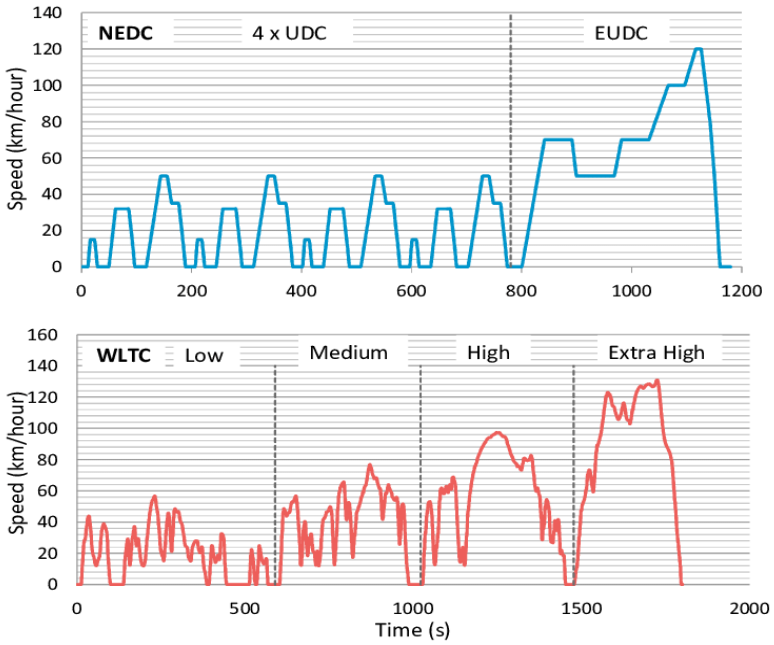

	NEDC	WLTC
Duration (s)	1180	1800
Total distance (km)	11.01	23.27
Average speed (km/h)	33.6	46.5
Maximum speed (km/h)	120	131.3
Stop duration (%)	23.73	13.00

Figure 1.2 Comparison between NEDC cycle and the more recent WLTP, in the table the main differences are summarized.

Nowadays a new testing procedure is also being introduced in a parallel way to the WLTP cycle, which is the so called RDE, which stands for Real Driving Emissions. The aim of the European legislation committee is to have a testing procedure which is as close as possible to the actual conditions encountered on the road by vehicles, along with reducing the most possible the chance of the car manufacturers to deceive the homologation procedure, as it has happened recently with Volkswagen and the “Dieselgate” scandal [5]. In that occasion vehicles had control logics which allowed them to recognize whether they were tested for emissions and acted consequently in order to minimize them loading a different engine map.

Going into more detail, the following master thesis will be structured as follows:

State of the art: in this section the current most advanced technical solutions in terms of engine technologies are presented, focusing on the current offer on the market regarding medium sized city cars and crossovers. The latest trends of the OEM world are analysed, in particular the downsizing of engine, pollutants reduction and engine control strategies.

Chapter one: this chapter contains a general overview of the Gasdyn engine simulation software from a theoretical point of view and a description of the engine object of this study, along with a comparison between the experimental data furnished by Renault and the simulated one.

Chapter two: this chapter contains a general overview of the Simulink environment software and a thorough description of the building of the vehicle dynamics model, exploring singularly every component adopted in the simulation and its development. Starting from the physical characteristics of the vehicle object of study, the definition of the testing procedures, the development and tuning of the driver PI controller and the coupling interface between Simulink and Gasdyn.

Chapter three: in this last chapter the results of different steps of simulation of driving conditions are presented. The WLTP homologation cycle is carried out with different strategies to optimize and reduce fuel consumption, and the results are successively analysed and commented. Beginning from the base engine model the analysis focuses afterwards on the Start&Stop strategy and the Deactivated Cylinder one.

Chapter 2 State of the Art

The vehicle under study in this work is a medium sized city car or crossover, powered by a turbocharged gasoline spark ignition (SI) engine. Analysing the current market offer we can divide this category into four different sub-categories based on the technology adopted to deliver the torque: Naturally Aspirated (NA) engines, TurboCharged (TC) engines, Hybrid powertrain layouts (HV) or Full electric propulsion (FE).

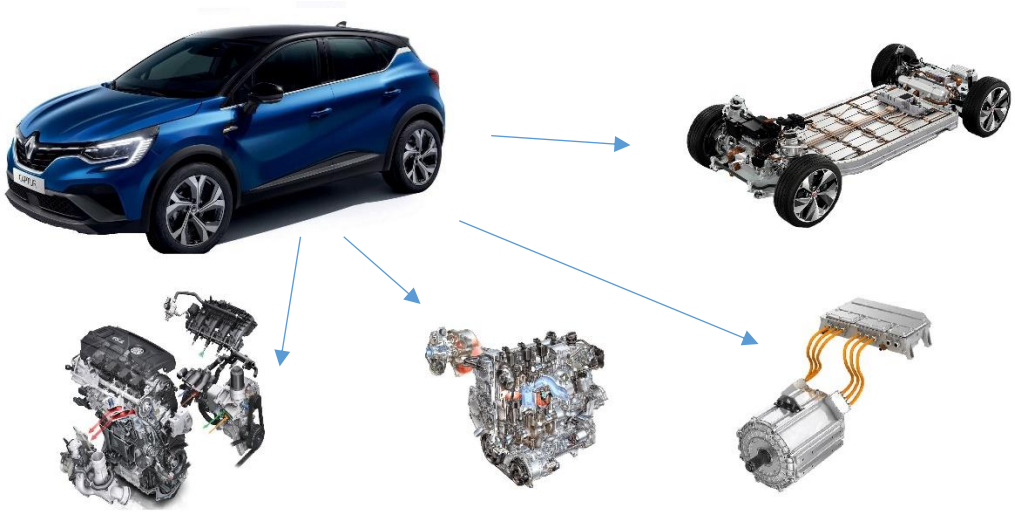

Figure 2.1 Different motorizations available nowadays on the medium city car market.

Regarding internal combustion engines, we can recall a formula that expresses the power developed by it as:

$$Power = \frac{\text{BMEP} * \text{V} * \text{rpm}}{\varepsilon} \qquad (2.1)$$

Where:

- BMEP : Brake Mean Effective Pressure, which is the average pressure which, if imposed on the pistons uniformly from the top to the bottom of each power stroke, would produce the measured (brake) power output.
- V: the displacement of the engine.
- Rpm: the engine speed in revolutions per minute.
- ε: parameter to distinguish between 2-stroke engines (ε=1) and 4-stroke engines (ε=2), based on the ratio between active and

At a glance, based on formula 2.1, we can immediately understand that in order to increase (or keep constant) the power output of an internal combustion engine we are able to act on the displacement and on the BMEP [6].

The trend in the early stages of engine manufacturing, before the year 2000 and before the pollutant restricting norms were introduced, has always been to increase the displacement of an engine to increase its power output, being mainly naturally aspirated engines, due to the fact that the BMEP could not have been increased over a certain limit imposed by the auto-ignition of fuel under a too high compression ratio.

Naturally aspirated engines are the most widespread type thanks to their simplicity in terms both of physical components and of control logic. They are able to satisfy the torque request rapidly compared to a turbocharged engine thanks to the much lower inertia of the different components thus making them more suitable in urban

driving conditions, and they are typically adopted on low-end models, also due to their lower cost and price and cost of services.

In the recent years, beginning from the introduction of Euro legislation on pollutant emissions emitted by vehicles, car manufacturing companies have always strived and studied in order to decrease them and comply with the limits imposed.

Different solutions were found, passing from the electrification of pre-existing powertrain layouts to the development of full electric vehicles or by maintaining the internal combustion engine philosophy and following the so-called *downsizing* trend.

A solution adopted in the recent years to reduce pollution has been the introduction of *electrification*, by coupling electric motors to internal combustion engine in a hybrid powertrain layout, or directly manufacturing full electric vehicles which do not install any kind of engine.

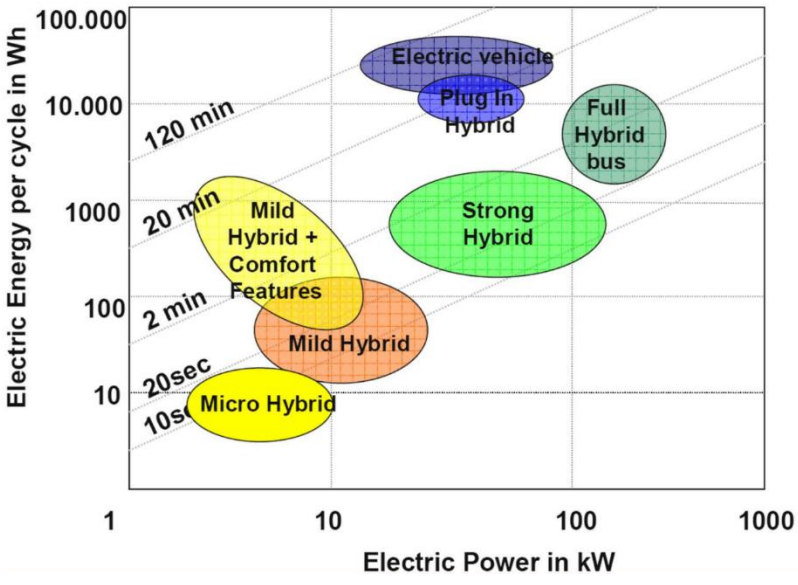

Figure 2.2 Bubble chart describing the different electrification levels on vehicles, depending on their power and electric energy use.

Nowadays the hybrid car market share can be categorized into four different types:

- Micro hybrid: this kind of vehicle uses preinstalled electric motors, such as for example the starter motor, to assist the vehicle only during take-off procedures, while during cruising only the internal combustion engine is engaged. They operate at a low voltage, 12V.
- Mild hybrid: this type is characterized by a small electric motor which assists at very low speeds (<10 km/h) the internal combustion engine, for example during parking or in the first part of the take-off phase. The systems are up to 6 kW in power and also include a supplementary battery in addition to the one used for basic vehicle services, operating at a tension between 12V and 48V.
- Full hybrid: these vehicles are able to drive uniquely using electric propulsion, exploiting the internal combustion engine as a generator to recharge the battery pack. They have an extended autonomy range and feature a complex control logic to optimize fuel consumption depending on several on board parameters. They include a large battery pack which operates between 60V and 200V.
- Plug in hybrid: hardware wise this category has the same layout of a full hybrid, but components are ulteriorly increased in size, capacity and power, and a charging port equipped with an on-board charger is included, giving the possibility to charge the battery pack directly from the electrical grid. They feature systems operating between 200V and 600V.

The last category on the market is the full electric vehicles, which do not feature any internal combustion engine onboard. They are becoming widespread especially in urban areas due to the delocalization of pollution, moving it from inside the cities to rural areas where the energy production plants are based. A few examples can be found in the full electric city buses and vans [7].

But following the latest trends on pollutant emission reduction, and thanks also to the ongoing technological studies and developments, car manufacturing companies have pushed the market with a trend known as the *downsizing* of internal combustion engines. The philosophy behind this trend has always been the reduction of fuel consumption and pollution, especially inside urban and highly populated areas, and this objective was obtained by designing and developing a new generation of engines which could meet the same performance goals of the latter ones, while reducing the displacement and the overall weight of the assembly [8]. Recalling formula 2.1, we see how now manufacturers began increasing the BMEP inside the engine to obtain power while keeping a contained displacement value.

With this, small-sized turbocharged engines became widespread on the market, typical examples can be the Ford EcoBoost125 or the Fiat TwinAir, which took the place of the previous generation powertrains with a reduced displacement and a supercharging system [9].

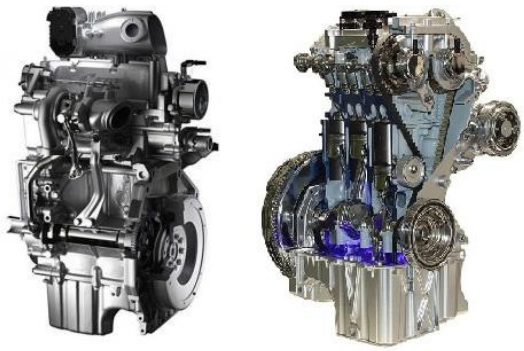

Figure 2.3 On the left, the Fiat TwinAir engine, on the right, the Ford EcoBoost 125. We can see how they are visibly very compact.

Turbocharged engines exploit the high enthalpy level of hot exhaust fumes exiting from the cylinders to put in rotation a turbine, which is mechanically connected through a shaft to a compressor, able to compress and increase the amount of air passing through the intake side of the engine. Once the inducted air is compressed, it increases its temperature which would be detrimental for the overall performances, thus a so-called intercooler is installed in this kind of setups. This is a finned radiator which cool down the compressed air back to around ambient temperature before delivering it to the combustion chambers.

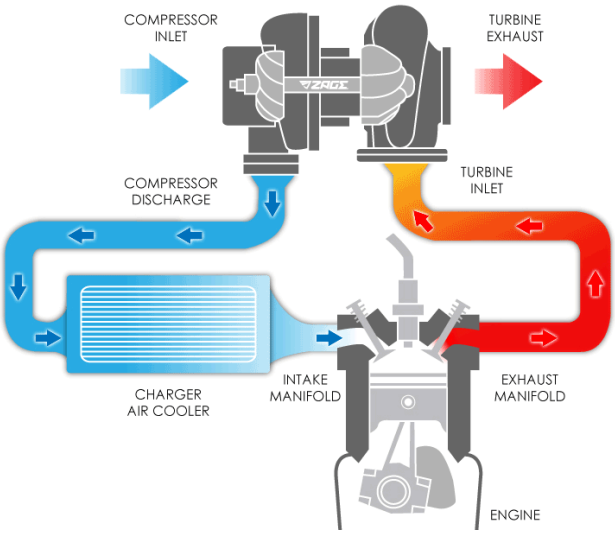

Figure 2.4 Schematization of a turbocharged engine.

There are different ways to compress the air inducted in an internal combustion engine [10]:

- Turbo Charging: adopting a so-called turbocharger, which is a component comprehending a turbine, responsible for harvesting the enthalpy from hot exhaust gases exiting from the engine head and spinning the compressor, compressing fresh air entering the intake ducts.

- Supercharging: this solution adopts only a compressor, without a turbine, which is mechanically driven by the engine crankshaft, this allows to remove the undesired turbolag effect but has the downside of harvesting mechanical energy, which reduces consistently the system overall efficiency by not exploiting the enthalpy of hot gases.

The advantage of adopting turbocharging systems can be easily understood by analysing the following figure.

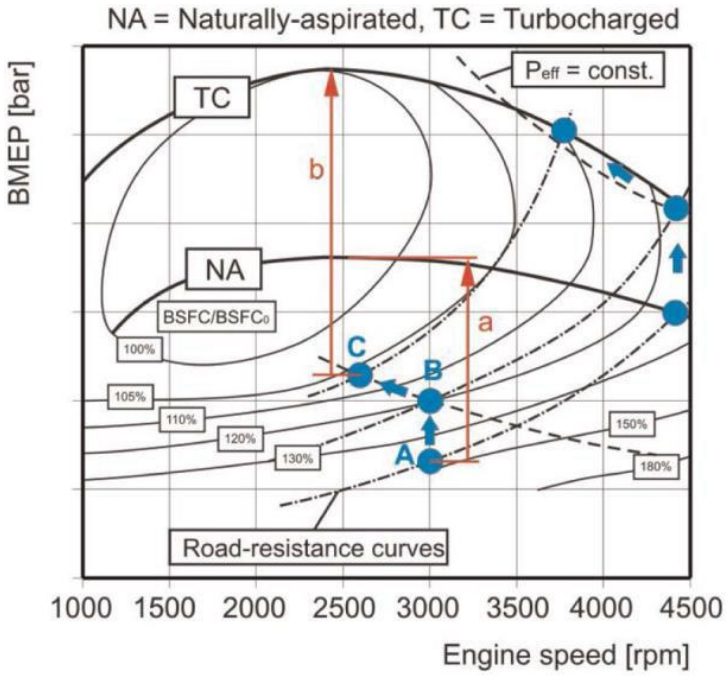

Figure 2.5 Comparison between a NA engine map and a TC one.

Figure 2.5 represents a comparison between an engine map of a Naturally Aspirated (NA) engine and a TurboCharged (TC) engine. The dashed-dotted lines are the constant resistance curves, and we can see how passing from a NA engine to a TC, thus from point A to point B, brings the operating point in a region of lower BSFC (Brake Specific Fuel Consumption) due to the increase in the BMEP value. This

translates in an overall increase in efficiency of the engine, and thus in a lower fuel consumption and pollutant emission. Moreover, another advantage in this terms of TC engines is that having a higher specific power allows to adopt gearboxes with longer transmission ratios, leading to a decrease in engine rpm value, from point B to point C, bringing the engine even more towards a lower BSFC region, which is advantageous. Finally, the two vertical red lines indicate the available BMEP in that operating condition, showing how from the same operating point, a TC engine has a greater available power output with respect to a NA engine, leading also to a better acceleration and driving behaviour.

Nevertheless, the downsizing of engines and the adoption of turbocharging strategies presents some drawbacks:

- The greater amount of BMEP and power expressed from these engines calls the need for stronger and more resistant components, due to the higher mechanical and thermal stresses arising, increasing its cost and weight.
- The number of components and the electronic control strategies required are greater and more complex, leading to cost increases.
- These engines present the problem of *turbolag*, which is the phenomena that expresses when a fast request of torque is demanded by the driver and the engine undergoes a slow transient before fulfilling the request. This is an effect of the increased fluid-dynamic and mechanical inertias with respect to a NA engine, given by the presence of compressor and turbine which absorb energy from the hot fumes exiting from the cylinders to increase their rotational speed. On top of this during the turbolag transient, the air-to-fuel ratio becomes significantly richer because the compressor cannot fulfil instantly the need for fresh air to the cylinders, leading to an increase in pollutant emission.

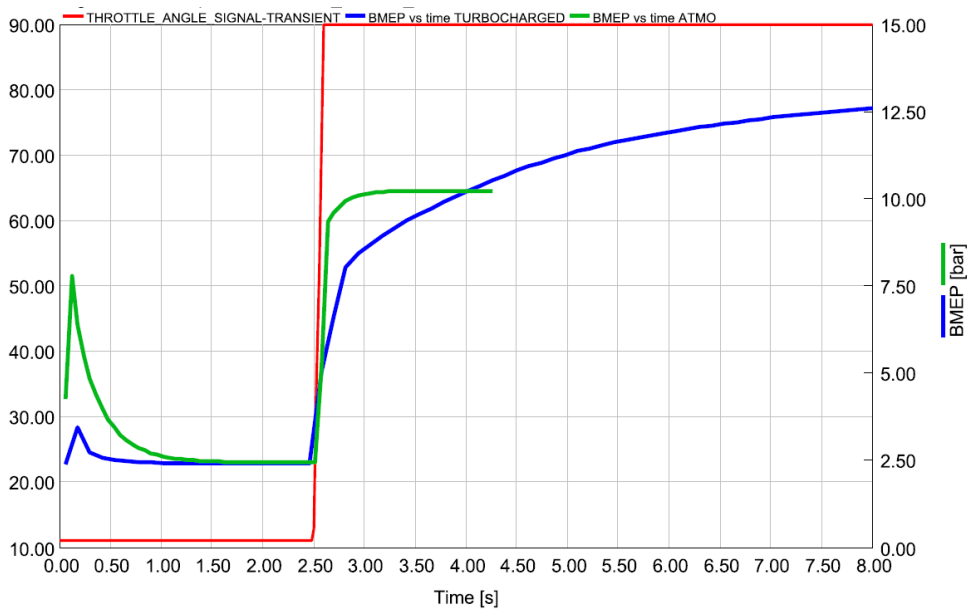

Figure 2.6 Comparison in torque request fulfilment between a NA engine (green line) and a turbocharged one (blue line).

Turbocharger assemblies must also be managed and controlled in order to pump the correct amount of boost pressure at the correct moment and in the correct operating conditions. Different solutions have been developed throughout the years, namely the wastegate valve, the Variable Geometry Turbine (VGT) and the more modern electrified turbocharger (etc.).

The most widespread and simpler solution nowadays is the wastegate valve one, in which a bypass valve electronically or pneumatically actuated is able to deviate a certain amount of exhaust gases away from the turbine, reducing its harvested work and limiting the amount of boost pressure produced [11].

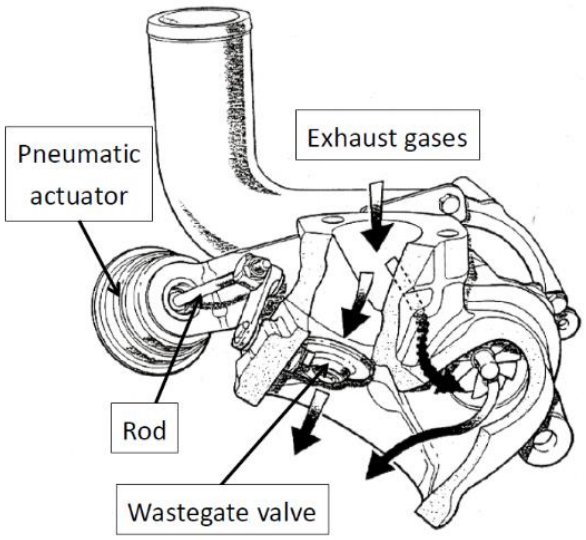

Figure 2.7 Turbine equipped with wastegate valve.

The need to control the turbocharger group power descends from the fact that, if not controlled, with the increase of rpm and air mass flow through the engine, the values of boost pressure generated would be excessive and counterproductive.

The variable geometry turbine, or VGT, instead adopts a series of deviator flaps placed radially before the entrance of the turbine. They act as a fluid dynamic stator and are able to modify both the air mass flow and the velocity triangles hitting the turbine blades, regulating the produced work at best.

Figure 2.8 Schematization of Variable Geometry Turbine guide flaps.

This technology was first patented back in 1953 by Garrett, a famous turbocharger manufacturing company based in Switzerland, and has first been installed on a mass production car in 1991 by Fiat, on the Croma.

Both these setups can also be used to counteract against the turbolag phenomenon, by increasing as much as possible the power generated from the turbine during transient operations, for example by shutting closed the wastegate valve or by directing accordingly the flaps of the VGT [12].

The eTC solution instead is composed by a turbocharger group coupled with an electric motor mounted on the rotating shaft. This allows the engine management unit to have complete control over the behaviour of the compressor and turbine, because it can inject power in the system, increasing thus boost pressure to counteract against turbolag, or it can harvest power from the system by “braking” the turbine and avoiding it from spinning excessively.

Figure 2.9 The new eTurboCharger developed by Garrett.

This technology is consistent also with the hybridization philosophy, because in urban and slow driving conditions it can act as generator to recharge the battery pack of the vehicle on the go. It has been studied and developed by Garrett and tested throughout the 2020 season equipping high end race cars, showing incredible potential on civil mobility also due to the upcoming new Euro7 regulations, which call for a strong hybridization of the current city car market offer [13].

The control on the behaviour of the turbocharger group is an engine management strategy which is often coupled with several other ones in order to put the engine always in an optimal operating condition. Some examples of these strategies that can be quoted are the control on spark advance, and the Variable Valve Timing (VVT).

The spark advance of an engine is the measure of how many crankshaft angle degrees (CA°) before the top dead centre of the cycle the spark plugs ignite the air-fuel mixture. A too low value sacrifices precious performance because the development of the combustion happens with an unfavourable and excessive volume of the combustion chamber, while a too high value leads to an excessive peak of pressure which can trigger autoignition of the charge and engine knocking problems.

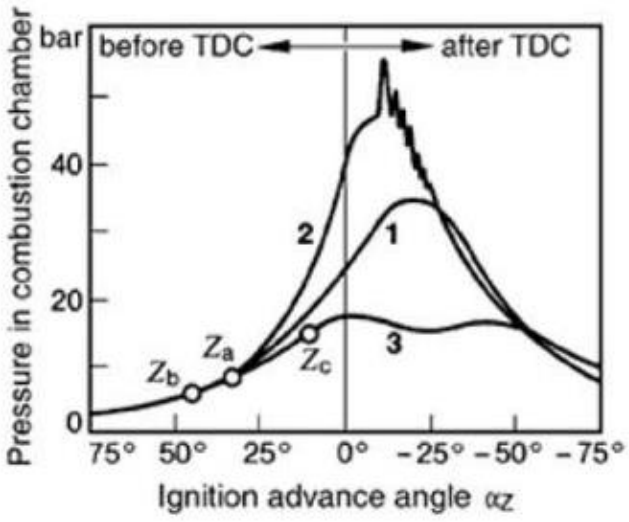

Figure 2.10 Effect of a correct spark advance (1), an excessive one (2) inducing knocking, and a too retarded spark (3), not developing a good amount of in-chamber pressure.

Nevertheless, this parameter can be controlled in turbocharged engines in order to reduce the turbolag effect. By retarding the spark advance, thus igniting the charge at a later stage of the compression stroke, the combustion develops consequently later and the exhaust gases that are fed in the turbine are much hotter. This means the fumes have a higher enthalpy level when flowing towards the spinning blades, being thus able to accelerate in a quicker way the compressor and containing turbolag.

A second example of a parameter that can be varied and controlled in order to manage at best the engine behaviour is valve timing. In all four stroke engines the valve timing is a fundamental parameter which regulates its behaviour and performance and must be tuned accordingly.

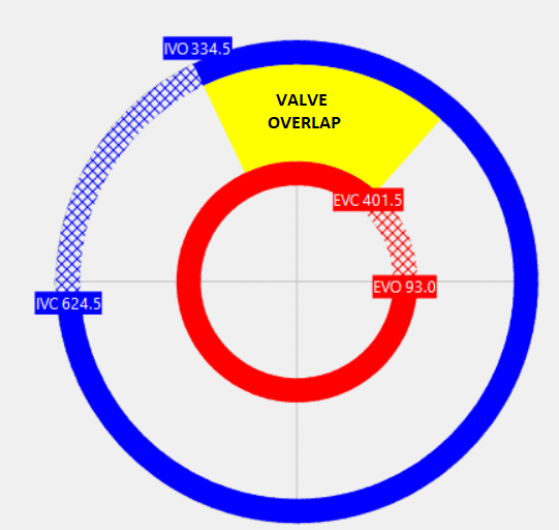

Figure 2.11 Example of valve timing chart, with indicated Exhaust valve opening and closing (EVO, EVC) and Intake valve opening and closing (IVO, IVC).

Conventional and older engines have a fixed valve timing, which presents only a range of engine speeds in which it is optimized, while outside of that it is detrimental for performance and pollution. For this reason car manufacturers have pushed toward the adoption of variable valve timing throughout the years.

The first generation of variable camshafts presented the possibility of only varying timing (and not lift) and in a discrete and discontinuous way, usually by twisting of a certain quantity the intake camshaft thanks to the adoption of a helical sleeve mounted on the timing chain gear and moved by the pressurization of the oil circuit.

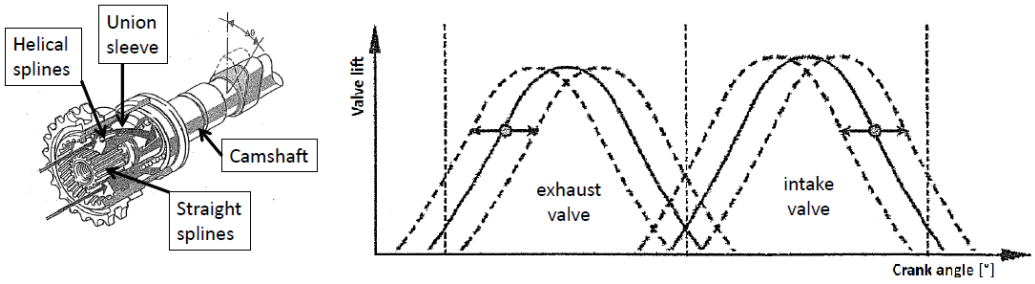

Figure 2.12 Operation of a typical first-generation variable valve timing system.

If the engine adopts the DOHC technology, meaning that it disposes of two separate camshafts for intake and exhaust valves, this also gives the possibility to vary and optimize the valve overlap in different operating conditions.

Successively, the second generation VVT was developed, introducing the possibility to also vary the lift profile of the cam. A famous example of this kind of technology is Honda's V-TEC, in which a set of low-lift and low-duration cams is built on the same shaft of a higher and longer shaft. At low loads and engine speeds, the slow cam is engaged and reduces fuel consumption and pollutants, while when the engine goes towards higher loads and regimes, a pin is moved by a hydraulic actuator and connects the rocker arm related to the higher cam, increasing the overall performance.

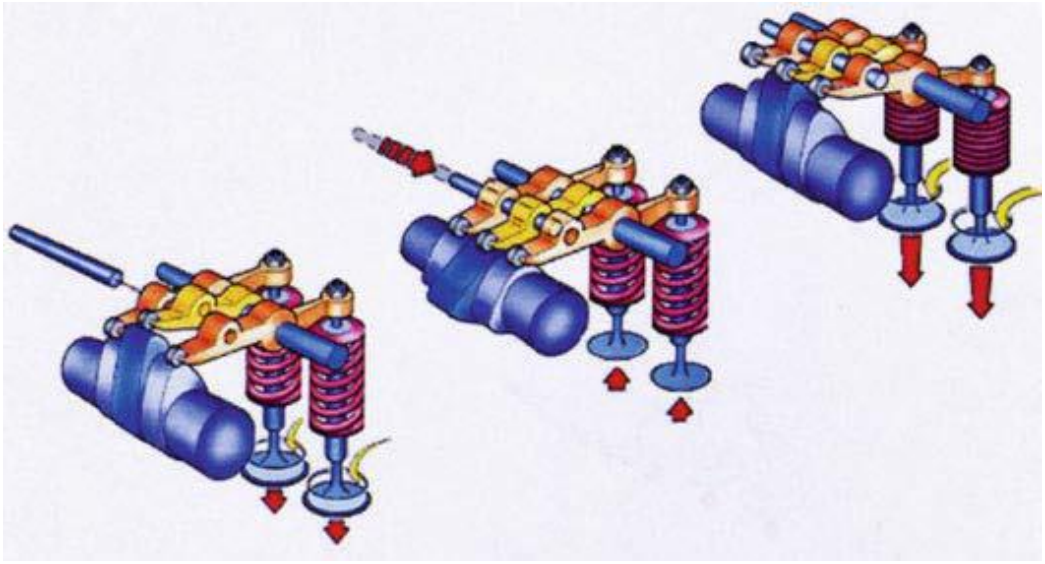

Figure 2.13 Schematization of Honda's VTEC technology, where a pin moved by oil pressure puts into operation the high-performance cam lobe.

Also in this case, the still present limit of the discontinuous operation of this device pushed car manufacturers to develop the third generation of variable valve timing, capable of operating in a continuous way throughout the operating points map of the engine and increasing consistently the level of optimization which could be reached. Examples of this technology are the BMW ValveTronic and the Fiat Multiair, the first one working tanks to a mechanical principle and an eccentric cam, while the latter's functioning is of hydraulic nature.

In the most recent years also the Camless technology was introduced, which excludes the adoption of camshafts to operate the opening and closing of the valves, replacing them with electromagnetic, hydraulic, or pneumatic actuators. Pioneer in this technology is the Swedish company Koenigsegg, developing a fully functional prototype in early 2015, but up to now this type of valve actuation is still reserved for prototypes and not for mass production engine models [14] [15].

Having the complete control over cam profiles opened to engineers the perspective of introducing several different strategies to optimize the combustion process for each engine load and speed, for example:

- Optimal valve opening and closing timings, maximizing in every condition the cylinder filling, thus improving performance and engine response during transients.
- Load control in spark ignition engines, now the mass of trapped air inside the cylinder can be regulated using the opening period of the intake valve, removing a consistent amount of pumping losses and the need of a throttle valve.
- In-cylinder charge motion can be now controlled by actuating in different ways the two intake valves, for example to introduce a strong swirl motion at low engine speeds.
- Introduction of the Miller cycle, a motor cycle which adopts a longer expansion stroke than the intake one. This results in higher efficiency values and lower final gas temperatures, which also contain the formation of pollutants.

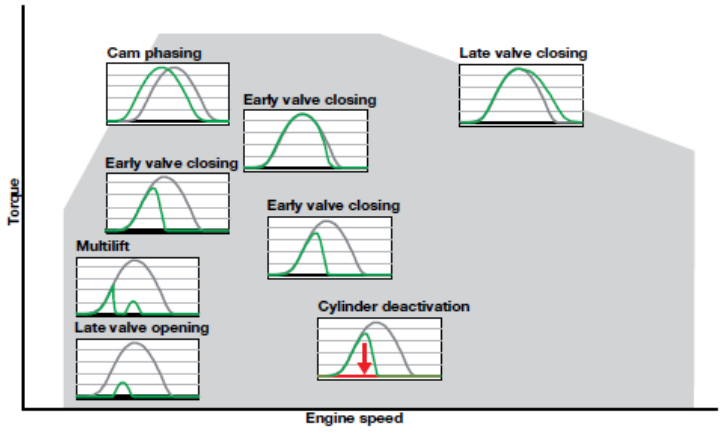

Figure 2.14 Different valve variable actuation strategies depending on the area of the engine map.

Chapter 3 GasDyn software and engine model

3.1 GasDyn software

GasDyn is a mono-dimensional thermodynamic and fluid dynamic simulation software, especially developed in order to be able to simulate and predict a wide amount of parameters regarding different typologies of internal combustion engines. It was first released in 1996 and was developed by the Politecnico di Milano Energy Department together with *Exothermia*, a Greek software development company. It is able to compute different engine quantities, for example the power and torque outputs, the fuel consumption, pollutant emissions, volumetric efficiency, air-to-fuel ratio, etc. Along with strictly engine related quantities, the software is able to solve the equations regarding inertial and wave effects inside the intake and exhaust ducts, which rule the general behaviour of an engine, and solve the thermal transients happening, for example, in a catalyst to be able to predict its conversion efficiency in time.

3.2 Conservation equations

The simulation environment is based on the solution of the conservation equations considering a mono-dimensional, unsteady, reactive, and compressible flow, considering both turbulence and friction phenomena [16].

Let us consider a control volume, as in Figure 3.1, in order to be able to write the conservation of mass, energy and momentum:

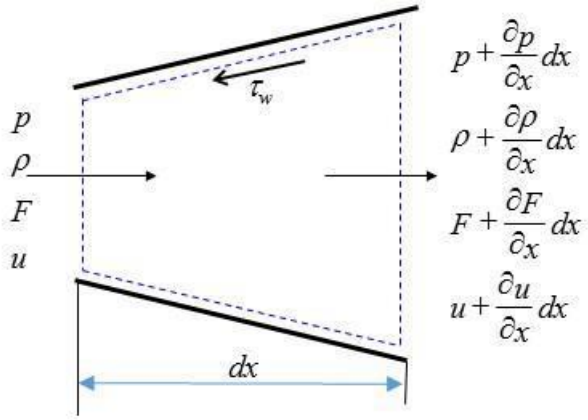

Figure 3.1 Control volume schematization adopted to write conservation laws

In this figure, the quantities described are:

- x : Coordinate along the axis of ducts.
- p : Pressure.
- F : Transversal section.
- u : Fluid velocity.
- ρ : Density.
- τ_W : Shear stress.

3.2.1 Mass conservation equation

Based on the previously described control volume setup, we are able to write the mass conservation, imposing that the mass flow inside the volume must be the difference between the one entering and the one exiting.

$$\left(\rho + \frac{\partial \rho}{\partial \mathrm{x}}\mathrm{dx}\right)\left(\mathrm{u} + \frac{\partial \mathrm{u}}{\partial \mathrm{x}}\mathrm{dx}\right)\left(\mathrm{F} + \frac{\partial \mathrm{F}}{\partial \mathrm{x}}\mathrm{dx}\right) - \rho \mathrm{uF} \;=\; -\frac{\partial}{\partial \mathrm{t}}(\rho \mathrm{F}\mathrm{dx}) \qquad (3.1)$$

The equation can be rearranged, and the second order infinitesimals can be neglected, obtaining a leaner equation form as follows:

$$\frac{\partial \rho}{\partial \mathrm{t}} + \rho \frac{\partial \mathrm{u}}{\partial \mathrm{x}} + \mathrm{u}\frac{\partial \rho}{\partial \mathrm{x}} + \frac{\rho \mathrm{u}}{\mathrm{F}}\frac{\partial \mathrm{F}}{\partial \mathrm{x}} = 0 \qquad (3.2)$$

3.2.2 Energy conservation equation

Regarding the energy conservation equation, we can recall the First Principle of Thermodynamics, which states that the difference between the heat flux through the control volume walls and the mechanical work done by the fluid, each one with its sign dictated by convention, must be equal to the sum of the time variation of the internal stagnant energy and the flux of enthalpy across the control volume surface. This leads us into writing the following expression:

$$\dot{\mathrm{Q}} - \dot{\mathrm{L}} \;=\; \frac{\partial \mathrm{E}_0}{\partial \mathrm{t}} + \frac{\partial \mathrm{H}_0}{\partial \mathrm{x}}\mathrm{dx} \qquad (3.3)$$

Where:

- $\dot{Q} = q \times \rho F dx + \Delta H_{Reaction} F dx$ is the heat entering the control volume.
- $\frac{\partial E_0}{\partial t} = \frac{\partial (e_0 \rho F dx)}{\partial t}$ is the variation of internal energy.
- $\frac{\partial H_0}{\partial t} = \frac{\partial (h_0 \rho F u)}{\partial x} dx$ is the flux of stagnation enthalpy.

Thus, by substituting, rearranging, and neglecting the second order infinitesimal terms we can rewrite the equation as:

$$\frac{\partial (\mathrm{e_0} \rho \mathrm{F})}{\partial \mathrm{t}} + \frac{\partial (\mathrm{h_0} \rho \mathrm{F u})}{\partial \mathrm{x}} - \rho \mathrm{q F} = 0 \qquad (3.4)$$

3.2.3 Momentum conservation equation

We can write the momentum conservation equation by stating that the sum of pressure forces and shear forces acting on the surface of our control volume must be equal to the sum momentum change rate inside the volume and the momentum exiting it. In mathematical terms, this means:

$$\frac{\partial (\rho \mathrm{u F})}{\partial \mathrm{t}} + \frac{\partial (\rho \mathrm{u^2 F} + \mathrm{p F})}{\partial \mathrm{x}} - \mathrm{p} \frac{\mathrm{dF}}{\mathrm{dx}} + \rho \mathrm{G F} = 0 \qquad (3.5)$$

Where the first term is related to the change of momentum inside the control volume, the second and third term are a rearrangement of the pressure forces on the volume's walls and the momentum exiting the volume, while the fourth term describes the shear stress effect.

3.2.4 Conservative form of equations

Once we have written the conservation equation in the previously described subchapters, we obtain the following system of equations to be solved:

$$\begin{cases} \dfrac{\partial(\rho \mathrm{F})}{\partial \mathrm{t}} + \dfrac{\partial(\rho \mathrm{uF})}{\partial \mathrm{x}} = 0 \\ \dfrac{\partial(\rho \mathrm{uF})}{\partial \mathrm{t}} + \dfrac{(\rho \mathrm{u}^2\mathrm{F} + \mathrm{pF})}{\partial \mathrm{x}} - \mathrm{p}\dfrac{\mathrm{dF}}{\mathrm{dx}} + \rho \mathrm{GF} = 0 \\ \dfrac{\partial(\mathrm{e}_0 \rho \mathrm{F})}{\partial \mathrm{t}} + \dfrac{\partial(\mathrm{h}_0 \rho \mathrm{Fu})}{\partial \mathrm{x}} - \rho \mathrm{qF} = 0 \end{cases} \qquad (3.6)$$

This system can be simplified in terms of resolution, by rewriting it in the conservative matrix form, where the momentum conservation equation is substituted by the equivalent impulse equation, in the form of a linear combination of the mass conservation equation and the momentum conservation one.

We must first regroup the considered variables in three vectors:

- The vector of conserved variable fluxes: $\bar{F}(\bar{W}) = \begin{bmatrix} \rho u F \\ (\rho u^2 + p)F \\ u \rho h_0 F \end{bmatrix}$

- The vector of source terms: $\bar{C}(\bar{W}) = \begin{bmatrix} 0 \\ -p\frac{dF}{dx} \\ 0 \end{bmatrix} + \begin{bmatrix} 0 \\ \rho G F \\ -\rho q F \end{bmatrix}$

- The vector of conserved variables: $\bar{W}(x,t) = \begin{bmatrix} \rho F \\ \rho u F \\ \rho e_0 F \end{bmatrix}$

The first vector represents the mass, impulse, and stagnation enthalpy fluxes, which are conserved throughout the control volume boundary. The second vector is composed by two different vectors itself: the terms due to a variation of cross section along the x axis of the duct, and the terms given by the friction between fluid and walls, along with the heat exchange term. The third vector contains instead the variables of our problem to be solved, they are independent and vary along x and t. Moreover, their fluxes are conserved along the shockwaves.

We can finally rewrite the conservation equation in a more compact and elegant form as follows:

$$\frac{\partial \bar{W}(x,t)}{\partial t} + \frac{\partial \bar{F}(\bar{W})}{\partial x} + \bar{C}(\bar{W}) = 0 \qquad (3.7)$$

Having four variables and only three equations, we must integrate our system with an additional condition, in particular a law describing the characteristics of the fluid object of our study.

We can exploit in this case the perfect gas law, describing the physical characteristics of a gas as follows:

$$\frac{p}{\rho} = R^* T \qquad (3.8)$$

This carries along a new variable, making them five, the temperature T, but for an ideal gas this can be exploited to write the internal energy and the enthalpy as a function of temperature, as follows:

$$e = C_v T$$
$$h = C_p T$$

Where C_v is the specific molar heat at constant volume, and C_p is the one at constant pressure.

Having finally our complete set of equations describing the thermal and fluid dynamics phenomena occurring in the ducts of the engine, by completing them with the suitable boundary conditions we are able to determine the flow conditions and parameters in every section of the duct.

3.2.5 Numerical method solution

Unless we have a problem with particular boundary conditions, for example the Poiseuille flux, we are not able to obtain an analytical expression of the flow state inside the ducts. It is thus for this reason that numerical solutions are required to solve these problems. The GasDyn software adopts a shock capturing second order finite difference method, which is able to solve the issue of solution discontinuity given by the presence of pressure waves.

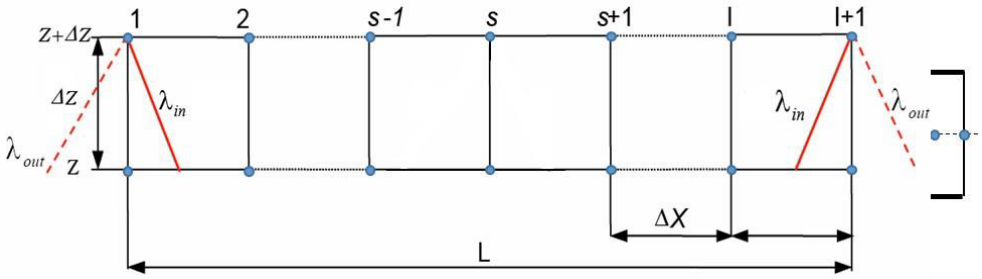

Figure 3.2 Mesh in a duct used to compute 1D numerical solutions

The previously described conservation equation is thus solved punctually in every discretization node in which the ducts are partitioned. Every intake and exhaust duct is divided in sub elements, which are partitioned in a mesh. The numerical algorithm is adopted only in the internal nodes, while for the boundary ones a characteristic based approach is used, exploiting Riemann variables.

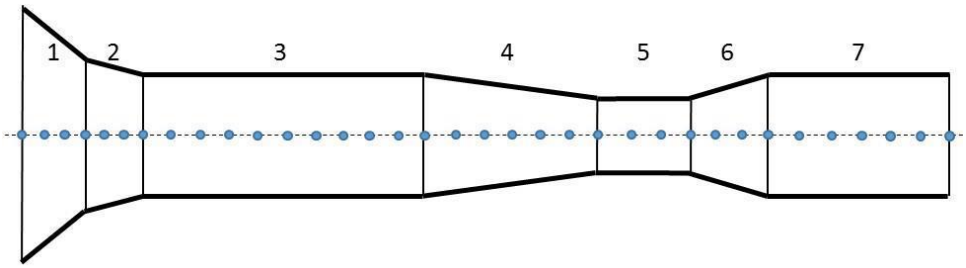

Figure 3.3 Example of a complex pipe made of several sub-elements connected together. The pipe is treated as a continuous duct by the numerical method.

Ducts mustn't be necessarily of constant diameter, or only straight, but can have more complex shapes including curvatures which the software is able to consider. Adopting this numerical method also gives the possibility to model a long and section varying duct in a unique block, successively discretized, and the sub elements communicate directly between each other.

3.3 Engine model object of the study

Hereby we present the GasDyn engine model which was adopted during this analysis.

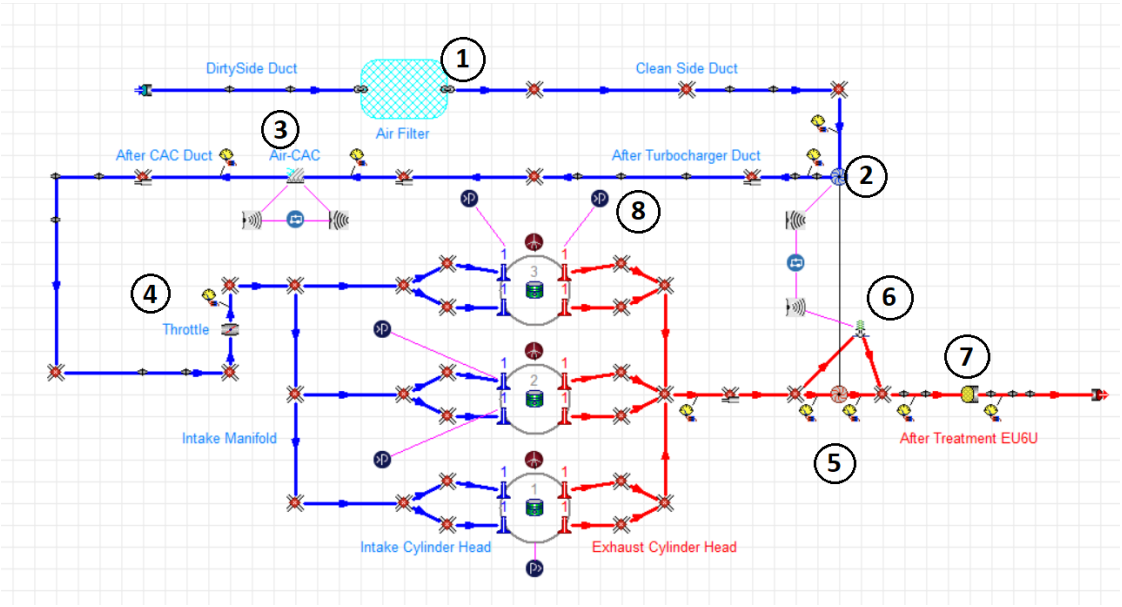

Figure 3.4 Overview of the engine object of this study modelled in the GasDyn environment

This model reproduces the characteristics of the Renault HR10DDTg2 engine, a 1000cc turbocharged three-cylinder engine which will equip different city cars of the French manufacturer, in particular the Renault Captur.

In Figure 3.4 we can highlight the following components:

1. Intake air filter
2. Compressor, model no. 037X76AL20B95GN (P92) manufactured by Borg Warner
3. Air intercooler
4. Throttle valve
5. Turbine, model no. 031X86FN28B01OG manufactured by Borg Warner
6. Wastegate valve
7. Three-way catalyst
8. Co-simulation input

Architecture	In-line 3 cylinders
Displacement	999 cc
Bore/Stroke	72.2 mm / 81.3 mm
Compression ratio	11:1
Compressor	Ø37mm, 5 blades, aluminium carter
Turbine	Ø31mm, 10 blades, steel carter
Torque	200 Nm @ 2250 rpm
Power	84.5 kW @ 5250 rpm

Table 1 Engine characteristics summary.

3.3.1 Stationary engine model

The first step made in order to create a vehicle transient simulation model is to have a correct and faithful stationary model, which is able to copy the experimental results at best. From an operative point of view, the engine model was already pre-existent and came along with a set of experimental data acquired by Renault on the engine test bench. By comparing the simulated results and the experimental ones we will be able to assess the correctness of the stationary model, having thus a good level of confidence before moving to the transient operating mode [17].

The first parameter to be assessed is the BMEP, being the main performance expression of the engine, which also defines the torque and power outputs for each operating point. An excessively high error on this parameter would lead, during the transient operations, to a misplacement of the engine regime and throttle percentage commanded, along with several other incorrectness.

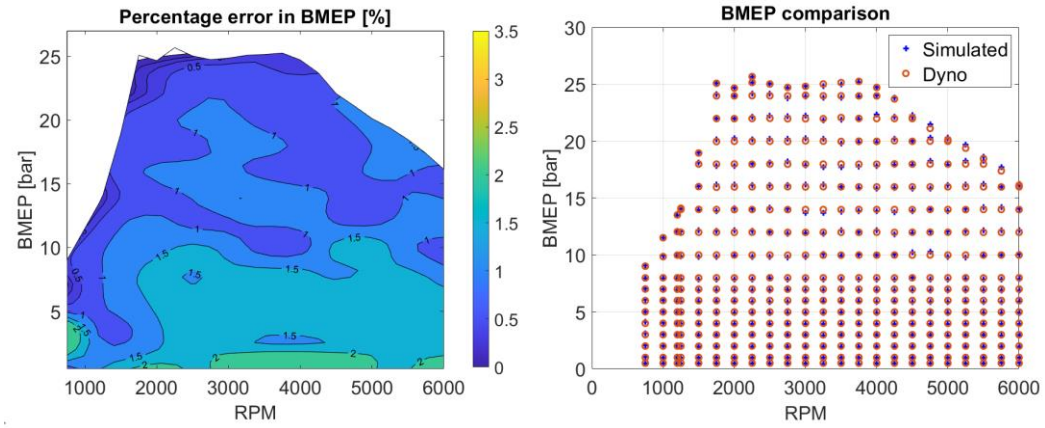

Figure 3.5 Comparison between experimental and simulated BMEP.

As it can be seen in Figure 3.5 the error in BMEP is contained throughout the map under 2%, which can be considered a very accurate and satisfying result. These results could be refined by imposing stricter tolerances on the model, but as said in the previous chapters, it would have led to an undesired increase in computational expense, making the model heavier and longer to be solved.

Carrying on we can pass on analysing the BSFC, or Brake Specific Fuel Consumption, of the engine.

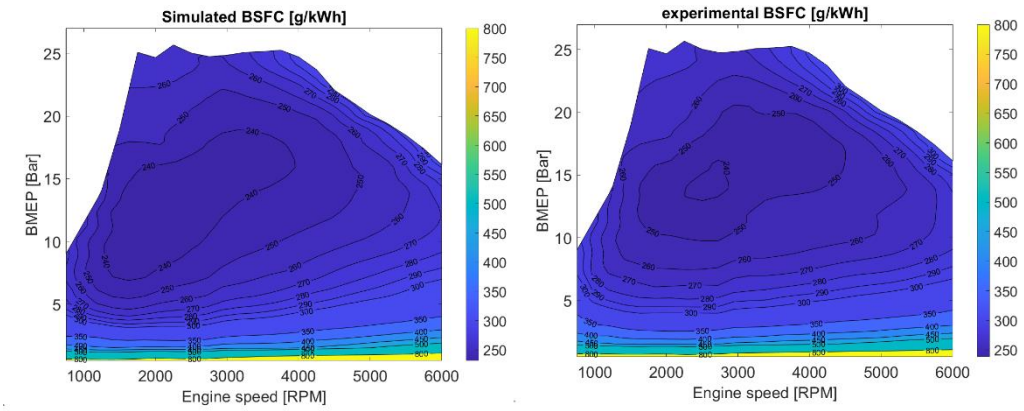

Figure 3.6 Comparison between experimental and simulated BSFC.

This is an important parameter when simulating real driving conditions because it directly determines the engine fuel efficiency, so how well the engine is able to generate energy from a gram of fuel. As shown in Figure 3.6 it can be immediately seen how the simulated BSFC map's trend and morphology well copy and reproduce the experimental one, having the minimum in a coherent area of medium-high load and medium engine speed. The error is contained under 5%, except in the very low loads and engine speeds, where the combustion model struggles to reproduce faithfully the real phenomena.

Finally another important aspect when considering vehicle simulations and homologation cycles is the pollutant emissions of the engine, in particular in this work the emissions of unburnt hydrocarbons (HC), of carbon monoxide (CO), of carbon dioxide (CO2) and of nitrogen oxides (NOx).

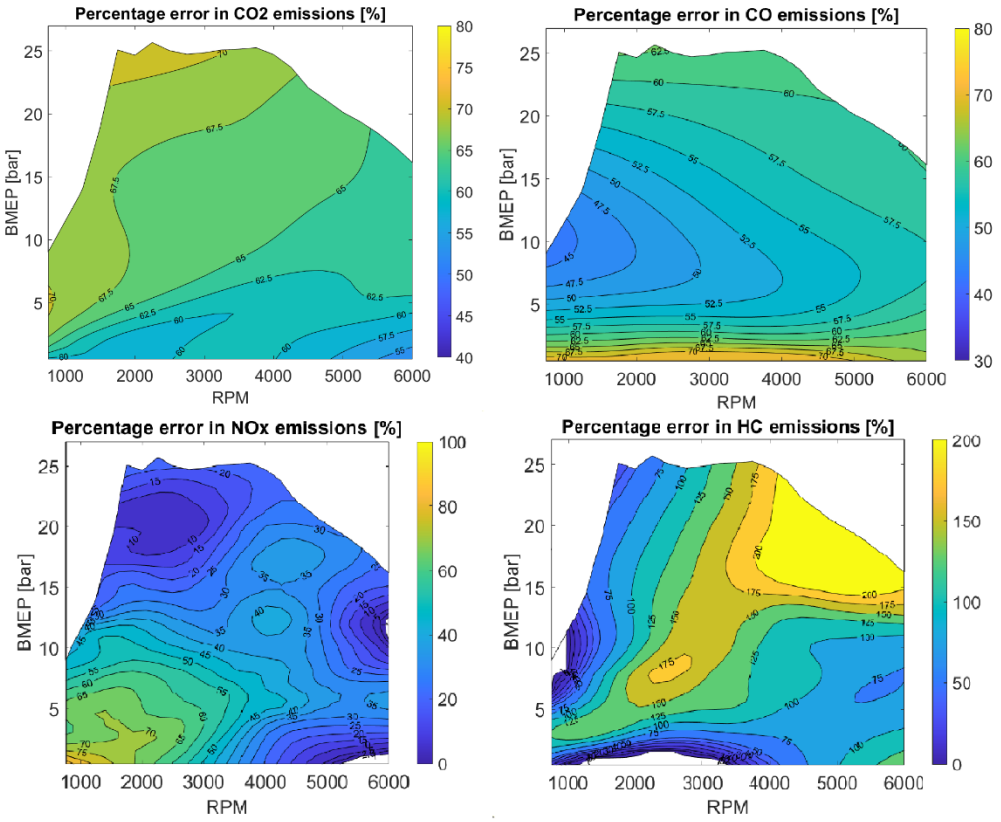

Figure 3.7 Comparison between experimental and simulated pollutant emissions.

In Figure 3.7 the percentage errors of each main pollutant are shown. As it can be seen there is a general trend of overestimation of the emissions, which will lead to the same effect in the vehicle transient simulations. This can be explained based on the fact that the mechanisms that lead to pollutant formations are several and very complex, while in the engine model the default values were adopted.

This opens the door to future refinements of the model, by working on calibrating the pollutant formation models at best.

3.3.2 Stationary, transient operation and co-simulation

The Gasdyn software can be adopted to simulate two different operating conditions. The first one is the stationary mode, in which the software solves different operating

conditions defined as a grid of Engine Speed – Load points, and each one is simulated until a steady state solution is found. This mode is useful when working with the validation of stationary maps, for example, when an engine is experimentally tested on the engine dyno bench and different operating points are acquired and logged.

The second computational mode is the transient mode, in which the software does not reach a steady state condition nor has a grid of operating points to follow, but instead it is given an engine load or an engine speed time history, and the transient operation of the engine is computed, simulating thus the inertial effects happening inside the engine assembly in a dynamic situation.

Gasdyn has also the capability of communicating with other softwares in a co-simulation environment, in particular Simulink. This opens the possibility to insert the engine model computed by GasDyn in a wider model, comprehending vehicle dynamics, in order to be able to simulate a full vehicle operation and execute driving cycles, real driving simulations, developing electrification strategies, etc.

Chapter 4 Simulink software and vehicle model

4.1 Simulink software

Simulink is a software developed by MathWorks and based on the famous MATLAB software. It is an extension of it and its working principle is based on visual programming, translating thus the needs of the programmer in blocks, charts, and state flows instead of code lines.

It is widely used to model time changing domains and dynamics of physical systems, in particular in this work it has been adopted to compute and simulate the longitudinal dynamics of a vehicle during a homologation cycle.

The complete vehicle scheme which was built for this thesis is the following one:

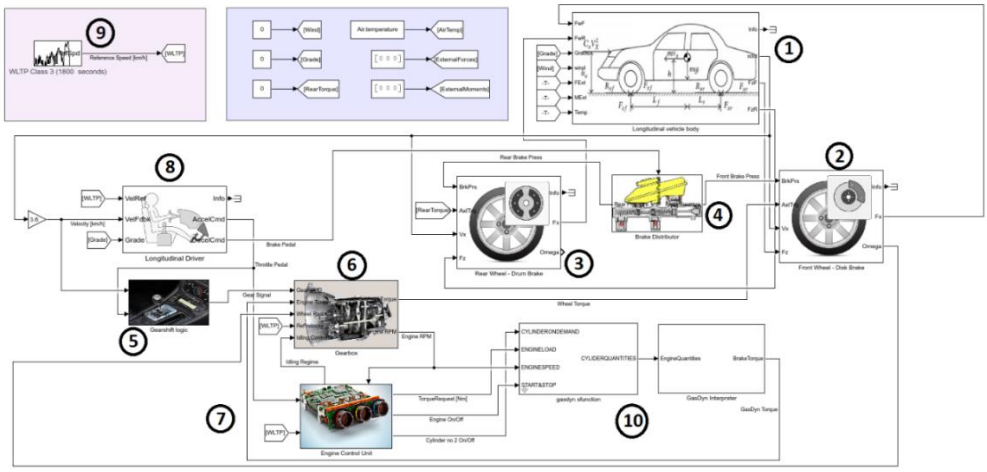

Figure 4.1 Overview of the Simulink full vehicle simulation model

Each different block is responsible of solving the equations related to a component of a car, in particular the highlighted ones are:

1. Vehicle car body
2. Front wheel with braking system
3. Rear wheel with braking system
4. Braking distributor
5. Gearshift logic controller
6. Gearbox
7. Engine Control Unit (ECU)
8. Driver controller
9. Velocity profile source
10. GasDyn S-Function

4.2 Longitudinal vehicle dynamics

Due to the fact that the vehicle must be placed on a rolling dyno when the homologation cycle is performed, it is possible to adopt a reduced dynamics model in place of the complete 14 d.o.f. one. To recreate the real driving conditions, the single-track longitudinal model was selected, neglecting thus any lateral component of the dynamics of the vehicle, which aren't necessary for our needs.

In the following subchapters each main component of a car is analysed and presented from a theoretical point of view and in the Simulink scheme [18] [19].

4.2.1 Car body

To model the carbody we can simply define the forces interacting with it as in the following scheme:

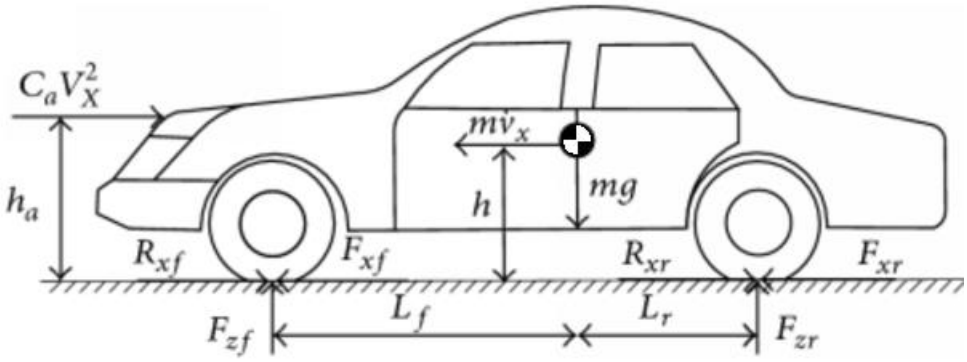

Figure 4.2 Forces scheme of a car body, used to formulate the dynamical equilibrium equations

Where:

- $m\dot{v}_x$ is the longitudinal inertial term.
- mg is the vehicle weight force.
- h is the centre of gravity (COG) height.

- F_{zf}, F_{zr} are respectively the front and the rear vertical load on the tires.
- F_{xf}, F_{xr} are respectively the front and rear longitudinal load on the tires.
- L_f, L_r are respectively the front and rear wheelbase.
- R_{xf}, R_{xr} are respectively the front and rear longitudinal resistance forces.
- $C_a V_X^2$ is the reduced aerodynamical load applied in the forces pole.
- h_a is the height of the aerodynamic force application point.

Given this setup we can write the following dynamical equilibrium equations:

$$\begin{cases} F_{zf} + F_{zr} - mg = 0 \\ m\dot{v}_x + F_{xf} + F_{xr} - C_a V_x^2 - R_{xf} - R_{xr} = 0 \\ F_{zr} L_r + R_{xr} h + R_{xf} h - F_{zf} L_f - F_{xf} h - F_{xr} h - C_a V_X^2 (h_a - h) = 0 \end{cases} \tag{4.1}$$

By solving this system of equations, we are able to compute the velocity of the vehicle in every time instant.

In Simulink this was managed by the car body block:

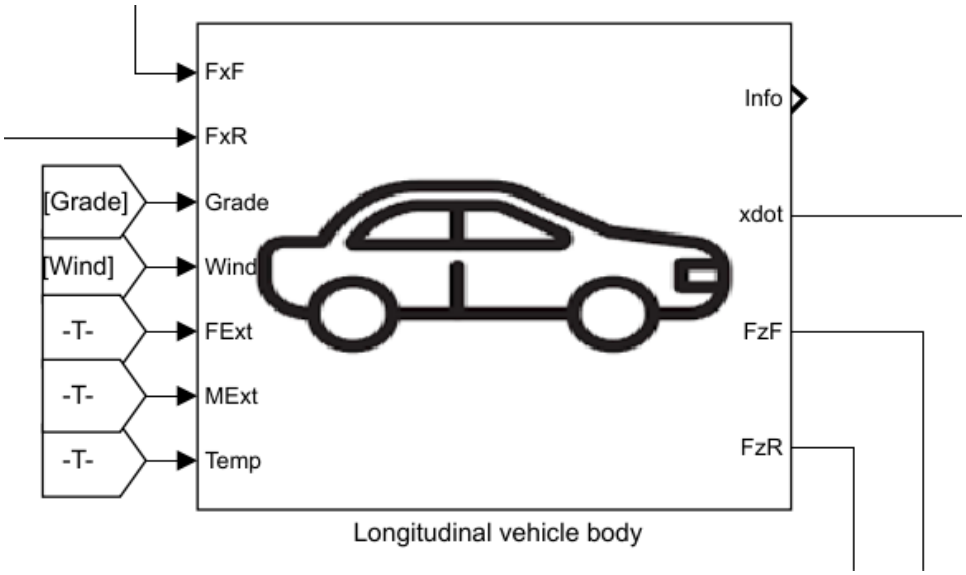

Figure 4.3 Carbody block in Simulink, having on the left the input signals and on the right the outputted quantities.

The inputs are on the left and comprehend the external ambient conditions, the road grade, and the longitudinal forces coming from the front and rear wheels. As output, it gives the vehicle longitudinal velocity along with the vertical loads acting on the wheels.

To specify which vehicle is being simulated the block gives the opportunity to set different characteristics of the vehicle, as it can be seen in the following image, along with other boundary conditions.

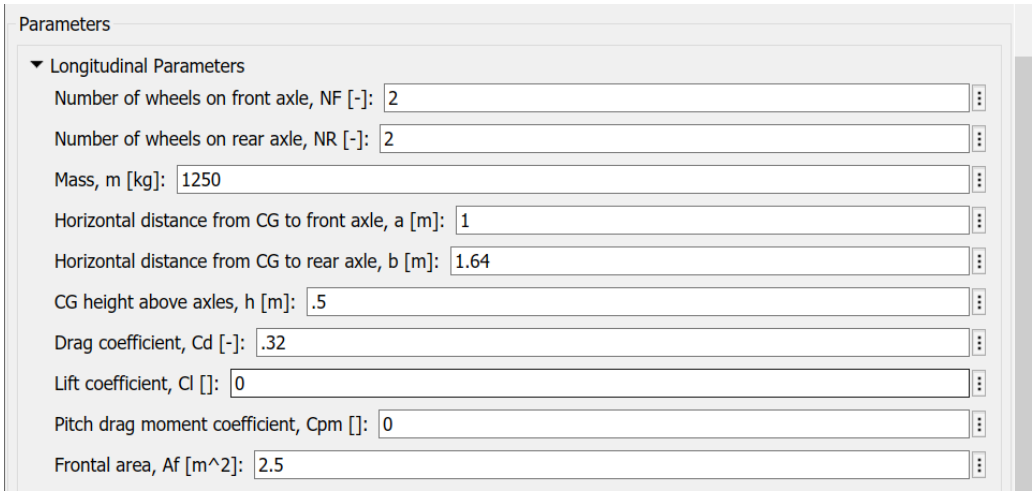

Figure 4.4 Carbody block parameters, set to reproduce the characteristics of the vehicle object of the study.

4.2.2 Front and rear wheel

The wheels of the vehicle have in Simulink a dedicated block, in which also the equations modelling the braking system are included. They communicate real-time with the carbody exchanging the values of wheel torque and longitudinal tractive force.

The mechanical model adopted is the following:

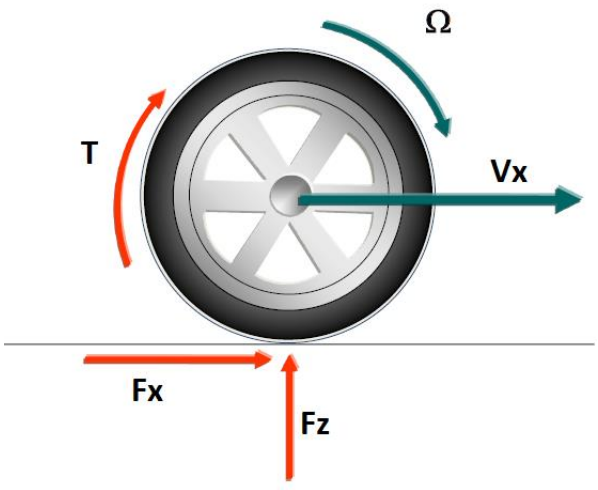

Figure 4.5 Force schematization of a car wheel

In Figure 4.5 we can see the different terms related to the wheel. The overall torque applied, which is labelled as T in the image, is the resultant torque coming from the algebraic sum of torque coming from the engine, from the brakes and the resistant one.

$$T = T_{Engine} + T_{Brakes} + T_{Resistant} \qquad (4.2)$$

The engine torque comes directly from the GasDyn block, it is passed inside the gearbox block and is delivered to the front wheels equally.

The braking torque is generated depending on the pressure inside the braking circuit, which is set by the driver applying a force on the brake pedal. The model adopted for the braking system is different between front and rear wheels, having at the front a disk braking system and a drum one at the rear.

The disk brakes can be modelled as follows:

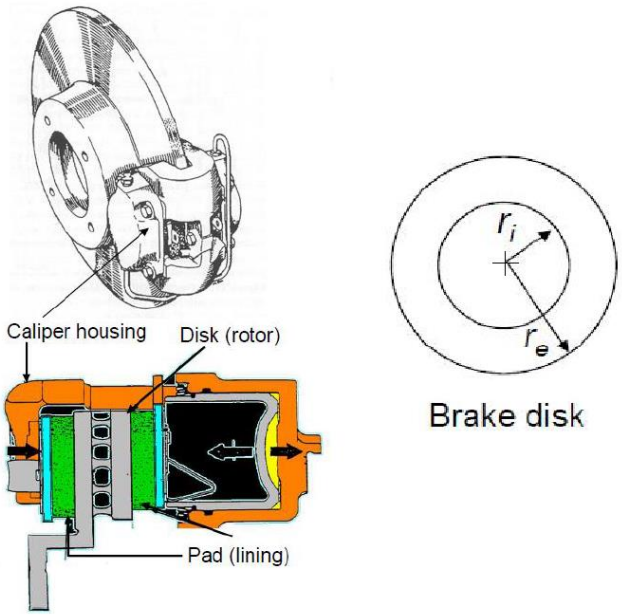

Figure 4.6 Disk brake schematization, on the right the image to compute the mean effective braking radius

$$\begin{cases} T_{DiskBrake} = 2\mu_{pad} R_{eff} A_{pad} p_{oil} \\ R_{eff} = \frac{2}{3} \frac{r_e^3 - r_i^3}{r_e^2 - r_i^2} \end{cases} \qquad (4.3)$$

The rear wheels instead are equipped with drum type brakes, which follow different equations and a different working principle.

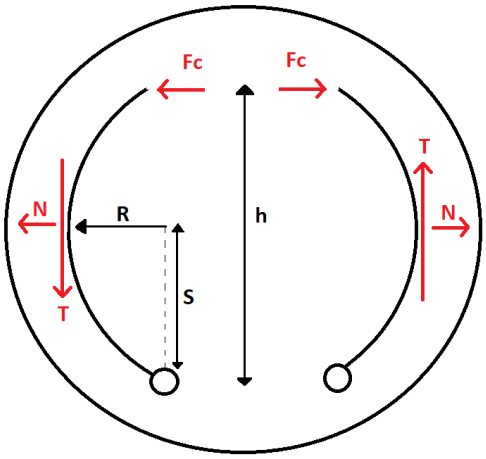

Figure 4.7 Schematization of a drum brake, with the external drum on which two shoes insist, pushed by a hydraulic piston.

$$\begin{cases} T_{DrumBrake} = \mu \dfrac{2F_c hS}{S^2 - \mu R^2} \\ F_c = p_{oil} A_{piston} \end{cases} \qquad (4.4)$$

Going more into depth, we can develop the terms related to resistant wheel forces and analyse successively how the longitudinal wheel forces arise.

The resistance forces are given by the rolling friction arising by wheel motion and the hysteresis phenomena related to rubber compounds. It is computed as a resisting torque as follows:

$$\begin{cases} T_{rolling} = -f_r(v_x, p) R F_z \dfrac{\omega}{|\omega|} \\ R_x = T_{rolling} R_{wheel} \end{cases} \qquad (4.5)$$

The tractive forces generated by the wheel are instead modelled adopting the Pacejka magic formula and describes the relation between the slippage of the tire in the contact patch and the longitudinal force generated.

This is because, for a tire, in order to be able to generate a longitudinal force, slippage is required and without it a tire would not generate any force.

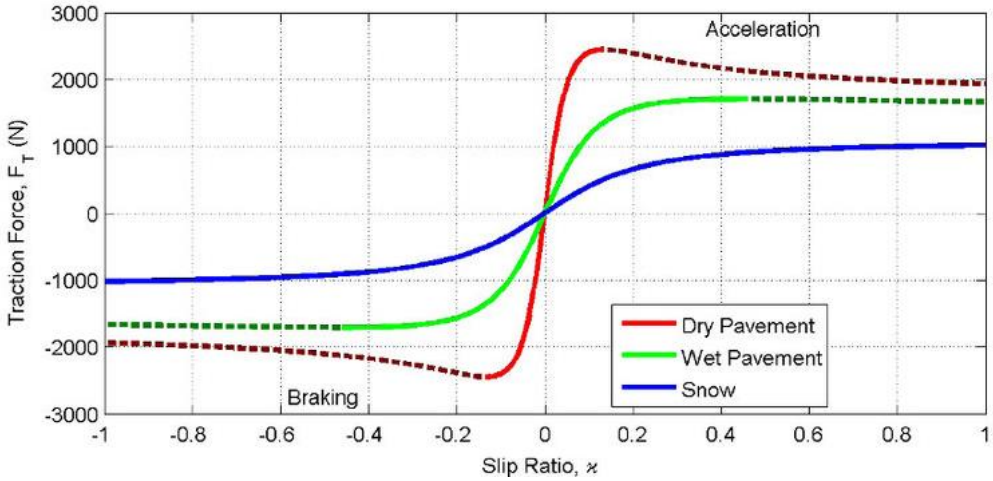

Figure 4.8 Typical tire behaviour in terms of longitudinal force as a function of longitudinal slip.

The expression of the formula is very complex and will not be reported in this text, while the coefficients which have been selected for the Pacejka magic formula are typical ones for a common road vehicle tire.

In the following figure, the selected coefficients are reported.

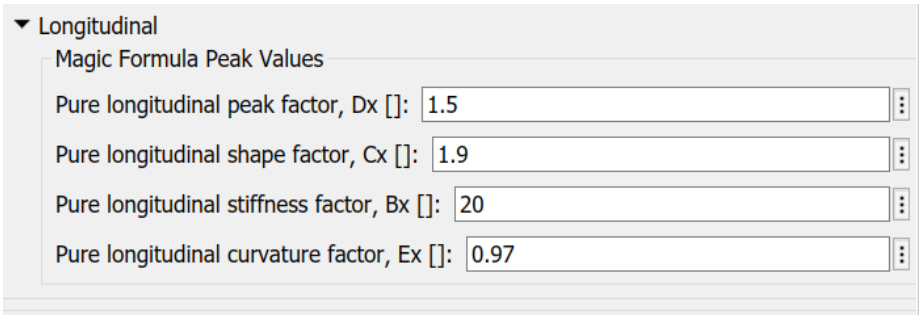

Figure 4.9 Simulink tire block settings of the Pacejka magic formula coefficients

The shape of the tyre characteristic depends strongly on several factors, for example external conditions, air temperature inside and outside of the tyre, internal air pressure, type of compound, damping and stiffness characteristics of the carcass, etc. The typical shape of a tyre characteristic plot presents a first quasi-linear area, for low slippage, until the value of 10%-12% is reached, which is where the maximum longitudinal force is delivered by the tyre. Over that value the dynamic friction coefficient prevails and an asymptotic value of Fx is reached, meaning that the tyre is excessively slipping.

All of the described phenomena are summarized in Simulink in the brake and wheel blocks:

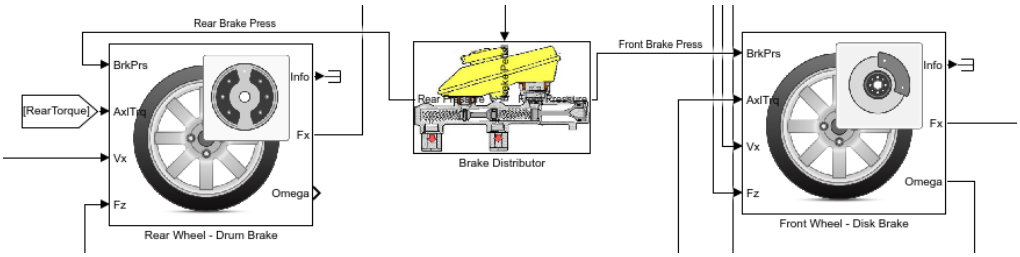

Figure 4.10 Front wheel, rear wheel, and brake distributor block in Simulink

Both wheels receive as input the axle torque, which has been set to zero for the rear wheel, being the vehicle a FWD.

Between the brake pedal and the brake calipers, we find the brake distributor, which is responsible for deviating the correct amount of braking pressure on the front and on the rear ones, following a distributed trend dependant on the longitudinal load transfer. The more the brake pedal is pressed, and the more the braking distribution must be redirected toward the front of the vehicle due to the higher vertical load on the tyres, and thus the higher braking capability. For the sake of simplicity in this model a fixed braking distribution has been adopted, meaning a repartition 70% front and 30% rear in the braking force.

In the following figure the settings adopted in the Simulink blocks are shown.

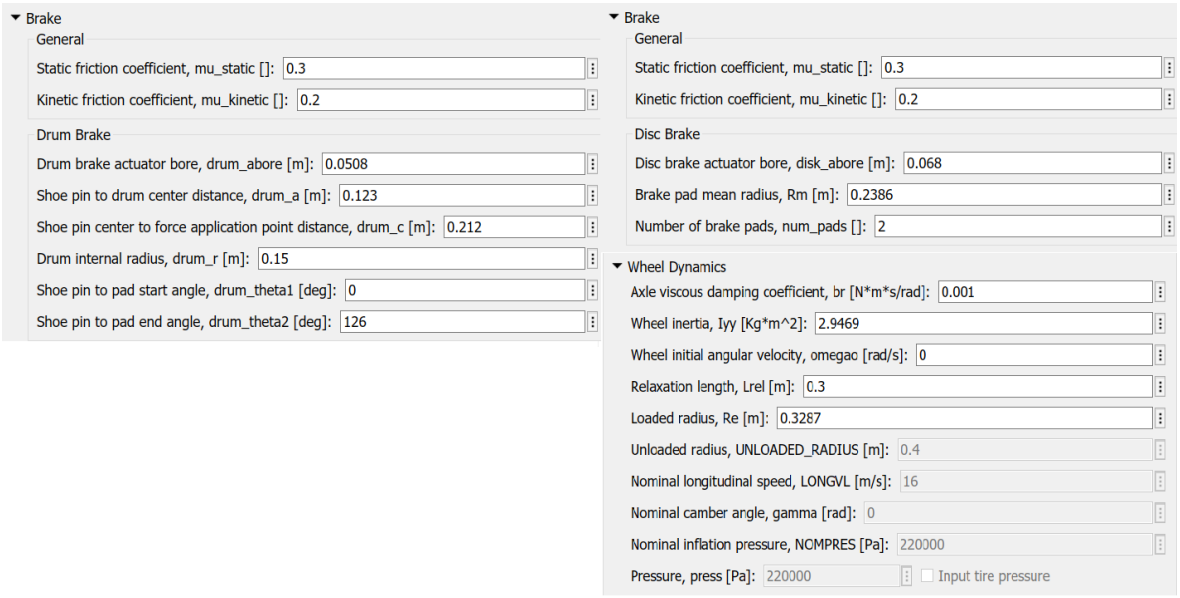

Figure 4.11 Technical data regarding front and rear braking systems, along with dynamical quantities regarding the wheels.

4.2.3 Gearbox

The component responsible of delivering the torque from the engine output shaft to the wheels is the gearbox. The vehicle object of this study is equipped with a manual gearbox, featuring 5 gears plus the reverse gear. Its mechanical function, along the torque transmission one, is the introduction of flexibility in the assembly, meaning that the engine characteristic can be varied depending on the road condition and the driver demand by varying the transmission ration accordingly.

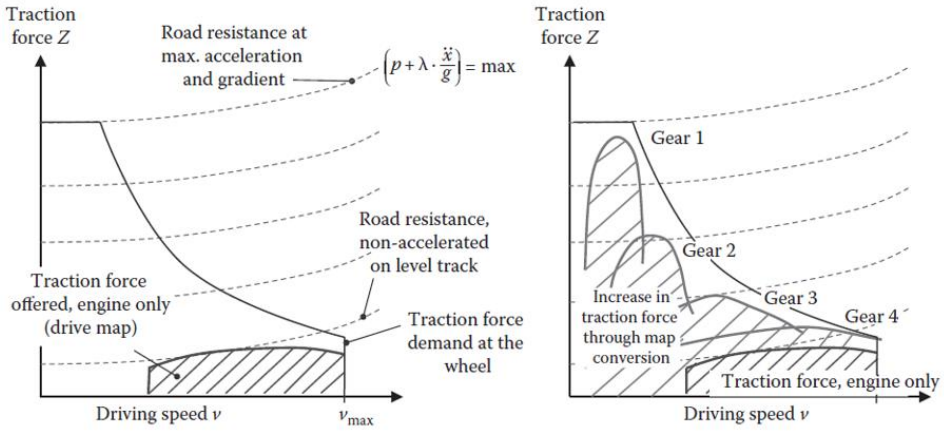

Figure 4.12 Visual representation of the elasticity given by a gearbox to an engine.

As it can be seen in Figure 4.12, a single transmission ratio would make impossible the movement of the vehicle because it cannot even intersect at low velocities the resisting force curve. By instead adopting different reduction gears it is possible to copy at best the resisting force curve, as it is shown on the right graph.

Recalling simple mechanical dynamics concepts [20], the gearbox can be analytically modelled through its characteristic transmission ratios.

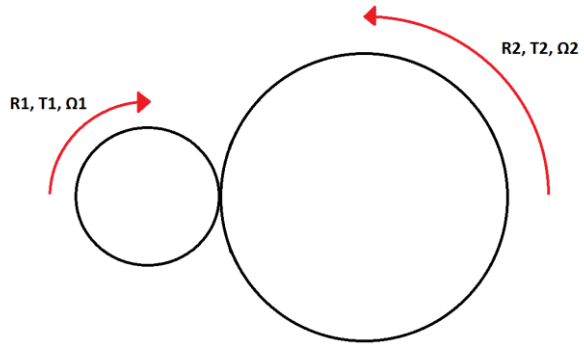

$$\frac{T_1}{T_2} = \frac{\Omega_1}{\Omega_2} = \frac{R_1}{R_2} = \tau \qquad (4.6)$$

Figure 4.13 Mechanical model of two coupled gear wheels

Each couple of gears is described through a transmission coefficient (τ) which correlates the proportionality both between the transmitted torque and the rotational

velocity of the two components. As it can be seen in Figure 4.14, describing mechanically a gearbox of a FWD – front mount car, the gears are mounted on a primary and a secondary shaft and are selected through the movement of dog clutches, which transmits the movement to the external housing of the differential, responsible of distributing accordingly to left and right wheels the driving torque. The differential plays a key role in the lateral dynamics of a vehicle, given that the outer and inner wheel during cornering spin at different rotating speed. As it has been stated before, because in this model uniquely the longitudinal dynamics are considered, the differential has been modelled only as a supplementary reduction gear.

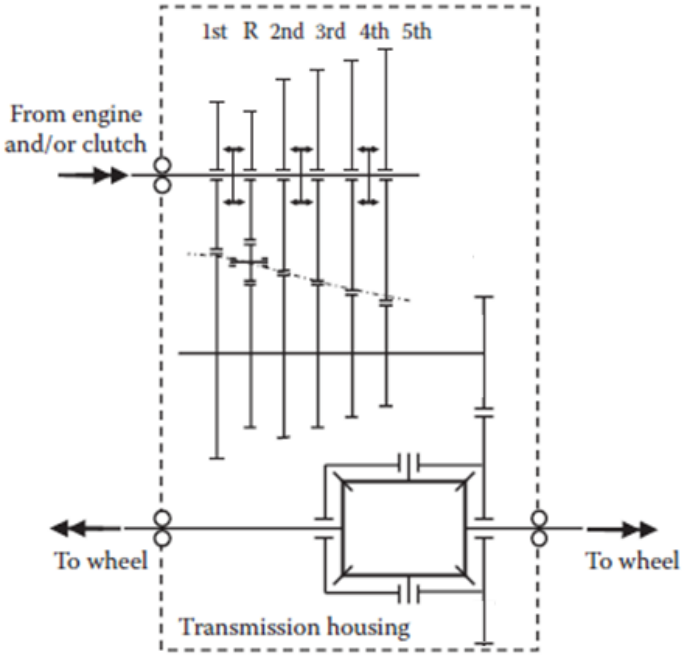

Figure 4.14 Schematization of a gearbox and differential for a front wheel drive car

The selected gear ratios have been taken from the manufacturer declared data sheet for the corresponding vehicle which will adopt this engine. It is typical of car manufacturers to adapt a pre-existing component such as the gearbox to a different

model by varying the final transmission ratio, the differential, rather than redesigning completely the internal geometries of the gearbox.

For this reason, the gear ratios adopted in this model are the ones already equipped in the existing 75kW model, and the differential transmission ratio has been corrected accordingly, by increasing slightly the final ratio to comply with the increased power and torque figures of the engine.

The gear ratios are thus:

τ_1	4.2771
τ_2	2.4237
τ_3	1.7734
τ_4	1.3465
τ_5	1.0852
$\tau_{differential}$	3.562

Table 2 Gear ratios characterizing the Renault Captur gearbox.

In the Simulink environment, this was obtained through a series of multiplications, where the multiplying factors are the gear ratios and the differential gear ratio.

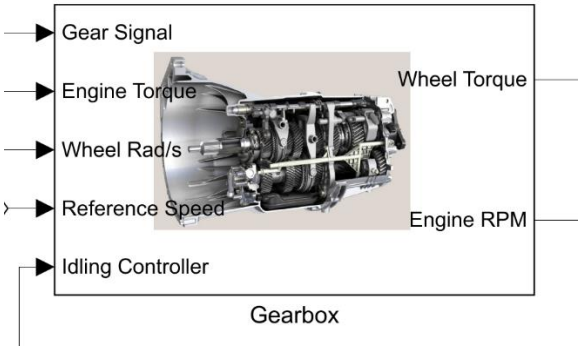

Figure 4.15 Gearbox Simulink block

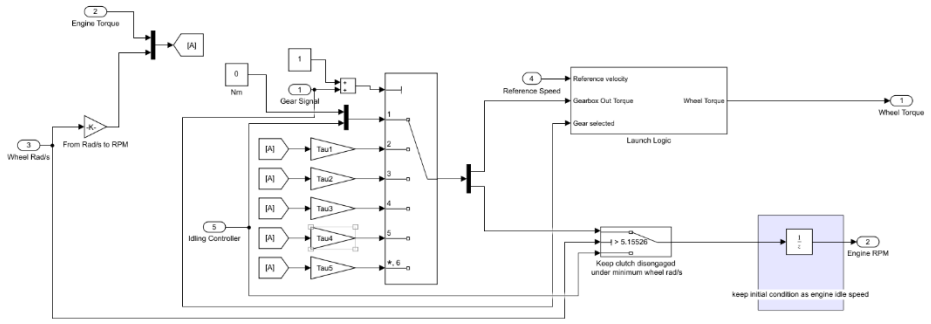

Figure 4.16 General layout of the modelled gearbox, on the left the different selectable gear ratios, on the right logical blocks to model the clutch engagement and disengagement.

In Figure 4.16, the inside of the modelled gearbox can be seen, where the central main switch is responsible of selecting the commanded gear from the driver, which redirects accordingly the engine speed and the engine torque signals, multiplying them by the gear transmission ratio. On the right there are two ulterior subsystems, responsible for the clutch engagement, sending a torque ramp signal to the driving wheels, and the clutch disengagement when the vehicle comes to a stop.

4.2.4 GasDyn S-Function

The Simulink environment also has the possibility to extend its computational domain outside the pre-existing libraries, by interacting with other softwares. This happens by building a so-called S-Function, which is a computer language description used to code a new block, in particular in this case, the engine object of our study. This block is generated directly from the Gasdyn environment and constitutes a complete co-simulation environment.

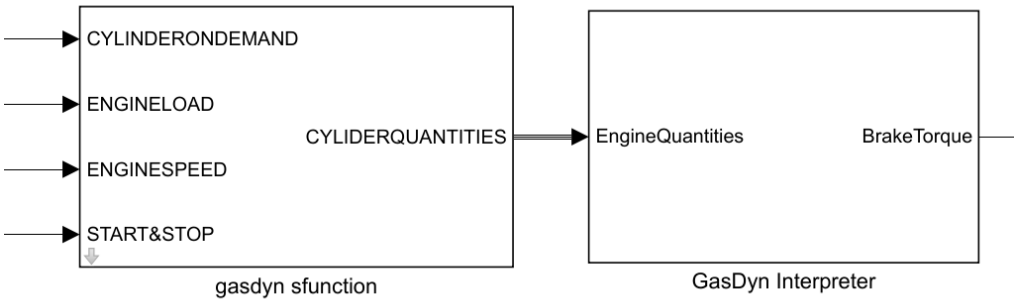

Figure 4.17 GasDyn S-Function block and interpreter to extract data coming from the cosimulation software

4.2.5 Control logics

The Simulink model features also control logic blocks, which are responsible in varying parameters based on several inputs coming from the model itself, in order to copy different demands. The first and most important controller present in the model is the Driver one.

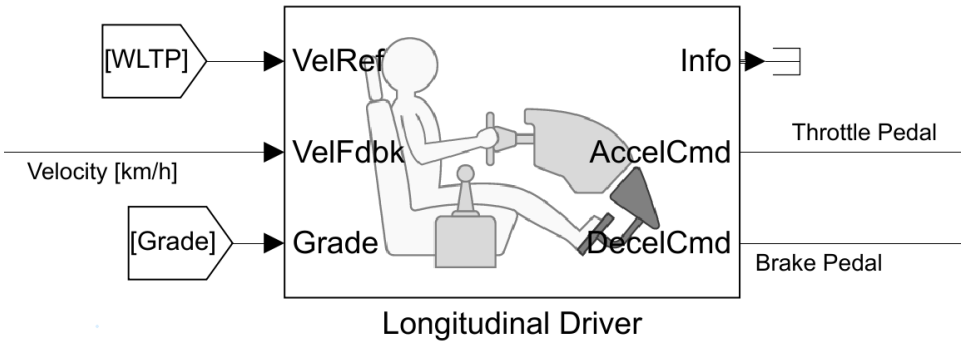

Figure 4.18 Longitudinal driver block, responsible of controlling brake and throttle pedals based on the velocity error.

The driver block is responsible of actuating the virtual brake and throttle pedals, by producing as output a logic signal varying between 0 and 1. This signal is outputted based on the PI Controller law, which receives as input the real longitudinal velocity

of the vehicle from the vehicle body block, it compares it to the reference velocity of the driving cycle, and based on the error it acts on the controlled variables through a proportional, an integral, a feed-forward and an anti-wind up gain. The equation of the controller is the following:

$$y = \frac{K_{ff}}{v_{nom}} v_{ref} + \frac{K_p e_{ref}}{v_{nom}} + \int \left(\frac{K_i e_{ref}}{v_{nom}} + K_{aw} e_{out} \right) dt + K_g \theta \qquad (4.7)$$

- v_{nom} is the vehicle nominal velocity, or the integral mean value of the cycle reference speed in time.
- v_{ref} is the reference speed to be followed.
- $e_{ref} = v_{ref} - v_{vehicle}$ is the velocity error.
- e_{out} is the difference between the output and the saturated value (0, 1).
- θ is the road grade value.
- K_{ff} is the feed-forward gain.
- K_p is the proportional gain.
- K_i is the integral gain.
- K_{aw} is the anti-windup gain.
- K_g is the road grade proportional gain.

The reference velocity input is taken by a dedicated block, in which it is possible to select different in-built driving cycles. For this job the WLTP class 3 cycle was selected.

Figure 4.19 Driving cycle block, which outputs the reference speed to be followed by the vehicle.

All the coefficients written in equation 4.7 have been selected through a first rough approximation based on mechanical system control theories, and successively refined through a trial-and-error process until a satisfying setup was found. In the following figure we report the finally selected coefficients.

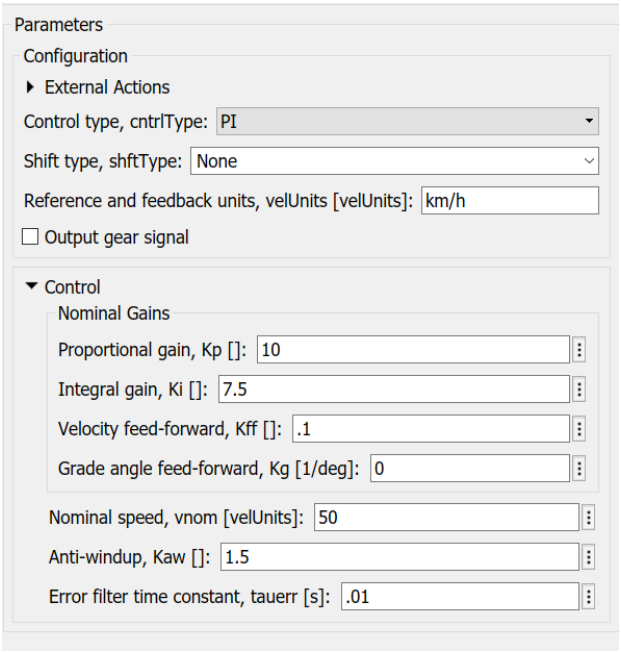

Figure 4.20 Final coefficients for the driver PI controller

Other two controllers are present in the vehicle model. The first one is responsible for sending the gear signal to the gearbox, and it features three different options, a simple gear strategy based only on the vehicle speed, a more evolved one based on speed and throttle position, which creates a 2D map of selectable gears, and finally the prescribed gear sequence from the European WLTP testing procedure.

This freedom of choice is useful to keep ourselves the possibility of implementing a real driving scenario in case of further developments of the model to adapt it to a RDE simulation.

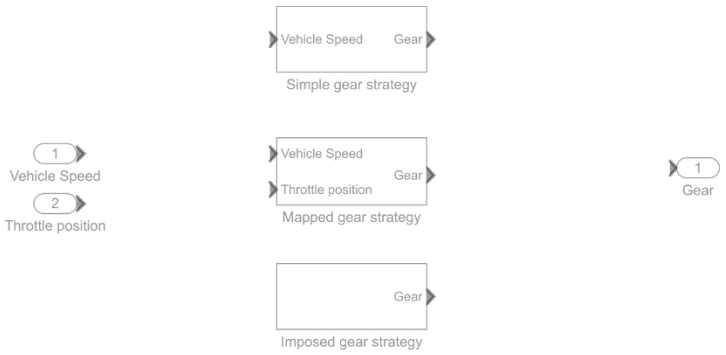

Figure 4.21 Variable subsystem in Simulink, giving the possibility to select the gearshift control logic to be adopted

The gear sequence which was adopted during the WLTP cycle simulation descends directly from the imposed norm regulation by the European Transport committee. It is a gearshift strategy developed through thorough statistical studies of the available car market offer in the present days and varies from vehicle to vehicle depending on several quantities.

The data required to compute this gear succession is:

- P_{rated} which is the maximum rated engine power as declared by the manufacturer.
- s, which is the engine's rated engine speed, point at which the maximum power is developed.
- n_{idle} which is the engine idling speed.

- $n_{\min\ _drive}$ which is the minimum engine speed which the engine can sustain during low load – low speeds operations, for example when driving slowly in traffic in an urban condition. It is determined solving the following equation:

$$n_{\min\ _drive} = n_{idle} + 0.125 \times (s - n_{idle})$$

- ng_{max} which is the number of forward gears installed in the gearbox, in this case 5.
- $i = [1, \dots, ng_{max}]$ as per the vector containing the number of possible selectable gears.
- $ratios = [\tau_1, \tau_2, \tau_3, \tau_4, \tau_5]$, the vector containing all the gear ratios.
- m_{test} which is the test mass of the vehicle.
- f_0, f_1, f_2 which are the road resistance curve coefficients, and depend on the vehicle adopted, the tires equipped, etc.
- The full load power curve of the vehicle.

Based on this data and through trial-and-error procedure, including successive corrections based on the time required to shift, the deceleration-acceleration phase and the engine idling speed, the gearshift sequence is created and is imposed in the model.

Figure 4.22 The final gearshift sequence as per European Committee Norm.

The other controller is the engine control unit, or ECU, which is responsible of selecting the engine strategies and sending the signals to the engine to optimize its operations, implementing for example the start & stop controller. Moreover it features a torque request controller, which is able to translate the throttle pedal position into a torque request for the engine, based on different parameters.

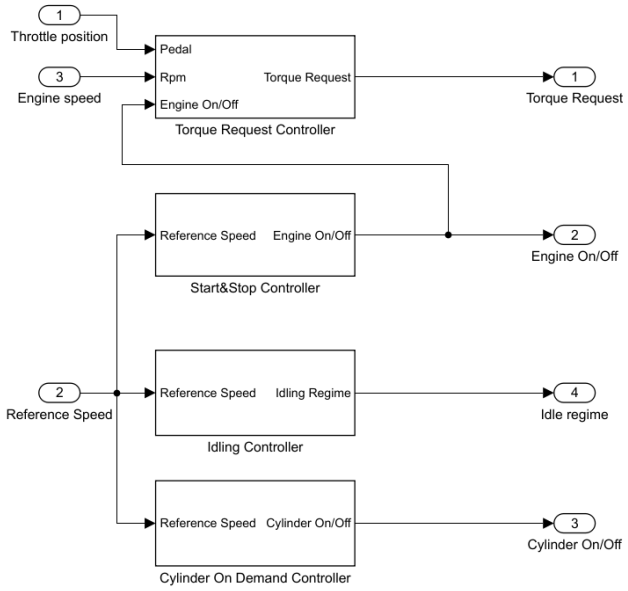

Figure 4.23 Engine control unit blocks, responsible of controlling the engine and its strategies

The first controller developed in this scheme was the torque request one, which based on the throttle position, so the acceleration requested by the driver, and the engine speed at which the engine is, it communicates a requested torque to the GasDyn software, which adapts different internal controllers to satisfy and fulfil the request, powering the vehicle. Based on the two input signals it enters in a table containing at each regime and each load a torque value. This table was obtained by previously simulating a full load and a zero-load engine map, with a sweep between the idling regime and the engine limiter.

Once the full load torque curve and the motored one were obtained, a linear interpolation was used to compute the intermediate loads.

In the following figure the obtained map is shown:

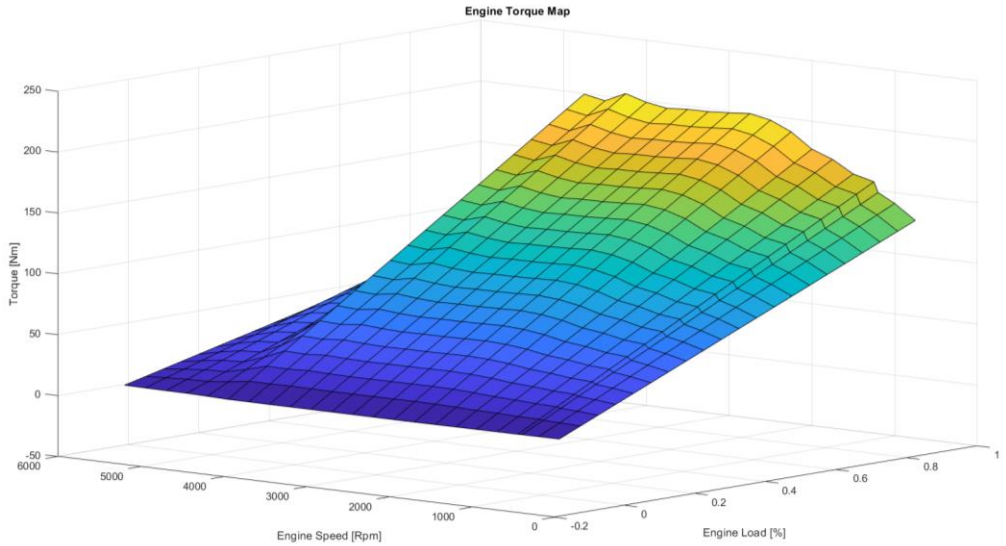

Figure 4.24 Engine torque map adopted for the torque request controller

As it can be seen in proximity of the zero-load area also the torque demand has slightly negative values do to the engine brake that must be generated.

The other controllers are instead responsible of managing the different engine strategies available for this engine.

The start & stop controller is able to detect when the vehicle is in a stand still situation, based on its longitudinal velocity, and it sends a shut-off signal to the engine. This strategy, especially in urban driving conditions where the traffic leads to a continuous driving and stopping situation, is able to reduce the fuel consumption and the overall pollution of the engine.

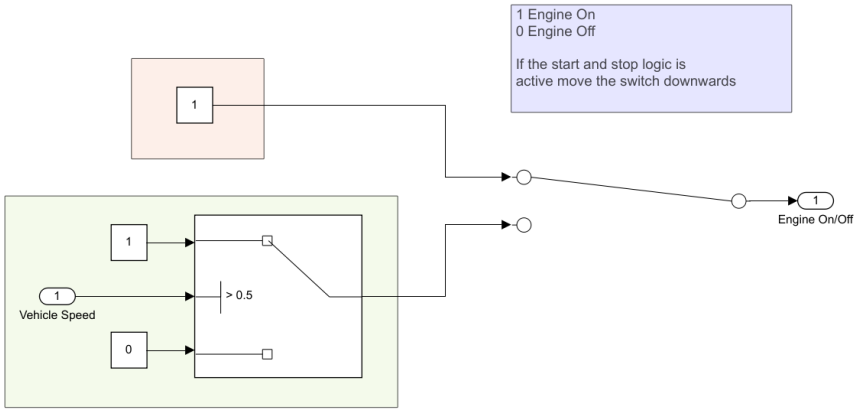

Figure 4.25 Start & Stop controller block layout

The other controller gives the possibility of activating the Cylinder on Demand strategy, which consists of deactivating a cylinder (or more than one, in case of more fractioned engines) in operative conditions where the full displacement and performance of the engine is not needed. For example, it is common in cylinder deactivation strategies to deactivate a cylinder during decelerations or during idling, decreasing once again the overall fuel consumption and pollution.

For this study, we selected a Constant Cylinder Deactivation case, where cylinder number 2 remains deactivated throughout all the operations of the engine.

Chapter 5 WLTP Cycle Simulation

5.1 Base Engine WLTP cycle

In this chapter the results of different vehicle simulations regarding the WLTP cycle will be presented. This cycle is adopted by the European legislation committee to test new vehicle models and grant them homologation in terms of pollutant emissions. It has been developed based on a multi-year statistical analysis of on-road driving conditions, by collecting more than 600’000 km of data. It is carried out in a norm prescribed procedure, where the vehicle undergoes a first break-in phase and is successively left to cool down and reach room temperature for a period up to 36 hours. This is done in order to normalize the most possible the results outcomes between different test centres, vehicle models and conditions. The test bench room is a strictly controlled and climatized ambient, set to be at 296 K in any condition, thus also the initial conditions and environmental conditions have been set accordingly in the simulation models, making as a consequence evident the thermal transient which engine, intake and exhaust ducts and three-way catalyst go through.

The first simulation that was carried out was the full vehicle model equipped with the base Renault engine, which gave the possibility to assess the correctness and well-running of the simulation, along with undergoing a process of trial and error to refine and tune at best the controllers and blocks found inside the Simulink model.

Successively, once the “Base Model” worked in a satisfactory way, two successive engine strategies were tested and compared with the benchmark, in particular the “Start&Stop” strategy, which turns off the engine at prolonged stops, and the “Deactivated Cylinder” strategy, which kept constantly deactivated cylinder number 2 throughout the driving cycle.

5.2 Vehicle dynamics

5.2.1 Vehicle velocity

In this section the results regarding the base engine model will be reported.

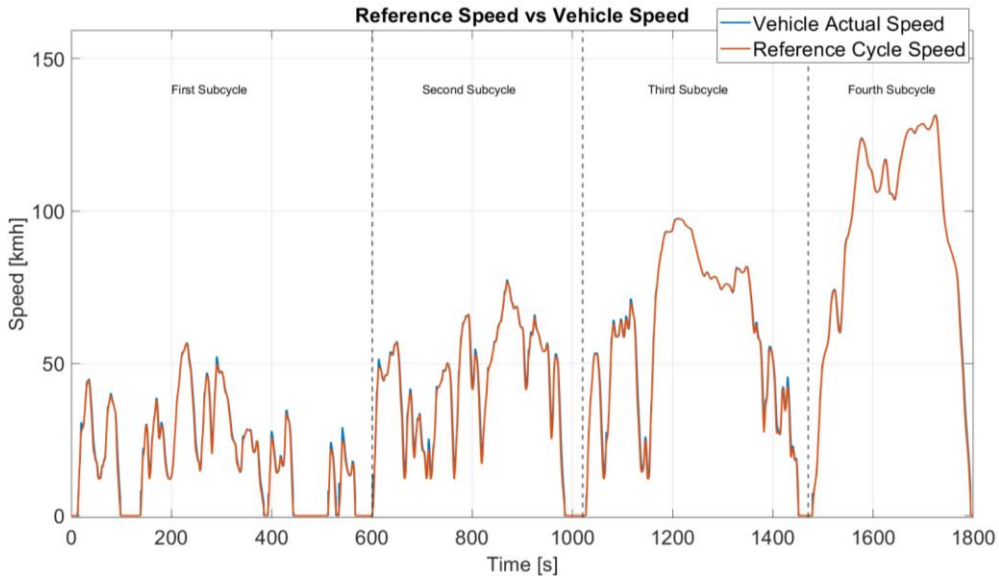

Figure 5.1 Comparison between the reference cycle speed (red) and the actual vehicle speed (blue)

The first result to be analysed is the correct operation of the driver PI controller, responsible of operating on throttle pedal and brake pedal in order to follow at best the reference speed imposed by the driving cycle norm. As it can be seen in Figure 5.1, and successively in a more detailed view in Figure 5.2, Figure 5.3, Figure 5.4

and Figure 5.5, the reference is well copied by the vehicle, leading to a maximum error of $+5\,km/h$ in the most overshooting areas, typically during the first two sub cycles. This can already be deemed as a satisfactory and correct result, as it complies with the prescribed speed tolerances in the homologation procedures, but the driver's behaviour can be ulteriorly improved by adopting a scheduled PI strategy or a PI controller with varying coefficients as a function of the vehicle speed.

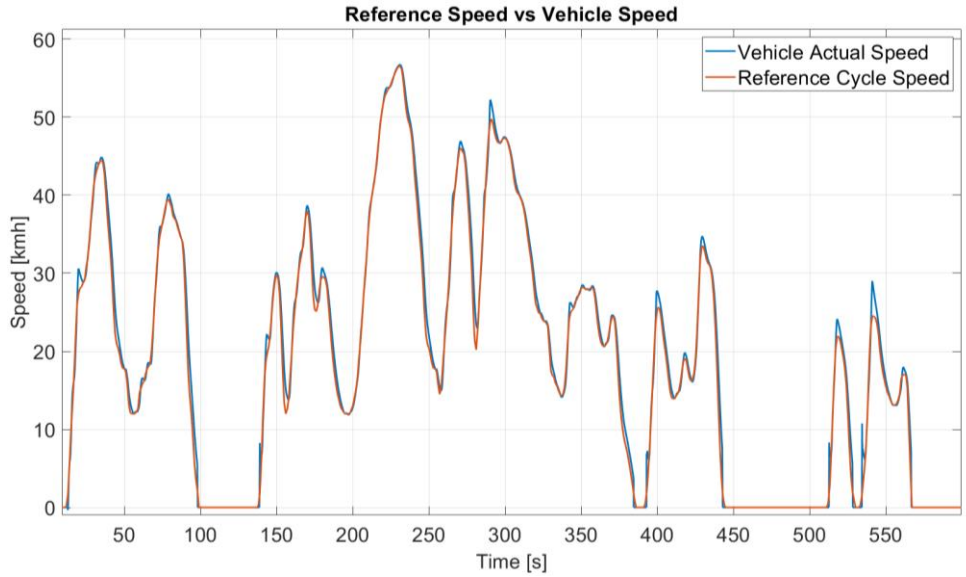

Figure 5.2 First driving sub-cycle detail.

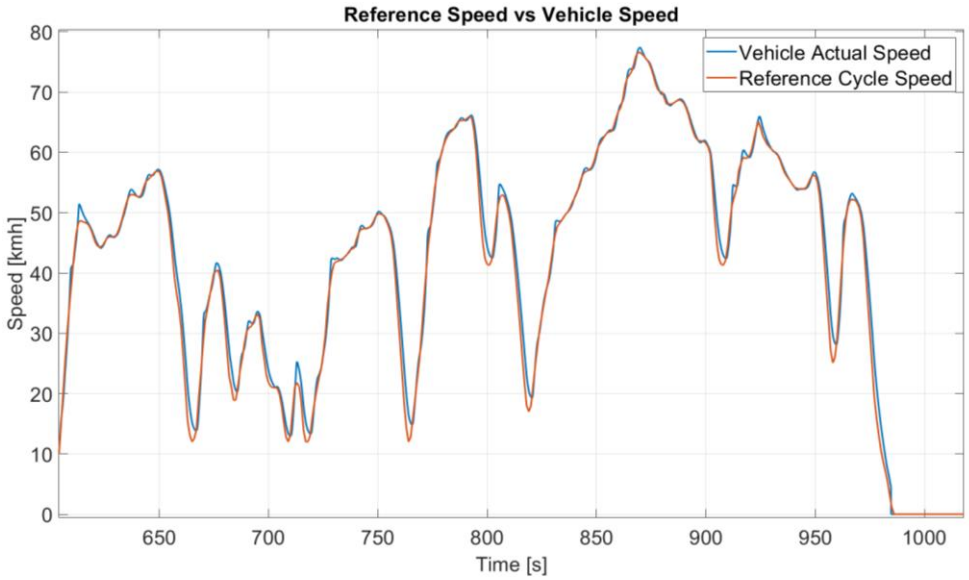

Figure 5.3 Second driving sub-cycle detail.

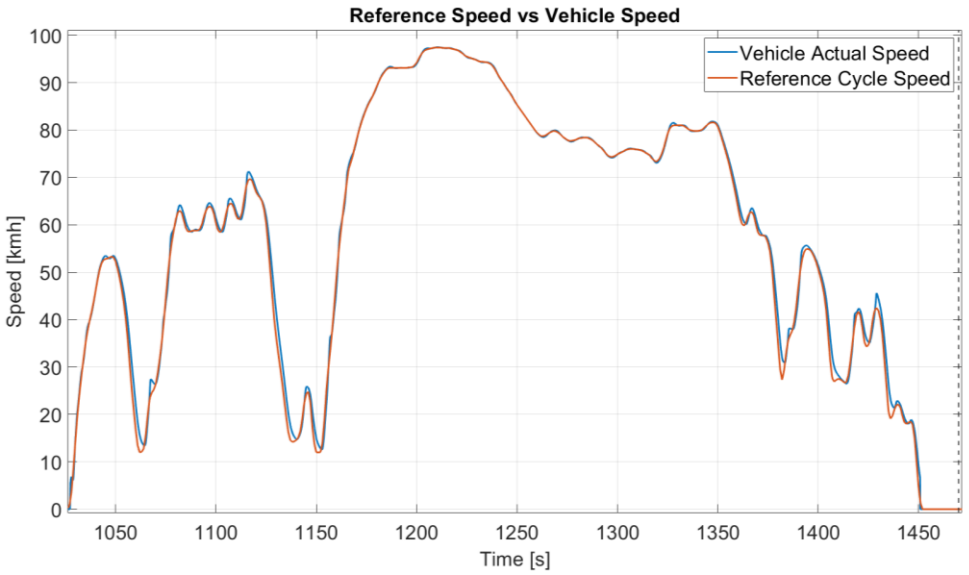

Figure 5.4 Third driving sub-cycle detail.

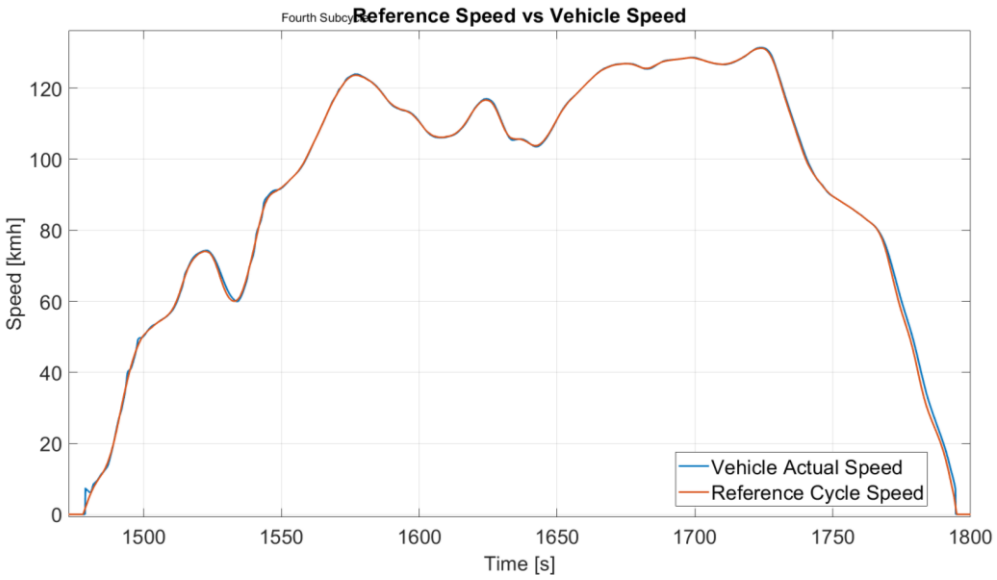

Figure 5.5 Fourth driving sub-cycle detail.

5.2.2 Torque request

Along with the correct operation of the driver controller which allows the vehicle to follow at best the velocity path prescribed, also the internal GasDyn controllers must be verified, in particular the internal throttle, wastegate and intercooler PIDs. These controllers co-operate in order to ensure that the torque requested by the engine control unit is fulfilled correctly, by setting the correct throttle angle and the correct wastegate opening to ensure the desired amount of boost pressure and thus BMEP is generated.

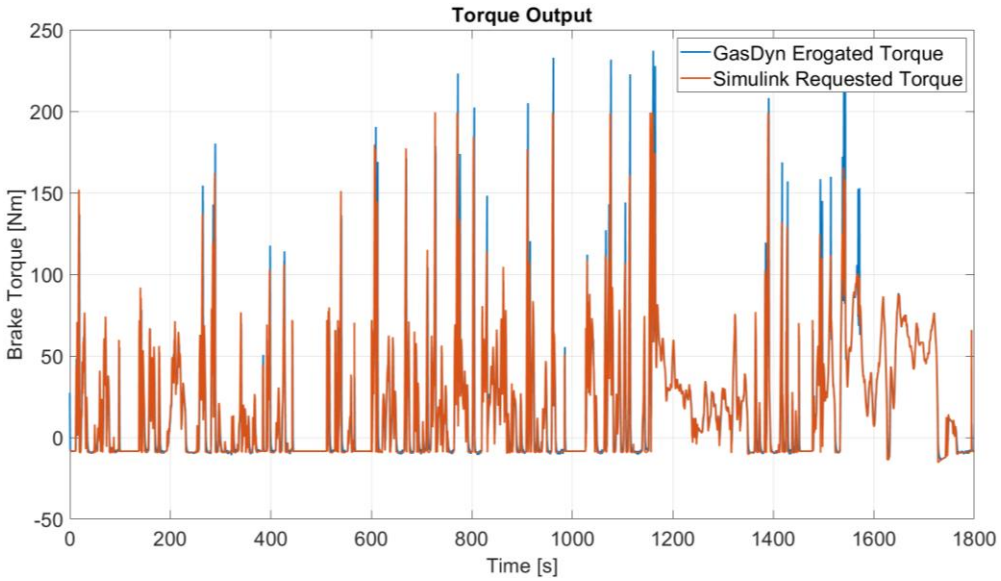

Figure 5.6 Torque requested by Simulink compared to the torque erogated by the GasDyn engine model

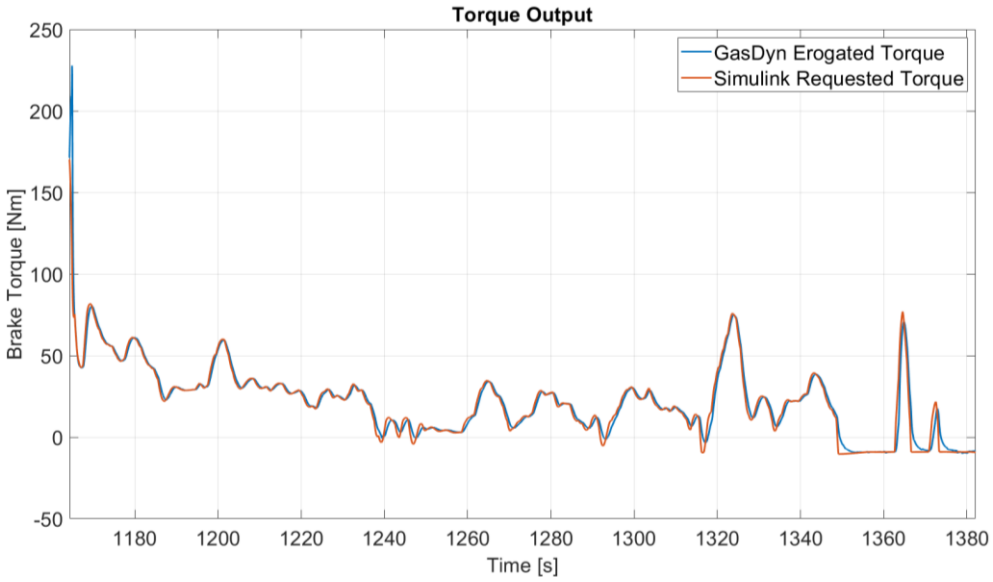

Figure 5.7 A more detailed view of the previous graph

As we can see in Figure 5.6 and more in detail in Figure 5.7, the torque request is well fulfilled by the outputted torque from the GasDyn software, meaning that the internal controllers are tuned well and work correctly.

5.2.3 Engine operating points

As shown at first in figure 5.6, and in a more detailed way in figure 5.7, the torque request and the generated torque have quite similar trends, exception made for some instantaneous overshoots which do not affect in any way the vehicle dynamics, being filtered by the dynamics of the system. This leads us to state that the internal GasDyn controllers work in a proper way. There is still room for improvement, because to have a steadier response from the engine and avoid torque overshoots, the internal controllers of the engine model can benefit from a finer tuning to the expense of a heavier and longer computational time.

Regarding the driving cycle we can analyse the area of an engine map in which the operative points are, dividing the analysis for the four different sub-cycles.

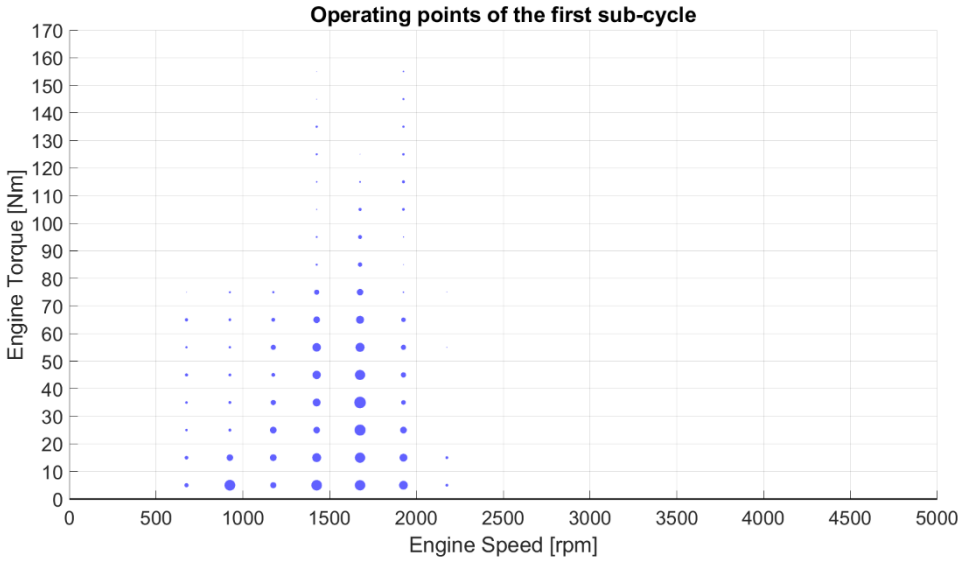

Figure 5.8 First sub-cycle operative points cloud

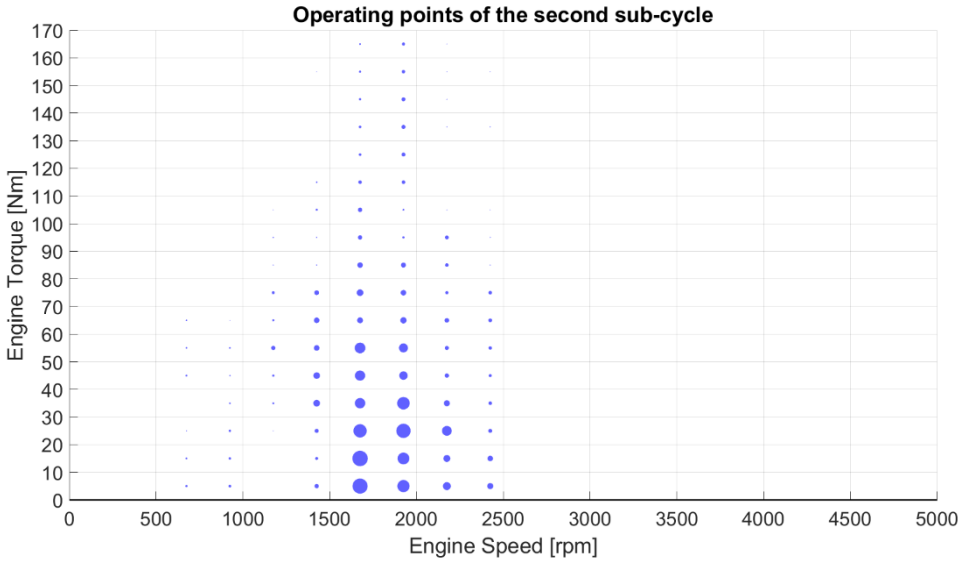

Figure 5.9 Second sub-cycle operative points cloud

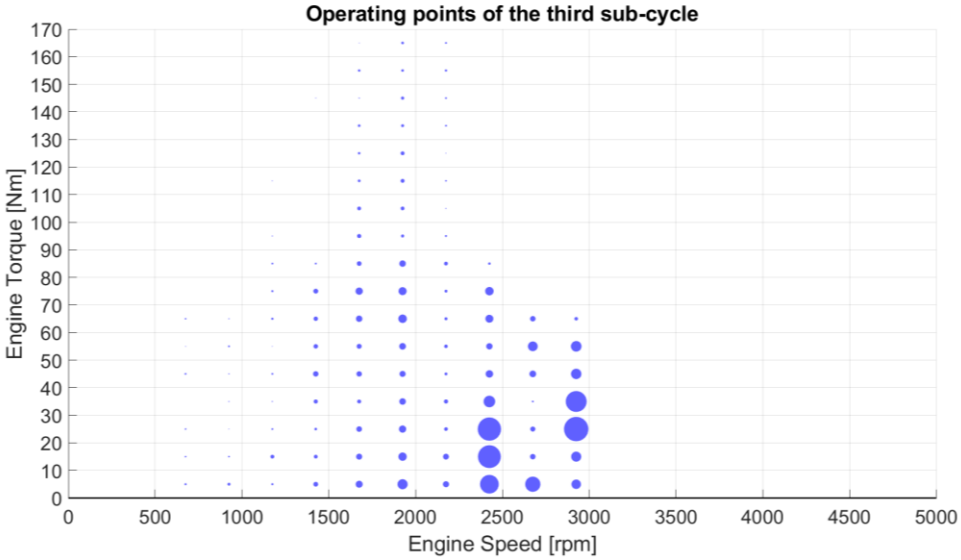

Figure 5.10 Third sub-cycle operative points cloud

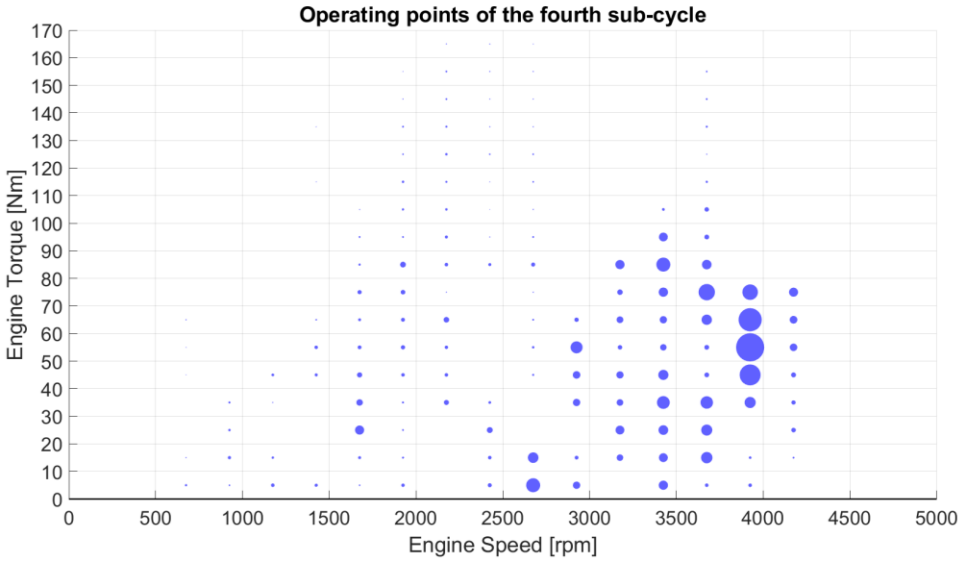

Figure 5.11 Fourth sub-cycle operative points cloud

In the first two sub-cycles, displayed in Figure 5.8 and Figure 5.9, we can see how the engine is kept under 2000 rpm and the area with a higher density of operative points is contained under the 50% load line. This shows how the first two sub-cycles

of the WLTP test are meant to test the slow driving and urban conditions, characterized by low accelerations and decelerations, with a maximum speed of 50 km/h for the first and 70 km/ for the second part. Moving instead onto the successive plots, in figure 5.10 the third sub-cycle is displayed, showing evidently how now the engine speeds used start becoming higher along with the loads, because this section is the one characterized by the strongest acceleration and deceleration values.

Finally, the fourth sub-cycle shown in Figure 5.11 aims to reproduce extra-urban driving conditions, for example on a highway, so the engine speeds are higher due to the higher vehicle speeds reached, but being the accelerations lower the load request is generally more contained.

5.2.4 Engine air-to-fuel ratio

Passing onto inspecting engine related quantities we can analyse the operative points that the engine passes through in terms of Air-To-Fuel ratio.

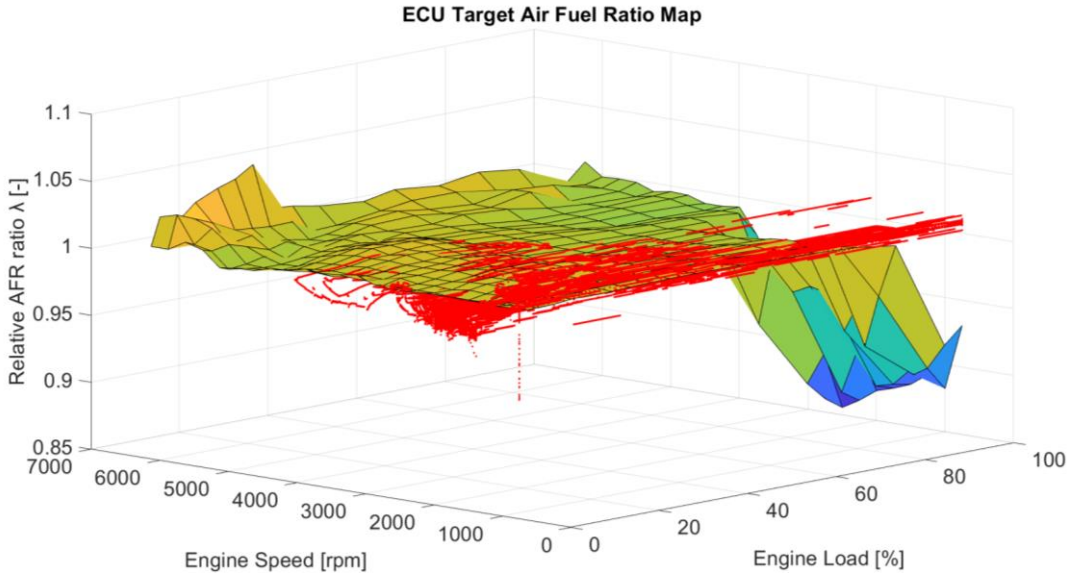

Figure 5.12 Engine fuel map compared to the effective AFR ratio during the driving cycle.

In Figure 5.12 the engine fuel map, which is the target relative AFR for every engine speed and load, is displayed along with the effective AFR obtained during the driving cycle. We can observe how the absolute error is contained throughout all the cycle in 0.03, which means that the controller is finely tuned. We can highlight two main areas which deviate from the prescribed values. On the right of the map, where the engine rpm is around the idling regime, a leaner operating condition is met, which can be explained as when the vehicle is starting from a stand-still condition or during a sudden and abrupt peak in torque request, and the GasDyn controllers undergo a transient during which the throttle opens before the correct fuel amount can be injected, thus creating a slightly lean operating condition. With the same principle, on the left of the map we can highlight an area which is richer than the objective AFR at a higher regime and in a zero-load condition. This can be identified when the torque request rapidly goes to zero, for example during decelerations, in which the throttle valve closes quickly and reduces the inducted air in the engine.

5.3 Fuel consumption and pollutant emissions

5.3.1 Fuel consumption

An important aspect when simulating driving cycles with a complete vehicle is the fuel consumption, especially in recent years when the struggle to reduce pollutants has become significant.

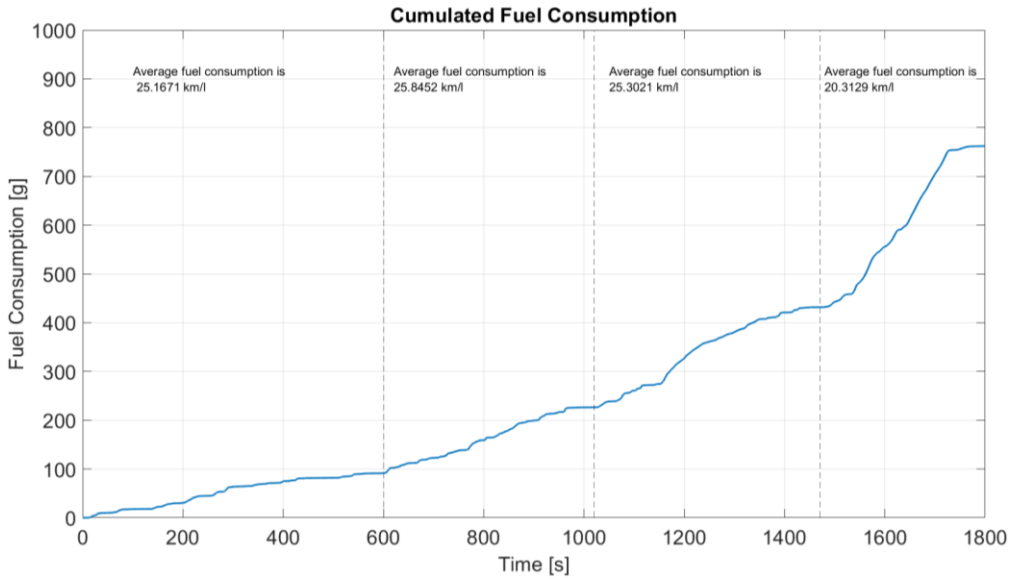

Figure 5.13 Cumulated fuel consumption trend, with the average consumption divided for the four sub-cycles

We can observe how in the first three sub-cycles, which represent an urban driving condition with only in the third part an extra-urban condition, the average consumption is stable around the 25.5 km/l figure, while only in the fourth sub-cycle thus the highway driving simulation the fuel consumption is increased up to reaching a value of 20.3 km/l, due to the higher speeds reached and the increase in torque request. This sums up to a total fuel consumption during the cycle of 22.3 km/l. This result can be considered as an underestimation of the real value of fuel consumption also by comparing it with vehicles of the same category and can be explained with an underestimation of the real condition rolling resistance and aerodynamic resistance coefficients, or by an overestimation in efficiency of the engine combustion process.

5.3.2 CO2 emissions

Directly following the analysis of fuel consumption we can pass onto the pollutant emissions one, being the two strictly related, beginning from the CO2.

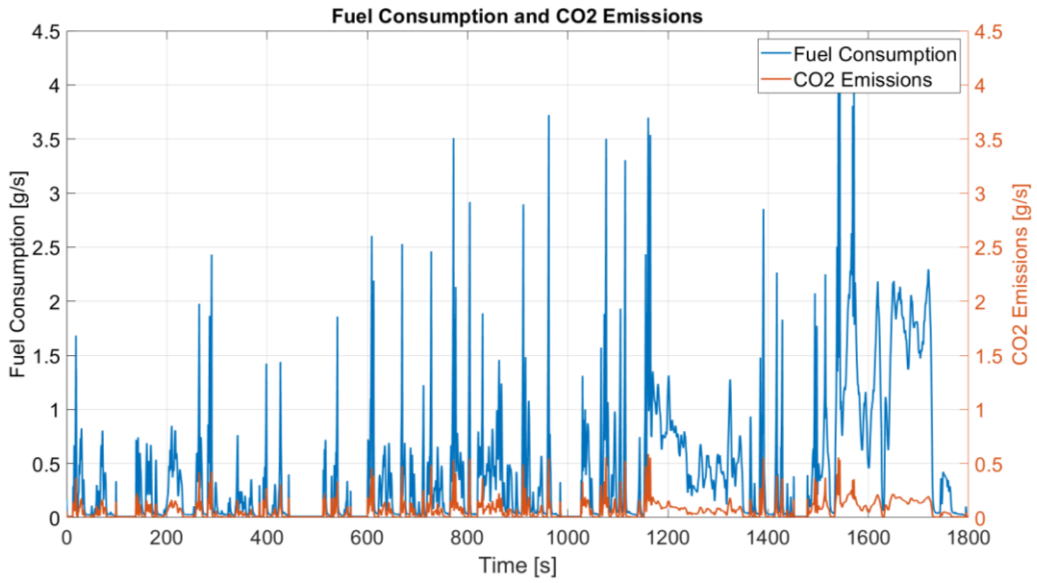

Figure 5.14 Instantaneous CO2 emissions in g/s compared to fuel consumption

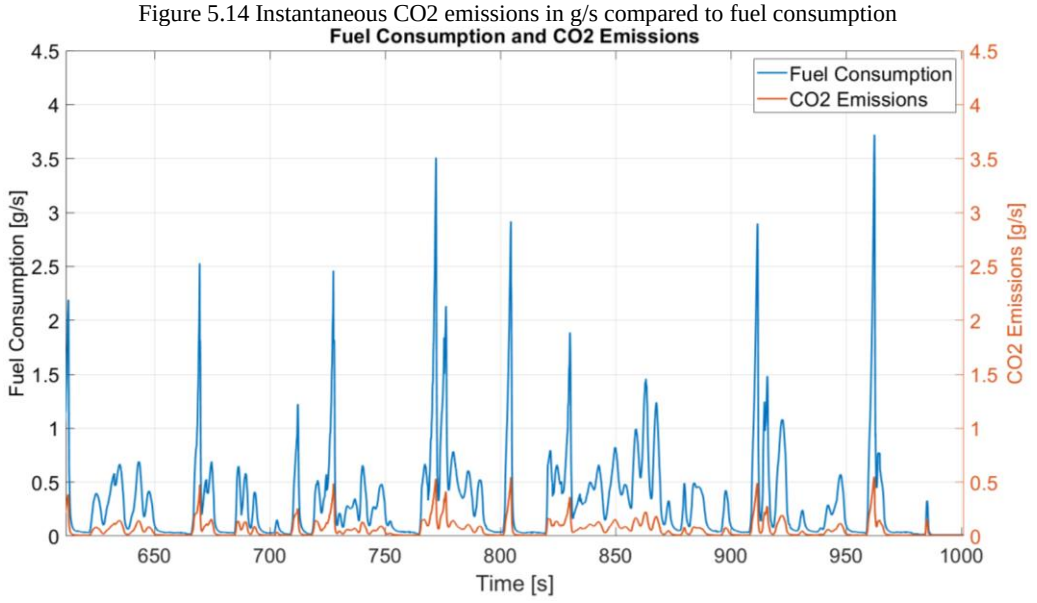

Figure 5.15 Detailed view of CO2 and fuel consumption comparison

In Figure 5.14 and in a more detailed view also in Figure 5.15 we can see the instantaneous fuel consumption expressed in grams per second (g/s), which exhibits a monotonically growing trend between the different subsections of the driving cycle as expected. The fuel consumption plot is also overlapped by the instantaneous CO2 emissions of the engine, and as expected the two quantities have a strict correlation and a comparable trend.

The visible peaks in the instantaneous emissions plot correspond directly to a sudden increase in torque demand by the driver during acceleration phases.

5.3.3 CO, HC, and NOx Emissions

The three main pollutants which are analysed during the Euro homologation procedure are carbon monoxide (CO), unburnt hydrocarbons (HC) and nitrous oxides (NOx). They are sampled constantly during the driving cycle and diluted in a precise quantity in order to be stored in calibrated bags. This allows to create a sort of moving average throughout the entire duration of the test and obtain a mean value of the emissions to be compared to the prescribed limits. It must be specified that for this study, the considered emissions are to be referred directly to the in-cylinder quantities, and not the tailpipe emissions, thus a comparison with the actual European legislation limits would not make sense and will not be reported.

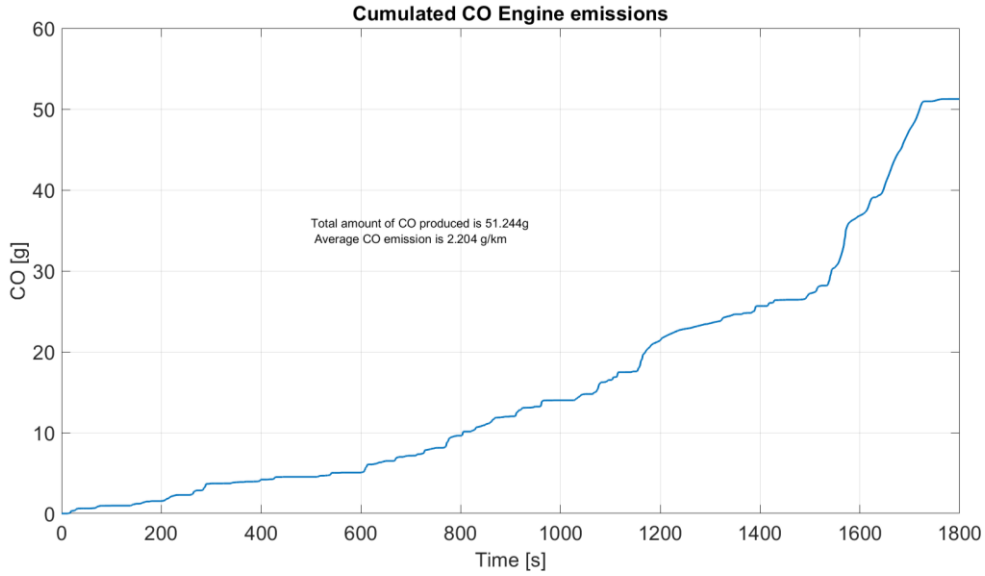

Figure 5.16 Cumulated CO emissions

In Figure 5.16 we can see the cumulated trend for CO emission, which correctly resembles the trend of fuel consumption and torque request in terms of monotony and successive increase throughout the four sub-cycles.

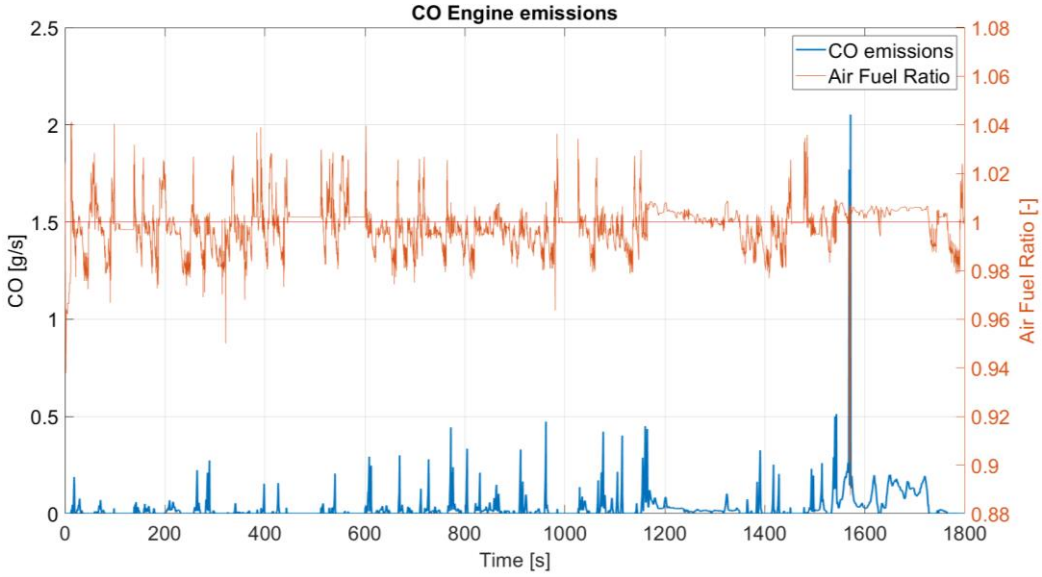

Figure 5.17 Overview on the instantaneous CO emissions, compared to the instantaneous air-to-fuel ratio

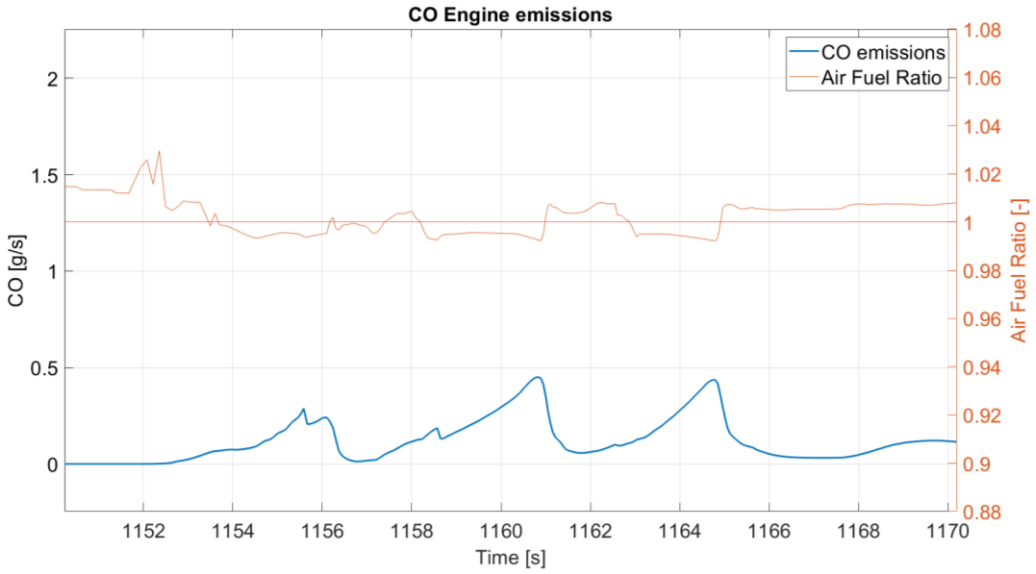

Figure 5.18 Zoom on the comparison between CO emissions and AFR

In figure 5.17 and 5.18 a comparison between the instantaneous emissions of CO and the engine relative AFR can be seen.

As expected, when the AFR decreases reaching a value under 1, meaning that the engine is working in a slightly rich condition, the CO is emitted in a more consistent way, as it is evident from the three successive peaks in figure 5.18 which correspond directly to the three depressions in the red AFR line.

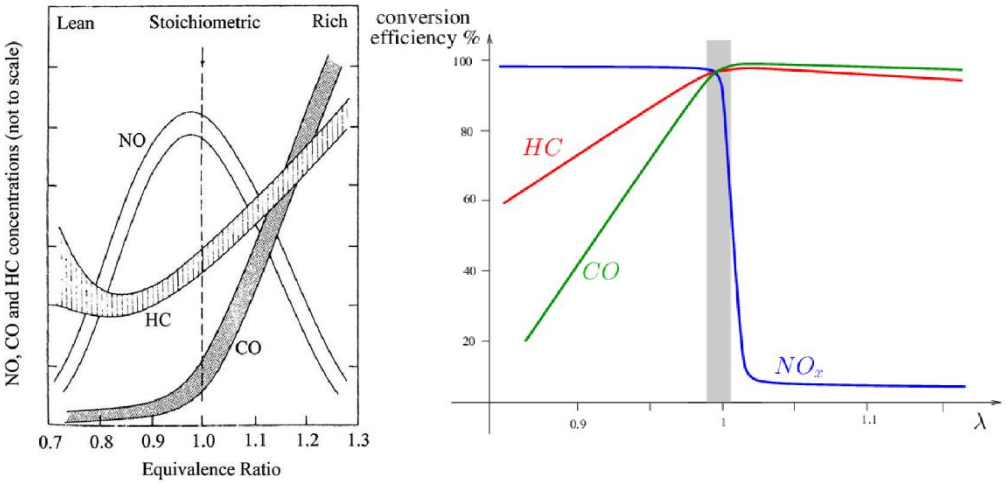

Figure 5.19 On the left, the emission of pollutants as a function of equivalence ratio, on the right the TWC conversion efficiency as a function of equivalence ratio.

This connection between AFR and emissions can be seen in figure 5.19, where the graph on the left shows how for CO the emission is more consistent in richer operating conditions, similarly to HC, while for NOx the trend is opposite because it is emitted mostly in slightly lean operating conditions. The air fuel ratio is not only important to contain a priori the pollutants formation inside the combustion chamber, but it is also critical when considering the tailpipe emissions and the conversion efficiency of a Three-Way-Catalyst, because as it is shown on the right of figure 5.19 the more the AFR is distant from a stoichiometric condition ($\lambda = 1$) the less it is efficient in converting either the lean or the rich derived products of combustion [6].

x

Another pollutant to be analysed during the testing procedures is the unburnt hydrocarbons (HC).

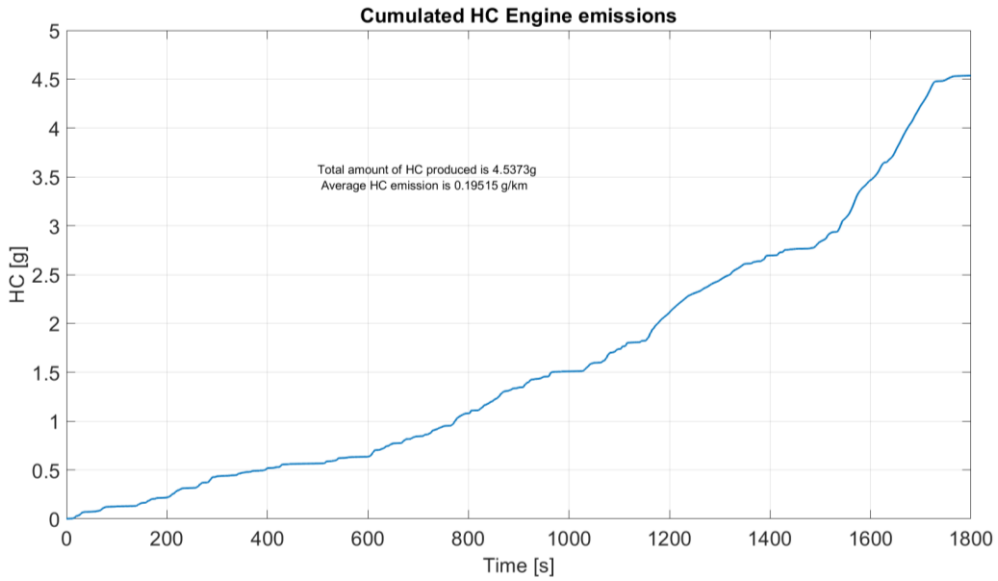

Figure 5.20 Cumulated HC emissions

Once again, the displayed trend corresponds to the four sub-cycles.

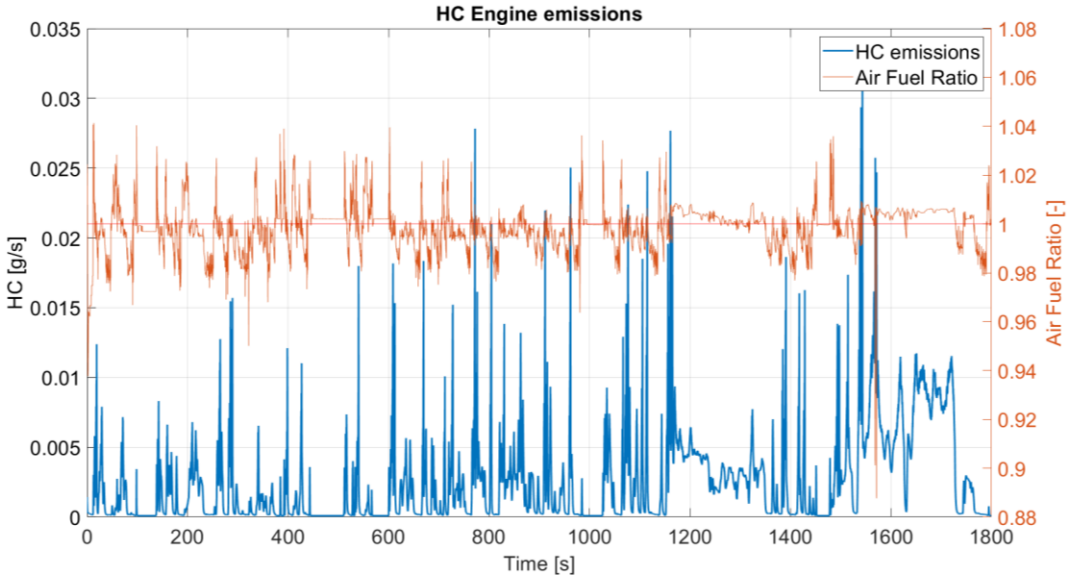

Figure 5.21 Instantaneous HC emissions compared with instantaneous AFR.

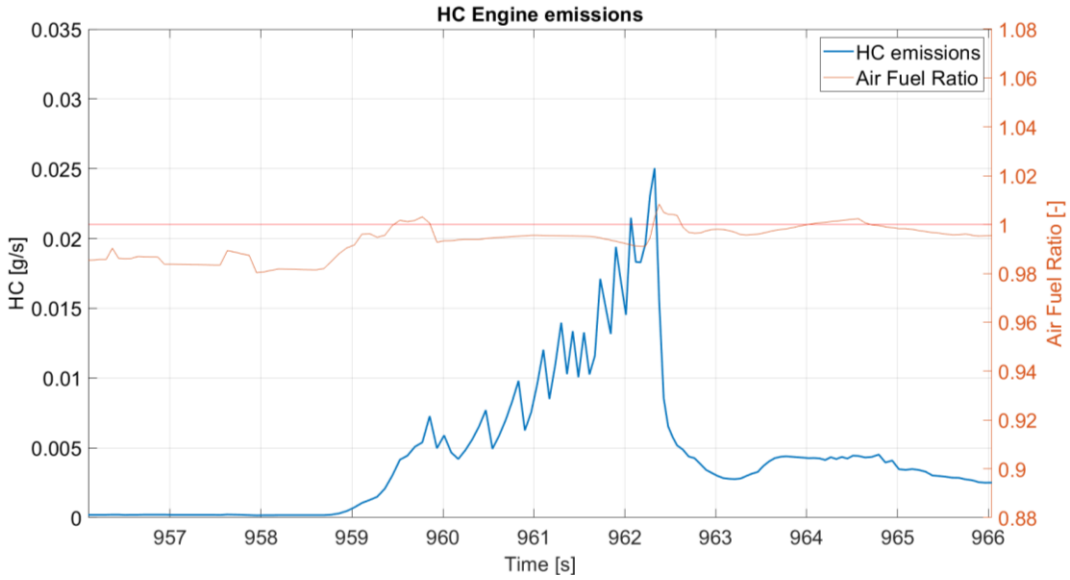

Figure 5.22 Detailed view of HC emissions versus AFR

Also in this case, in figure 5.22 we can see how when the operating conditions of the engine drift towards a richer area the HC emissions spike and increase.

Finally, let us pass onto showing the NOx emissions.

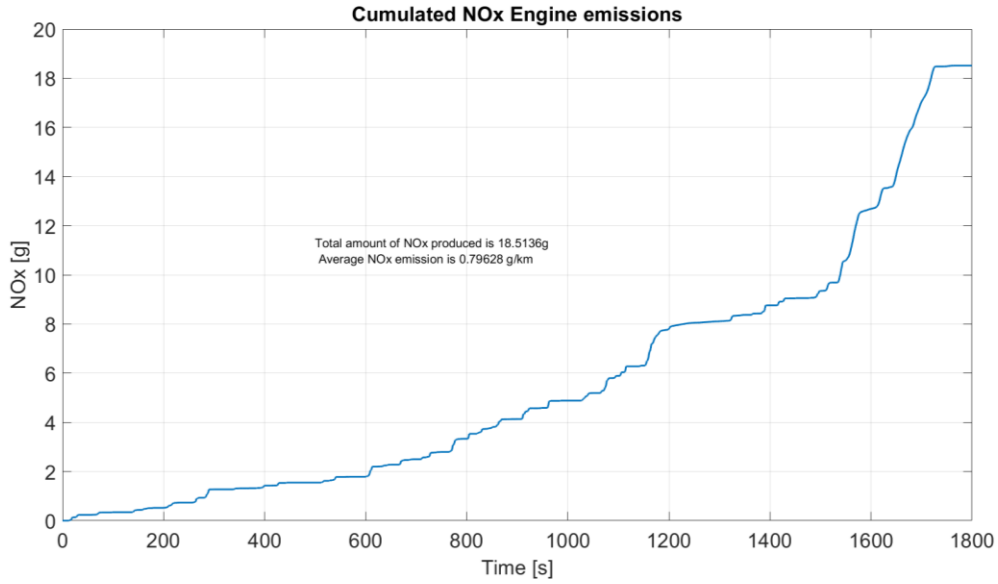

Figure 5.23 Cumulated NOx emissions.

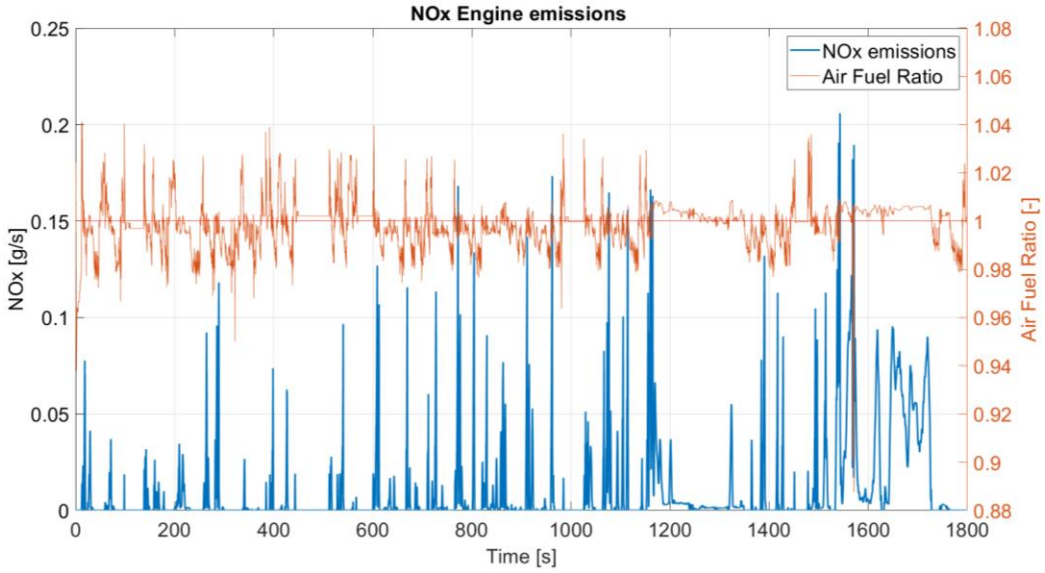

Figure 5.24 Overview on instantaneous NOx emissions and engine AFR

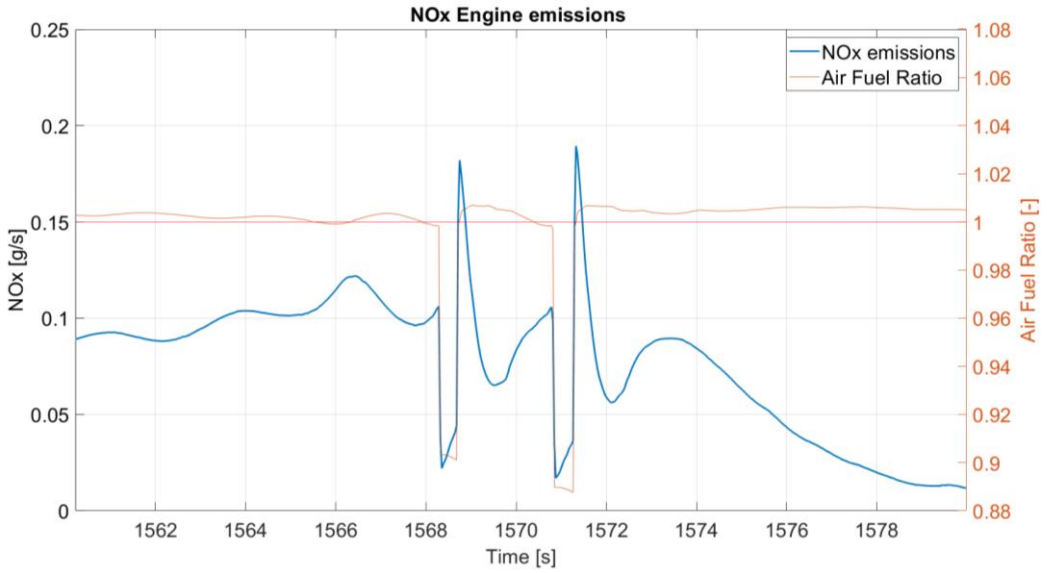

Figure 5.25 Detailed view of NOx emissions compared to engine AFR

As it is displayed in figure 5.25, in this case the behaviour of pollutant emissions is opposite compared to the two previous ones. When the engine finds itself in a richer operating condition, which is described by the two downward peaks in red, the NOx emissions instantly decrease, and only when the AFR goes back up to around 1.01, corresponding to slightly lean operations, the emissions have a positive peak.

5.4 Engine temperatures

An interesting aspect when considering homologation cycles simulations is the evolution of temperatures in the engine intake and exhaust systems.

When speaking about temperatures along the intake side of the engine, they can be considered as a vital and fundamental parameter determining engine performance and pollutant emissions. For example, in turbocharged engines especially, having the control over the evolution of inducted

Inspecting the temperature gradient inside the catalyst during the warm up procedure can be considered as fundamental given that to have the best attainable conversion efficiency, modern three-way catalyst converters must operate in a range between 500 K and 700 K.

It is especially for this reason that on recent models, car manufacturers have adopted a split catalyst philosophy, with a first smaller one placed near the engine in order to heat up quickly and begin reducing pollutant emissions as soon as possible, coupled then with a secondary converter more distant from the engine head. In the engine object of this study, a more conventional layout was adopted with only one main catalytic element placed after the turbine.

The European testing procedure imposes that vehicles, when being tested for homologations, must undergo first a so-called “pre-conditioning” phase in which the engine and all fluids are brought up to exercise temperature and successively let cool down naturally for a period up to 36 hours in a controlled room set at 296K, thus the following figures must be analysed considering that the initial temperature of all the engine components corresponds to the test room temperature [3].

5.4.1 Turbine temperatures

In the following section we present the temperatures before and after the turbine.

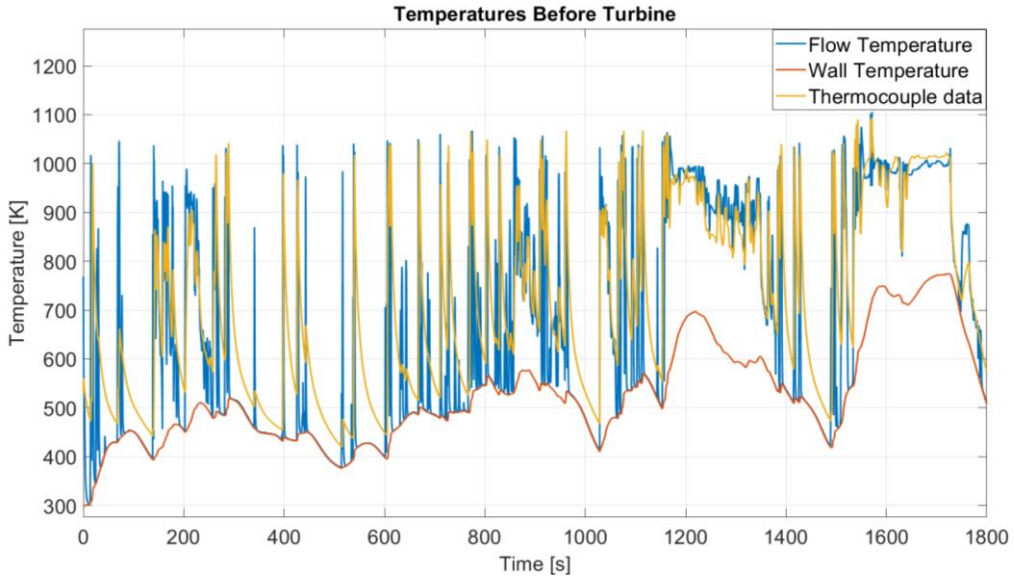

Figure 5.26 Temperatures before the turbine inlet of flow, wall and the reading a thermocouple would produce.

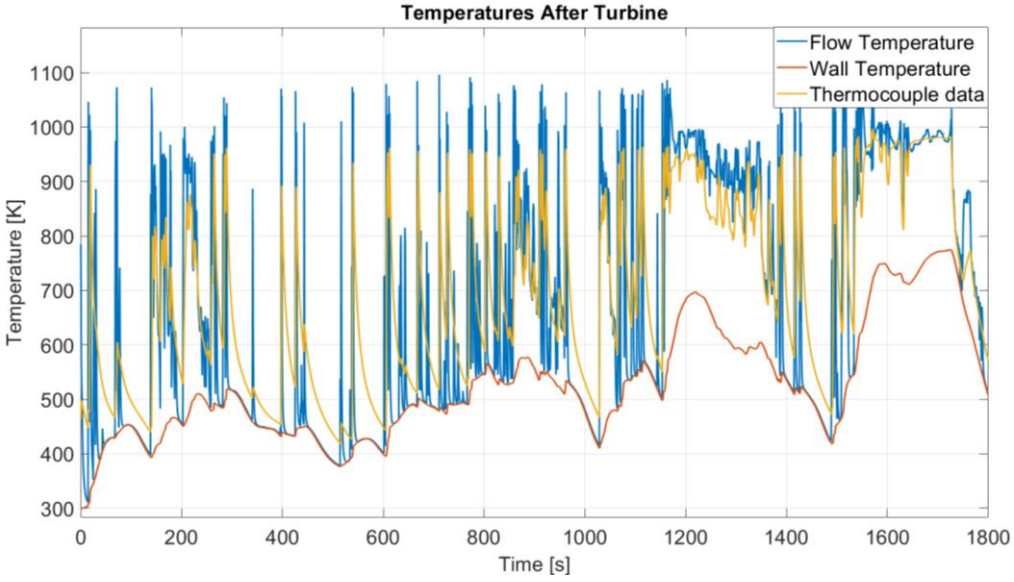

Figure 5.27 Temperatures after the turbine outlet of flow, walls and the reading a thermocouple would produce.

By observing figure 5.26 and 5.27, regarding the wall temperature there is no substantial difference between turbine inlet and outlet, being these two locations very close to each other and sharing the same duct wall, the turbine housing. The trend well copies a real-world situation, in which during accelerations and when the engine torque demand is rising, the temperatures in the exhaust duct begin increasing, while when decelerating the temperatures slowly decrease.

Regarding the flow, as expected, the temperature before entering the turbine blades is always higher than on the outlet side, and we can appreciate the thermal transient by observing the yellow line on these figures. For example, between the 400 and 600 seconds marks, the cycle exhibits a period of time where the vehicle is stopped and remains idling, and this can be clearly seen from the descending thermal transients of the thermocouple data.

5.4.2 Catalyst temperatures

Carrying on with analysing the temperature trends in the exhaust side, let us see the evolution of temperatures inside the catalyst.

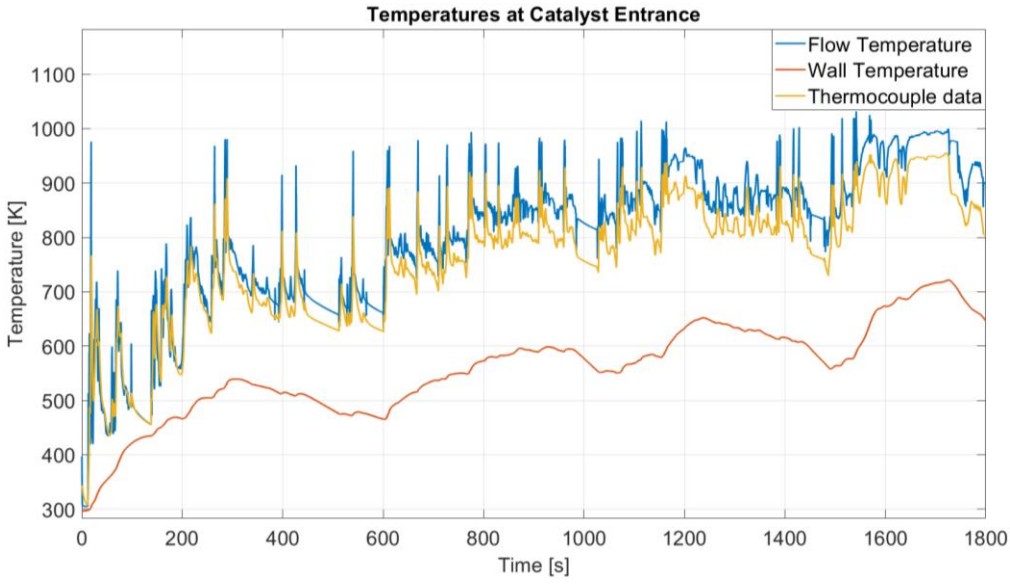

Figure 5.28 Temperatures before entering the catalyst of flow, walls and the reading a thermocouple would produce.

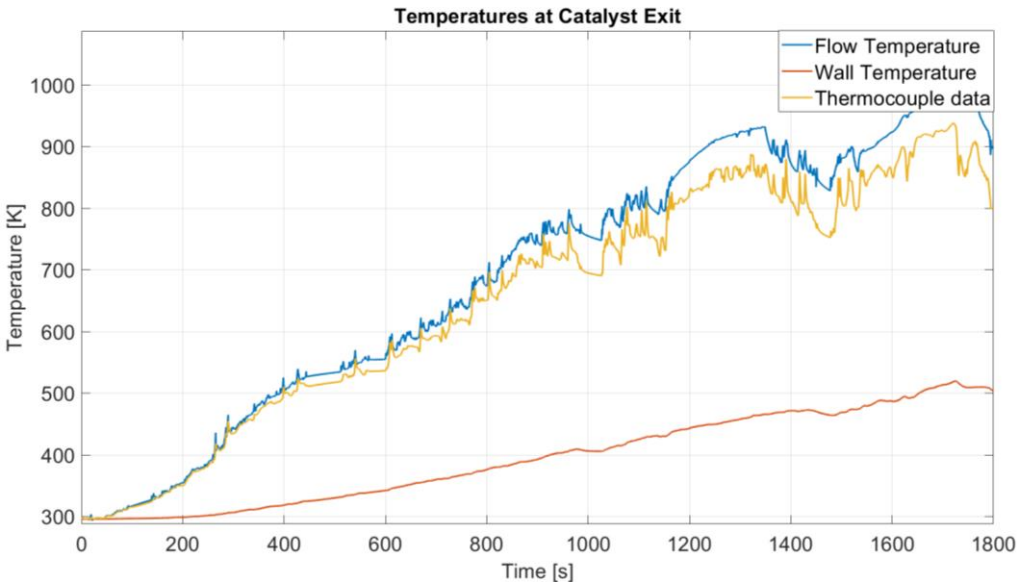

Figure 5.29 Temperatures after exiting the catalyst of flow, walls and the reading a thermocouple would produce.

Compared to the plots describing the turbine temperatures, which were only exhibiting slight differences, in this case the trends in the two locations are noticeably different.

The catalyst adopted in the engine model is 12 cm long, yet the difference in temperature along the axis is strong. Considering the entrance of the catalyst, we can state that it is able to enter in an acceptable operating temperature range only after 5 minutes from the start which can be deemed as a good heat-up time. Instead to fully enter in the correct exercise temperature we must wait until almost the end of the driving cycle, when around the 1600 seconds mark also the exit section of the catalyst reaches a temperature above 500K.

Another interesting aspect that can be noticed in Figure 5.28 and Figure 5.29 is the difference especially in flow and thermocouple temperature of oscillation amplitude, which is quite more evident at the entrance of the catalyst. This is easily explained with basic thermodynamic principles, due to the fact that the bulk

material inside the catalyst between entrance and exit acts as a buffer for transferred heat and reduces the amplitude of temperature oscillations.

5.4.3 Intake side temperatures

The analysis of the intake side temperatures of an engine has a minor role when compared to the exhaust side because it does not include any pollutant reducing elements such as a catalyst, but for this reason it must not be ignored. Especially in turbocharged layouts, the trend of the airflow temperature throughout compressor, intercooler and engine intake head is an interesting aspect.

Let us begin from the compressor.

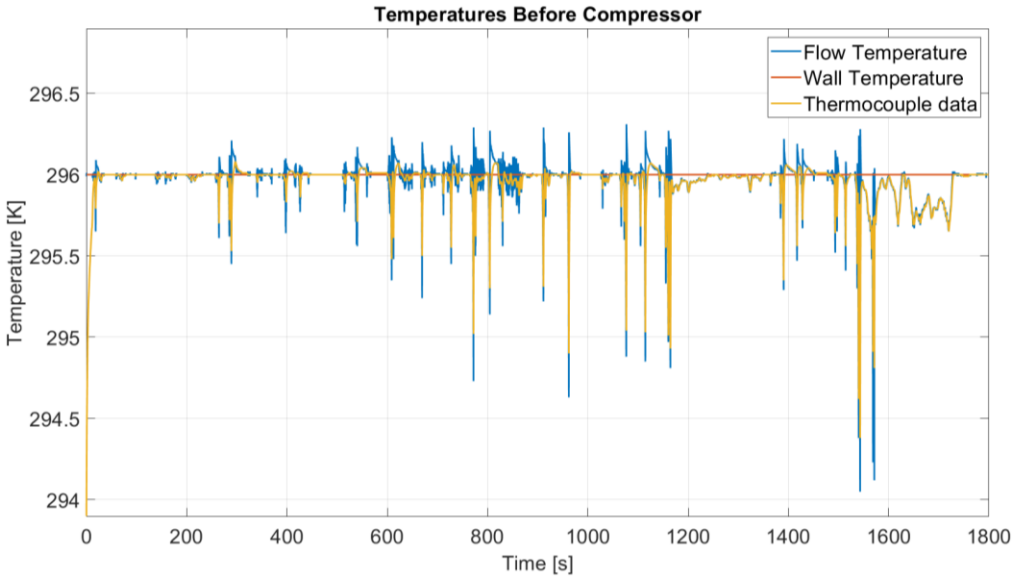

Figure 5.30 Temperatures before the compressor intake of wall, flow and thermocouple reading.

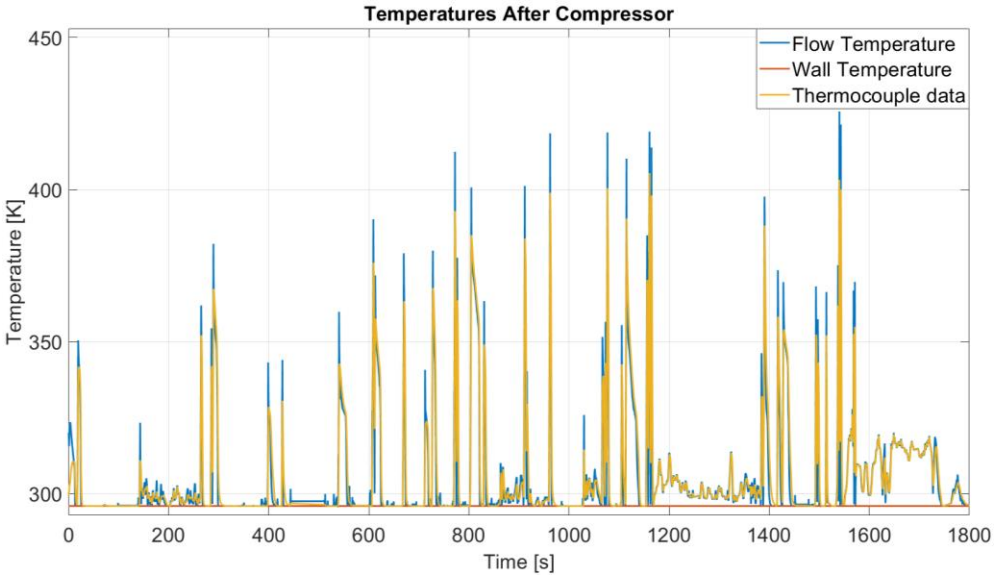

Figure 5.31 Temperatures after the compressor intake of wall, flow and thermocouple reading.

The first thing that can be noticed, which has been set differently from the exhaust side of the engine, is the fact that in this case the wall temperatures do not undergo an evolution in time but instead are kept constant at room temperature, which is 296K.

In Figure 5.30, thus before the compressor intake blading, we can see how the temperature is generally stable around the ambient temperature, except some singular and isolated cases in which the depression created by the engine is able to reduce of around 2K the air temperature.

It is different instead the trend at the exit side of the compressor, shown in Figure 5.31, where we can immediately notice some abrupt increases in temperatures, reaching peaks of more than 100K difference.

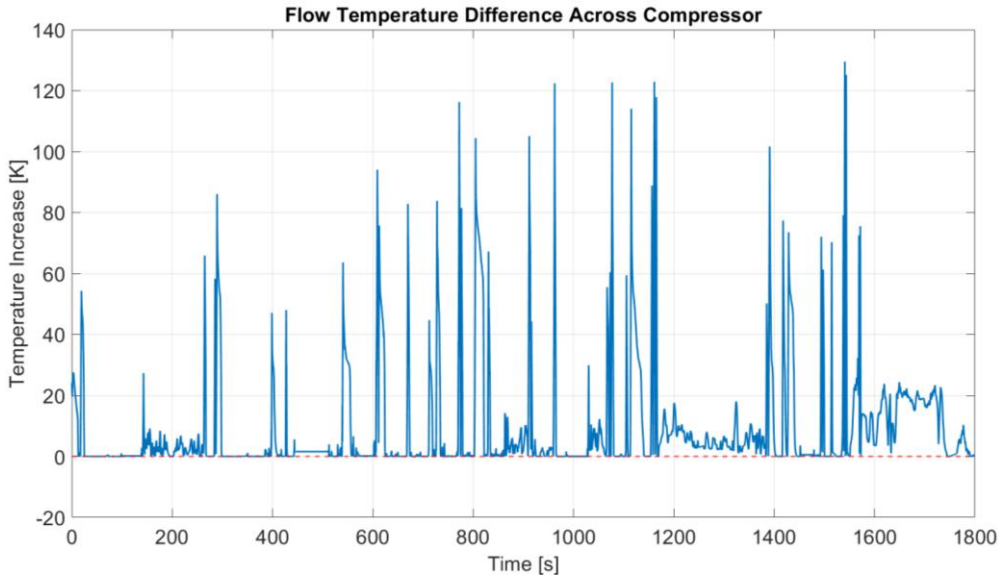

Figure 5.32 Flow temperature difference across the compressor.

In Figure 5.32 we report the absolute difference in temperature between entrance and exit from the compressor housing. We can see how, as expected, the difference is always positive due to the increase in pressure and the consequent increase in temperature. We can also highlight two areas, the first between 1200 and 1400 seconds and the second one between 1600 and 1800 seconds, which directly correspond to the third and the fourth sub-cycle, where excluding the peaks which arise with sudden torque demand peaks, the mean value of the difference in temperature is increasing, resembling thus faithfully the expected trend from the driving cycle.

Once the airflow exits the compressor outlet, in turbocharged engines it is now common use to install an air intercooler, which reduces the compressed air's temperature before being inducted inside the engine.

In the adopted engine model the intercooler was connected to a PID controller which was able to mimic the experimental temperature reduction recorded at the test bench by Renault, which can be seen in the following figure.

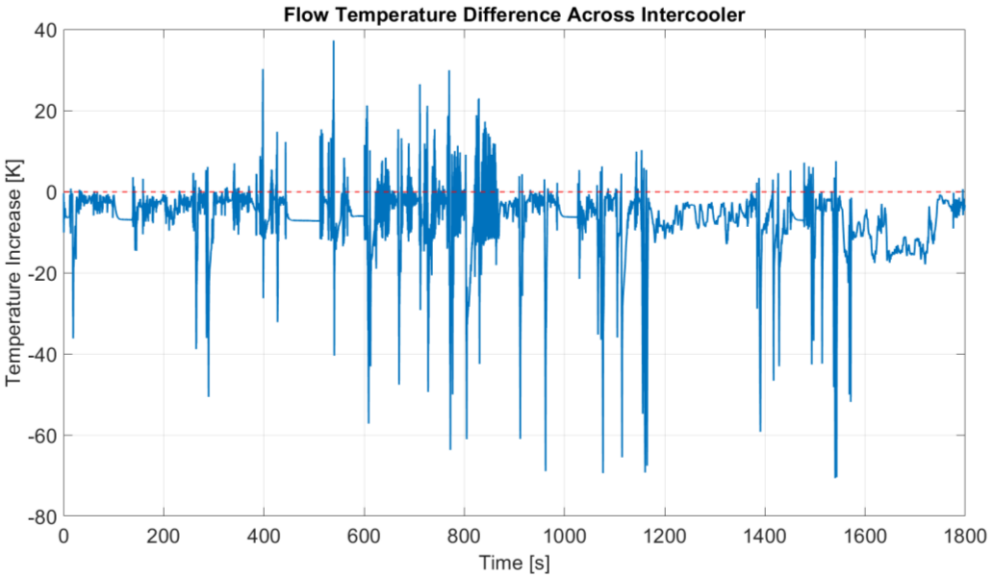

Figure 5.33 Temperature difference in the flow between entrance and exit from the intercooler.

It can be seen how there is always a temperature reduction across the intercooler block, except for some isolated and negligible peaks. The increased mean value in temperature which was discussed in the previous paragraph regarding Figure 5.32 can be seen mirrored here, where the intercooler must work into cooling back the flow towards room temperature during the last two sub-cycles.

5.5 Wastegate valve control

Finally, another parameter which the model is able to simulate and give as output is the behaviour of the wastegate valve, in terms of opening percentage and boost pressure created. The wastegate valve is the way of managing and controlling the turbocharger group in this engine and is controlled through a PID controller found inside the engine GasDyn model. The coefficients were found through a trial-and-error procedure during several launches of the full vehicle simulation.

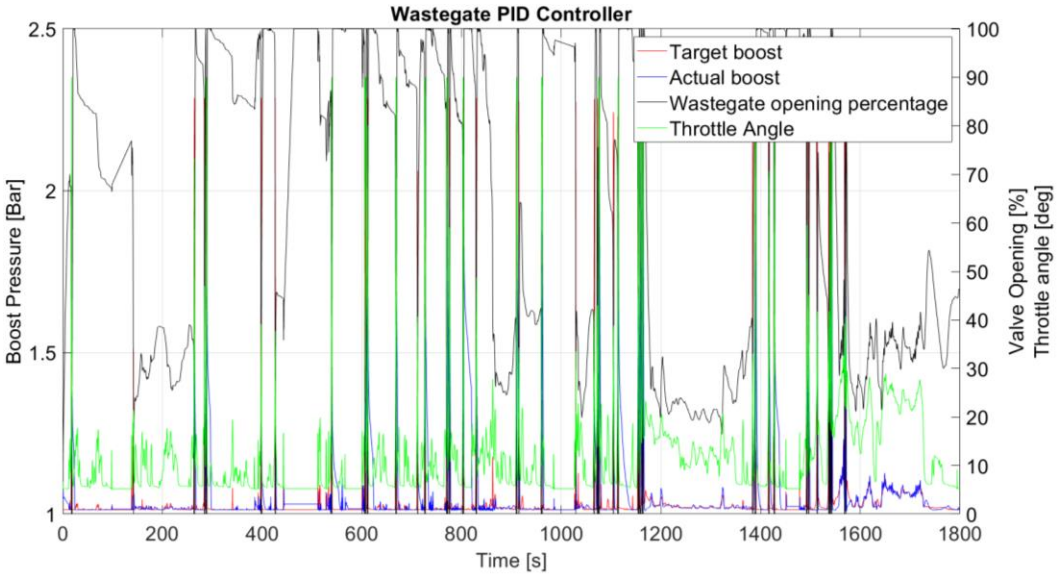

Figure 5.34 Full overview of the wastegate valve behaviour

To analyse the behaviour of this component we compared in a plot the trend of throttle opening, wastegate valve opening, and both the target boost pressure and the actual boost pressure. This is because in turbocharged engines, the load control is not uniquely done by managing the opening degrees of the throttle valve, but there is a cooperation with the wastegate valve to regulate the inducted air given by the compressor.

As per the fuel and the spark advance map of a naturally aspirated engine, turbocharged engines also feature a target boost pressure map to be followed.

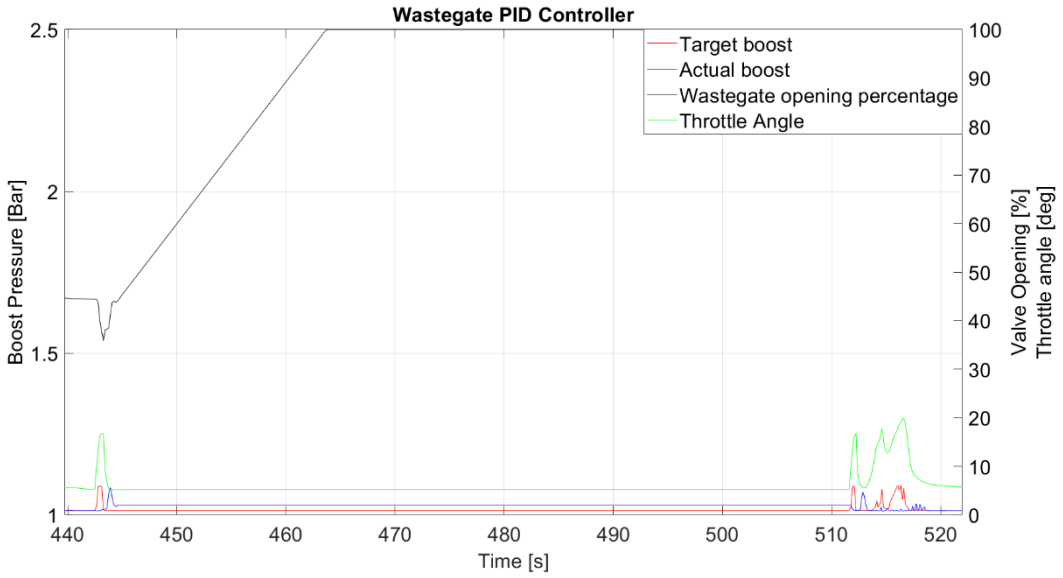

Figure 5.35 Detailed view during an idling phase of the engine

In Figure 5.35 we display an idling phase during a stop in the driving cycle. As we can see, the target pressure and the actual pressure reach a stable value quite quickly and remain at the prescribed value in a stable way. The same behaviour is exhibited by the values of throttle valve opening, which stabilizes on the 6° value as prescribed during idling,

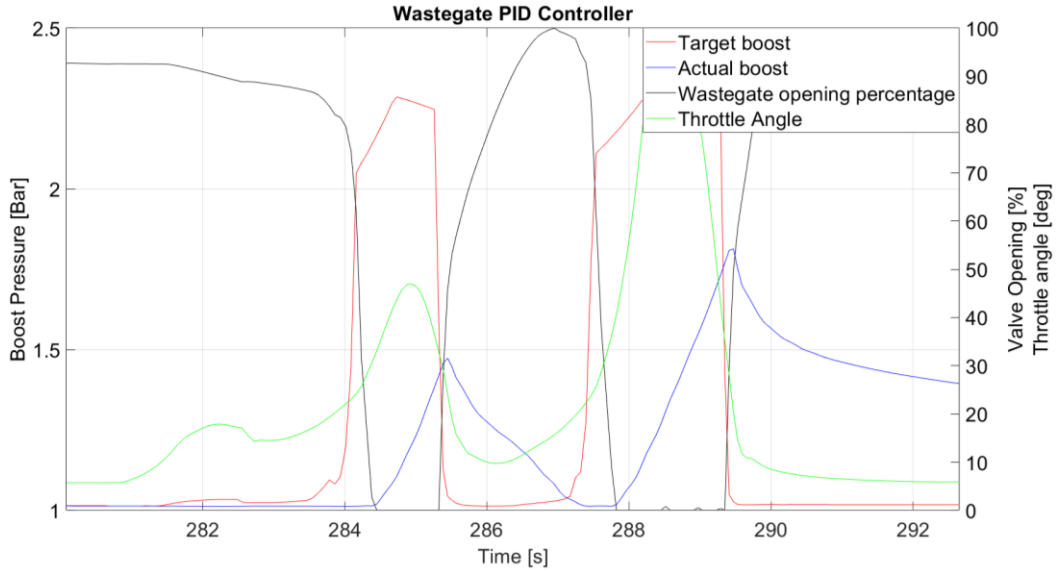

Figure 5.36 Detailed view of an acceleration phase of the vehicle.

In Figure 5.36 instead, we can see a clear example of an acceleration phase, in two successive moments. When the driver controller inputs an increase in torque request, the engine responds by opening the throttle valve from approximately 20° up to 50° in the first part and up to 90° in the second part. Consequently, we can see from the red line on the plot that the target boost pressure rises, and the blue line, which represents the actual boost pressure, begins rising by following the reference. The boost pressure in a turbocharged engine, recalling the concept of turbolag previously exposed in Chapter 2, is generally characterized by slow dynamics, explaining thus the controlled rise in boost pressure compared to the spike in objective pressure. Along with these, on the plot we can appreciate how also the wastegate valve controller operates during an acceleration transient, where it immediately reacts to the increase in demand of boos pressure by shutting closed the bypass valve and directing the entirety of the exhaust fumes flow inside the turbine impeller.

Chapter 6 Alternative engine strategies

In this chapter, once we have assessed that the co-simulation model works in a correct way and is able to compute results which can be considered as truthful, we will analyse how two different engine strategies can affect the engine behaviour in terms of fuel consumption, pollutant emissions and temperatures throughout the engine.

The two selected strategies for this case of study have been the Start & Stop strategy and the Deactivated Cylinder one.

Nowadays, it is of common use to implement the Start & Stop strategy for car manufacturers, because as we will see more in detail in the following pages, it is a very easy and unexpensive way to reduce fuel consumption and pollution, especially useful in urban driving conditions where the time during which the engine remains idling for example, at a red light or in a traffic jam, is considerable.

The second strategy proposed, thus the Deactivated Cylinder one, is a simplification of the more complex Cylinder on Demand strategy, in which for a multi-cylinder engine, in operating conditions where the torque demand can be satisfied with less than the entire number of cylinders at disposal, one or more of them are switched off, to reduce fuel consumption and consequently pollutant emissions.

6.1 Simulink model modifications

To implement the two engine strategies and simulate the driving cycle, two additional subsystems were introduced in the Engine Control Unit block.

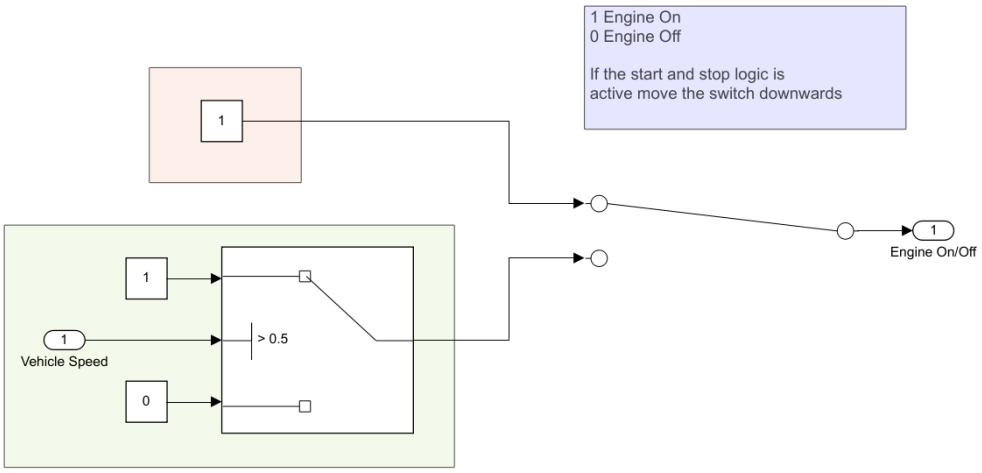

Figure 6.1 Start & Stop control unit logic

The subsystem shown in Figure 6.1 gives the possibility to the user to select by moving downwards the manual switch the Start & Stop strategy, which by detecting when the vehicle is at a stop sends a signal to the GasDyn software, imposing the shut-down of the engine.

Along with this, an additional controller that selects the idling regime was coded, which in the start & stop case corresponds to 0 rpm, instead of the base engine's 750 rpm.

In the second strategy, keeping cylinder number 2 constantly shut off, it was sufficient to introduce a constant block sending a logical 1 (the number one) to the GasDyn software in order to deactivate the cylinder.

6.2 Driving quantities comparison

While the base engine and the start and stop one produce virtually the same dynamic quantities during the driving cycle, due to the fact that the only substantial difference is the shutting off of the engine at a halt of the vehicle while all the other parameters are kept the same, the more interesting differences can be noted between the base engine and the Deactivated cylinder one.

The first parameter to be analysed can be the way in which the engines output brake torque. Being the driver controller programmed to follow a reference velocity, the overall trend and values of the outputted torque can be deemed as very similar but show different dynamics of fulfilment.

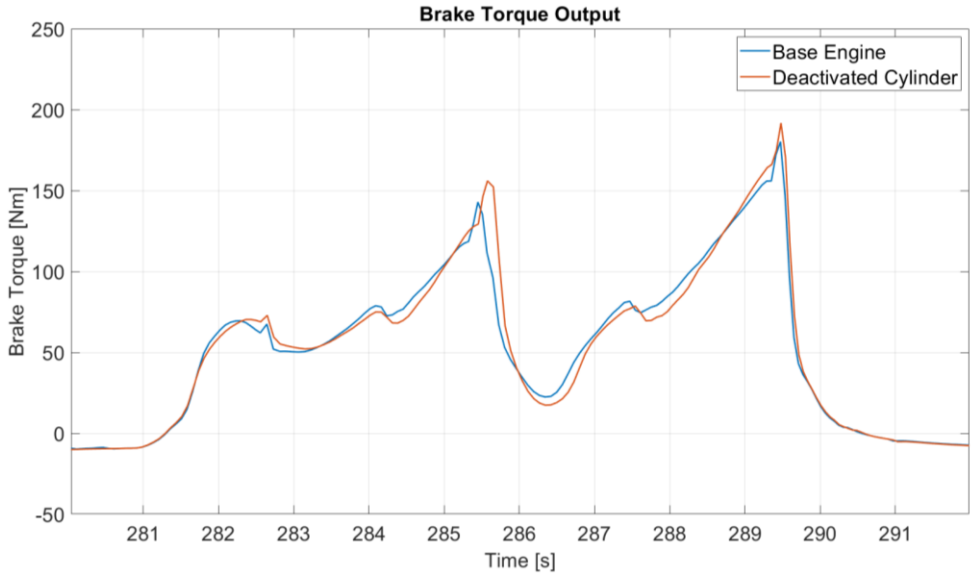

Figure 6.2 Brake torque output comparison between base model and deactivated cylinder model

As it can be seen in Figure 6.2, the general trend of brake torque output from the two engines is very similar, but the deactivated cylinder one exhibits a latency. This

can be explained because of the lower effective displacement of the engine, which makes the engine be affected by a slower dynamic behaviour and the internal GasDyn controllers must work to counteract this tendency, as we will see later on.

In order to output the same brake torque value, this engine is working throughout the driving cycle with a higher throttle valve opening and a higher boost pressure, as it is shown in Figure 6.3 and Figure 6.4.

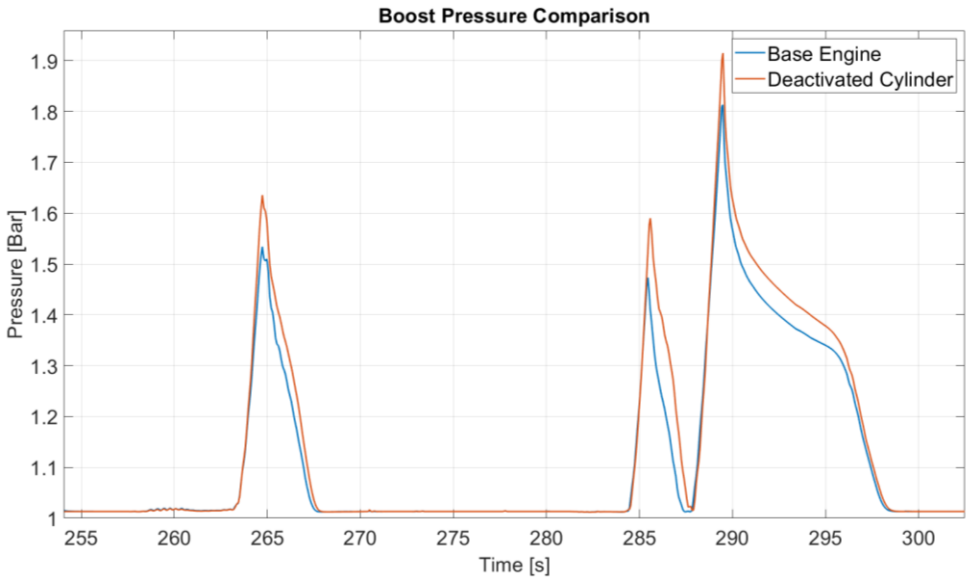

Figure 6.3 Detail of the boost pressure, compared between base model and deactivated cylinder model.

Here, to output the requested brake torque, which is around 90 Nm, the deactivated cylinder engine must work with a constant 0.1 Bar difference in pressure compared to the base model.

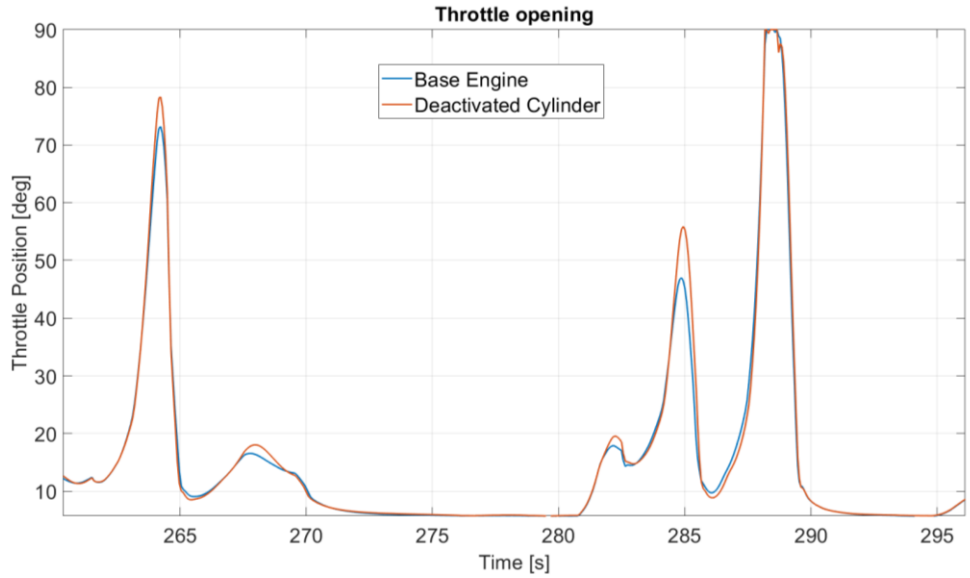

Figure 6.4 Detail of the throttle opening, compared between base model and deactivated cylinder model.

The throttle also exhibits a similar trend to the boost pressure, with a general overshoot of around 10° in opening, which is not a negligible quantity.

6.3 Fuel consumption and pollutants comparison

Let us now carry on in the analysis by comparing the fuel consumption and the pollutant emissions of the three analysed models, which from the point of view of a car manufacturer and in the optic of undergoing a European committee homologation procedure is one of the most interesting aspects.

Beginning from the fuel consumption, let us inspect Figure 6.5 and Figure 6.6.

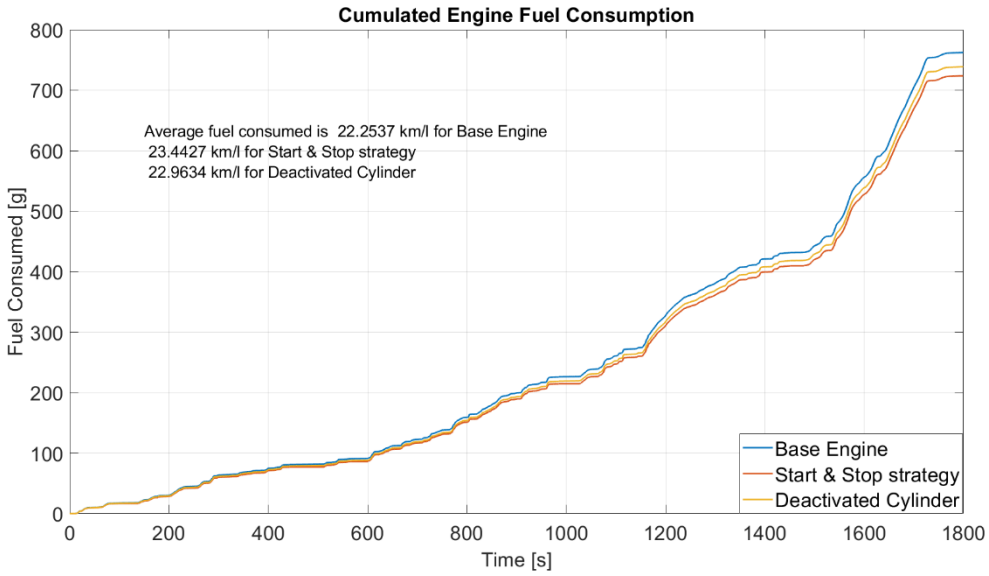

Figure 6.5 Cumulated fuel consumption plot, comparing the three engine models.

As we can see, the two newly proposed strategies are both able to reduce by a slight percentage the average fuel consumption during half an hour of driving cycle, bringing it from the original 22.25 km/l to 22.96 km/l for the Deactivated Cylinder case, and 23.44 km/l for the Start & Stop one. This can be explained by passing onto the following figure.

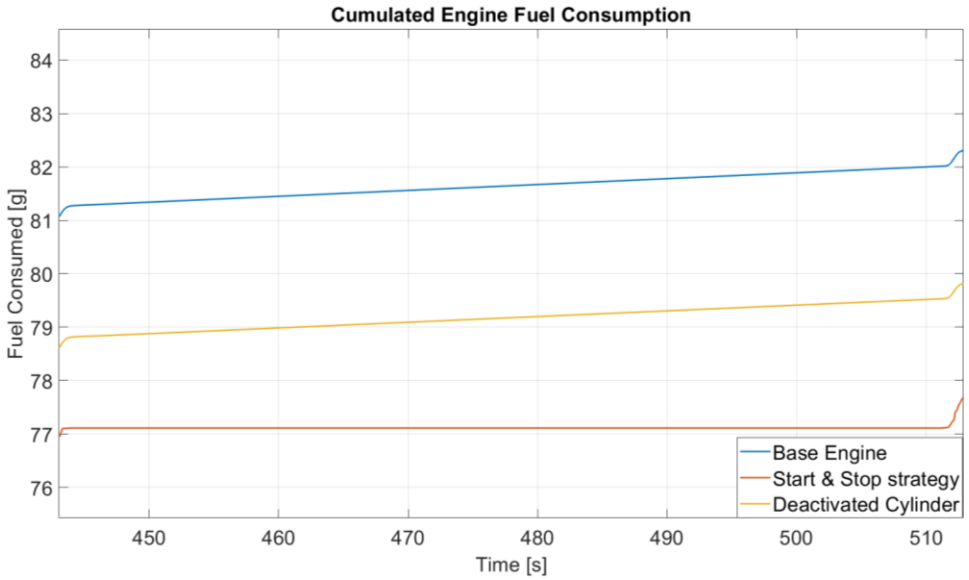

Figure 6.6 A detailed view of the fuel consumption during a stop in the cycle.

Here, in Figure 6.6, a section of the driving cycle in which the vehicle is at a stop is shown. As it can be clearly seen, the main advantage for the two proposed strategies comes during the idling phase. It is more evident for the Start & Stop case, depicted with the red line, where during stops it does not have any sort of fuel consumption, while in the Deactivated Cylinder case the reduction in idling fuel consumption is still present but not so evident.

The advantage seen in the case of the Deactivated Cylinder engine model can be explained by taking a look at the engine BSFC map, in Figure 3.6. Having less displacement, to fulfil the same torque request this engine had to operate at the same engine rpm range and with an overall higher load, as shown in the boost pressure and throttle angle comparison plots.

This, combined with the fact that the most of the WLTP cycle is spent in the range between 1500 and 3000 rpm, as can be seen in Figure 5.2, Figure 5.3, Figure 5.4, and Figure 5.5 where the operating point is the four sub-cycles are shown, leads to understand that the engine finds itself to operate in a lower BSFC area, exhibiting thus a lower fuel consumption.

During a WLTP cycle, the overall stopping time sums up to 4 minutes over a total of 30 minutes. By estimating an idling fuel consumption for the base engine of around 0.7 l/h, the Start & Stop engine is able to save up to 6% of fuel during these stops, meaning around 0.05 L, which results in the previously shown average consumption reduction.

Although the numbers may seem contained, the difference is quite noticeable. This is another strength of the upgrade from the previous NEDC cycle to the more recent WLTP one, because of its longer duration it is able to highlight also slight differences between car models.

In a parallel way, let us analyse the difference in engine pollutant emissions between the three engine strategies.

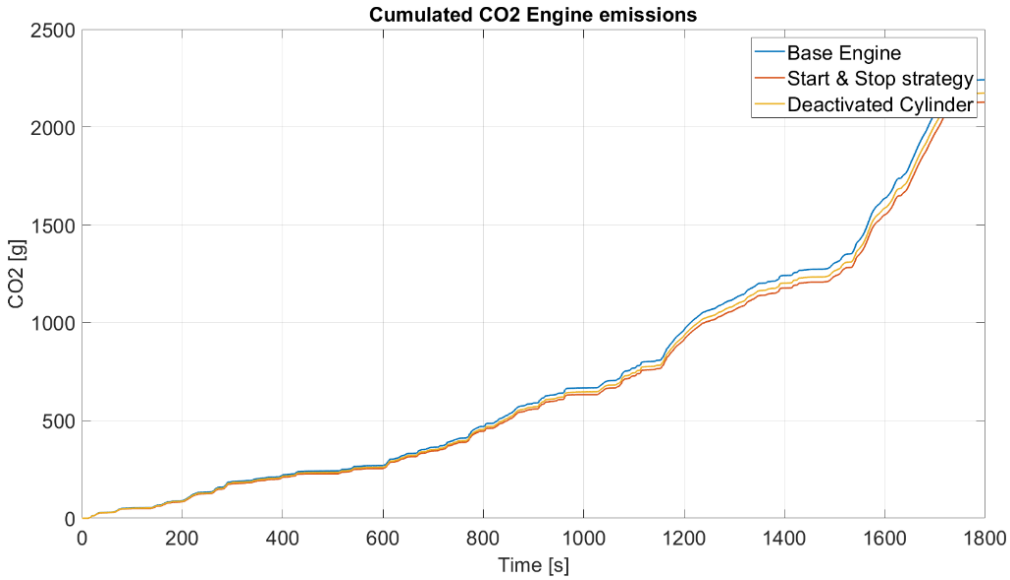

Figure 6.7 Comparison between CO2 emissions of the three engines.

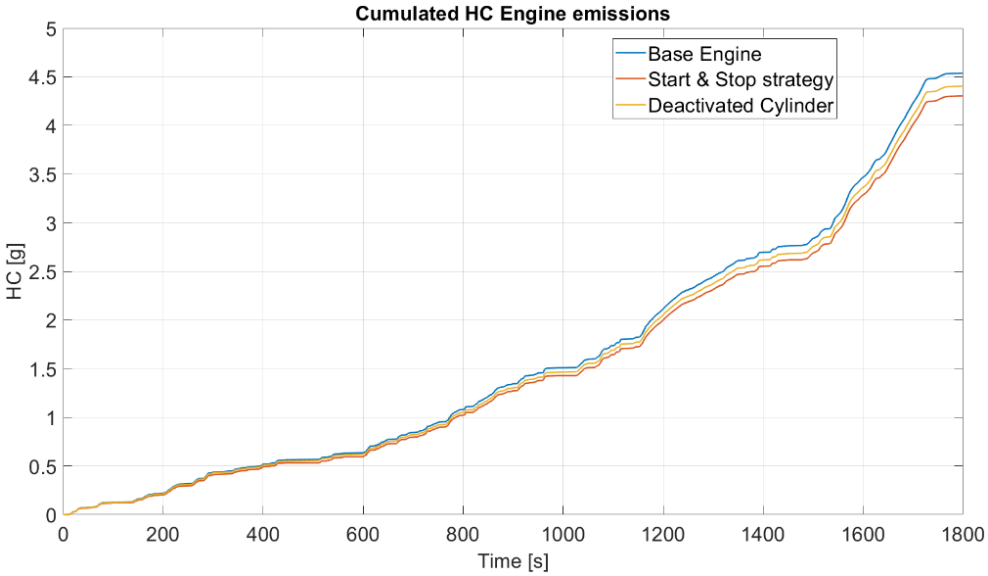

Figure 6.8 Comparison between HC emissions of the three engines.

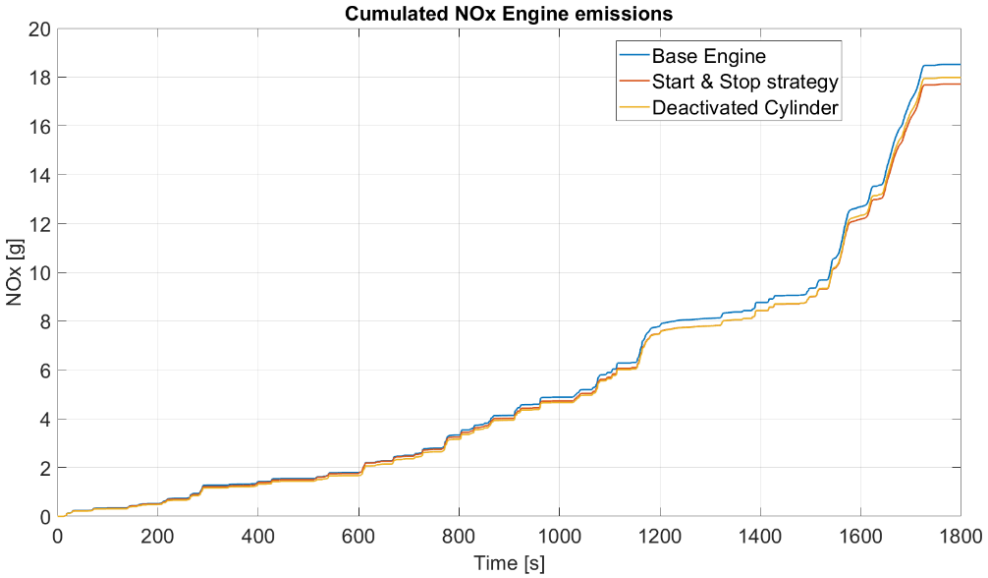

Figure 6.9 Comparison between NOx emissions of the three engines.

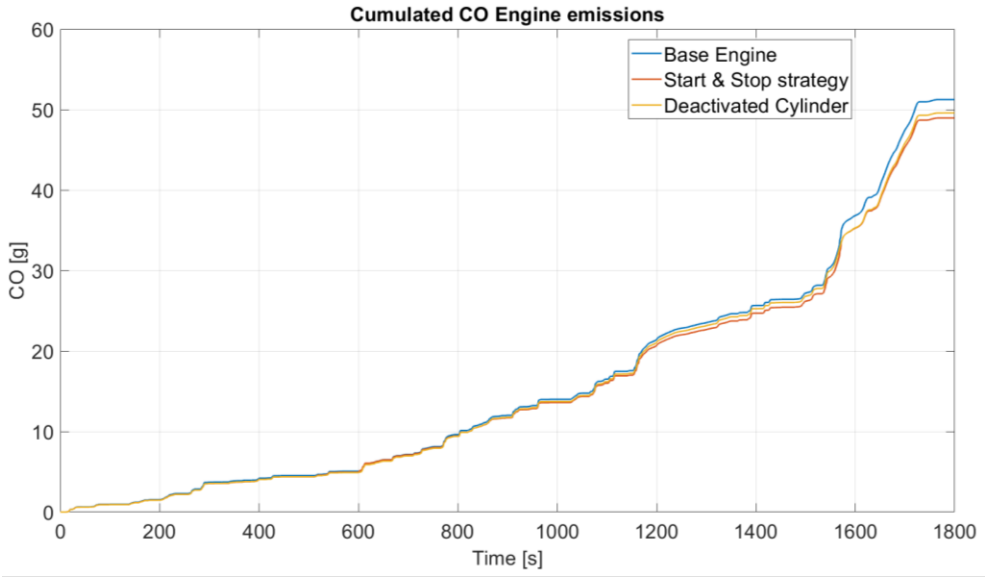

Figure 6.10 Comparison between CO emissions of the three engines.

Once again, also in this case the main difference between the base engine model and the Start & Stop strategy can be identified in the four minutes where the vehicle is at a stop and the engine is shut down. As it can be seen in Figure 6.7, the CO2 emission trend correctly resembles the fuel consumption trend show in the previous pages, where the Start & Stop strategy is seen as the one which requires the least fuel and thus emits the least CO2 and pollutants of the three.

In the following table we summarize the main characteristics of the three engine strategies in terms of pollutants and fuel consumption, highlighting the differences compared to the base model.

	Base Model	Start & Stop	Δ	Deactivated Cylinder	Δ
Fuel	762.17 g	723.51 g	-5.1%	738.61 g	-3.1%
CO2	2241.4 g	2126.8 g	-5.2%	2173.7 g	-3.1%
CO	51.24 g	48.94 g	-4.5%	49.58 g	-3.3%
HC	4.54 g	4.30 g	-5.3%	4.40 g	-3%
NOx	18.51 g	17.71 g	-5.4%	17.98 g	-2.9%

Table 3 Summary of the differences in terms of engine emissions and consumption between the three proposed engine strategies.

6.4 Engine temperatures comparison

Finally, let us now analyse the differences emerging between the three proposed engine strategies in terms of temperatures, by starting from the wall temperatures. As an example we inspected the temperatures at the exit of the catalyst.

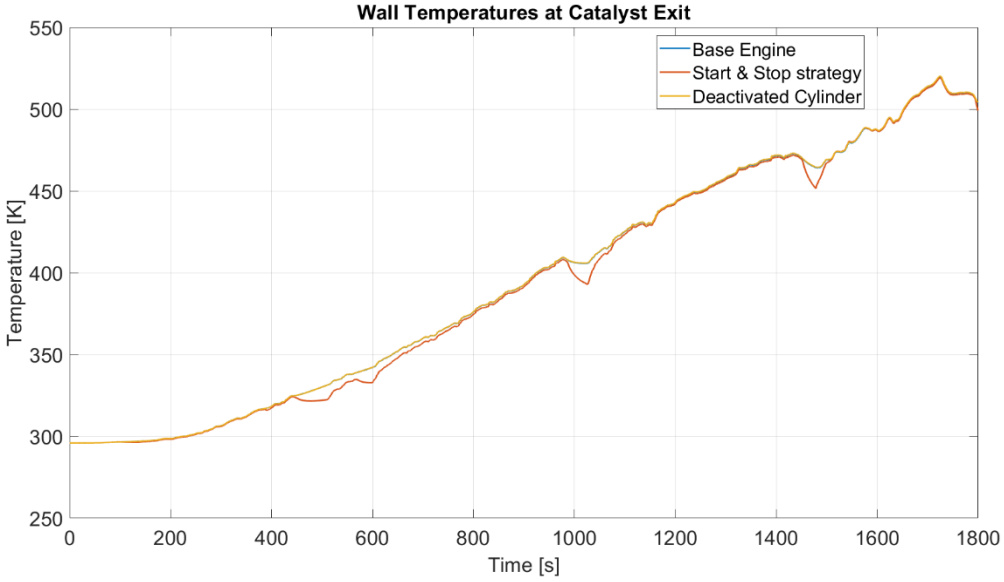

Figure 6.11 Wall temperatures compared between the three models.

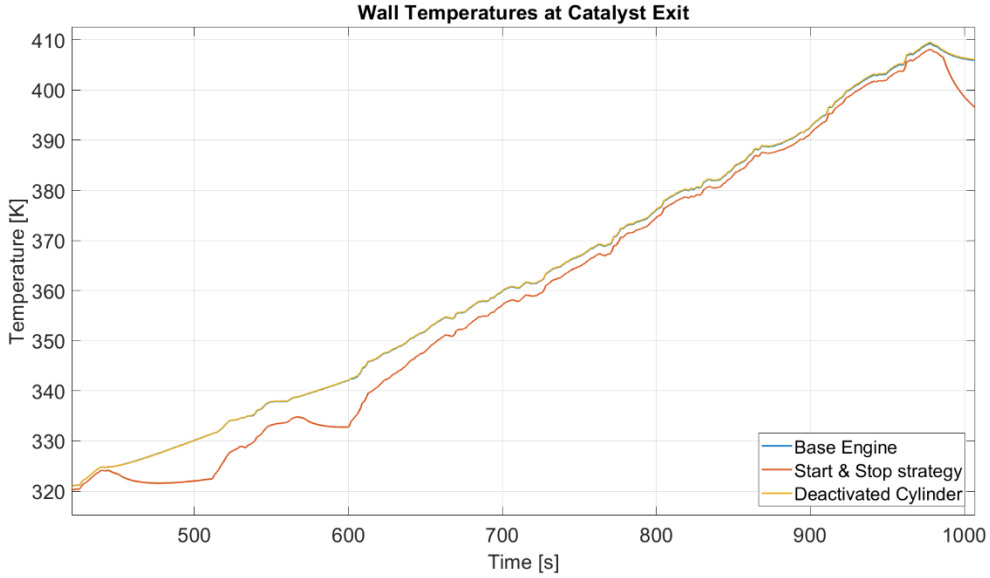

Figure 6.12 A more detailed view of the wall temperatures.

As we can see in Figure 6.11 and Figure 6.12, the wall temperatures in this point of the exhaust line are quite similar between the three models, except for the Start & Stop strategy. The trend shown differs from the other two models mainly due to the stopping times of the cycle, in which the cooling effect is much stronger given that the engine is shut off, while in the other two analysed cases there is a constant outflow of hot gases that contains the temperature gradient in those sections. Once the cycle restarts, we can see that the Start & Stop model asymptotically comes back to copy the temperatures exhibited by the other two models in terms of wall temperatures.

Going on, let us analyse instead the readings of a virtual thermocouple item in parallel with the actual computed flow temperatures.

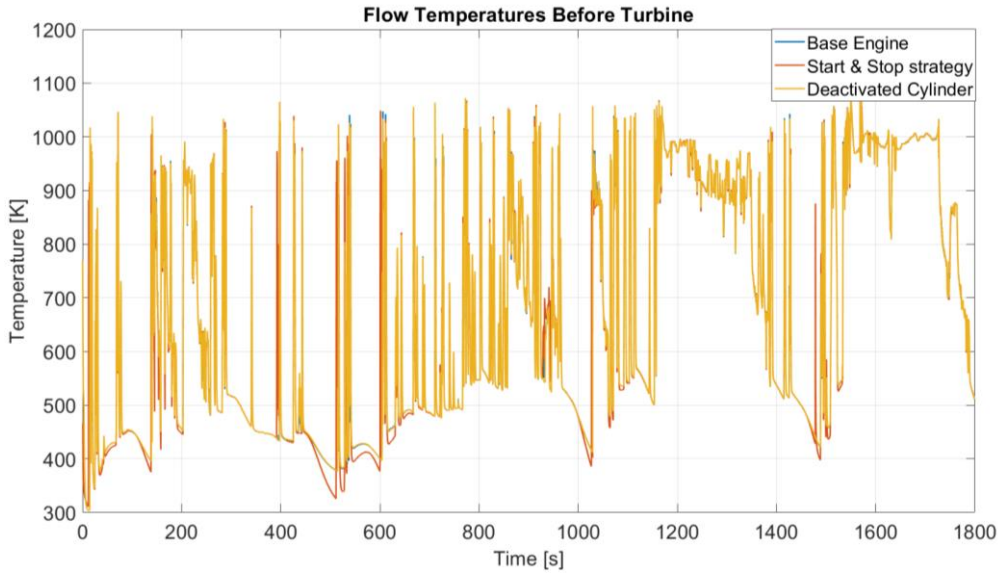

Figure 6.13 Flow temperatures before entering the turbine inlet.

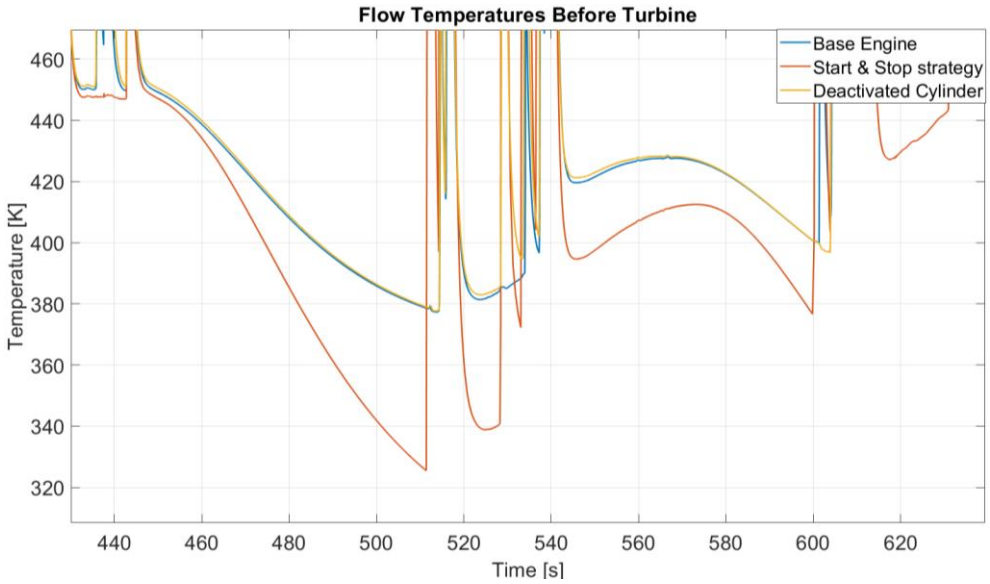

Figure 6.14 A more detailed view of the flow temperatures.

Once again, the temperatures computed for the base engine and the Deactivated Cylinder case are quite similar, while the Start & Stop exhibits a noticeable difference. In Figure 6.14, in detail, we can see how once again during the stopping periods of the WLTP cycle the Start & Stop engine has a steeper cooling ratio which

is also reflected in the thermocouple readings shown in Figure 6.15, and once the cycle restarts the temperatures in the gas flow realign with the other two models.

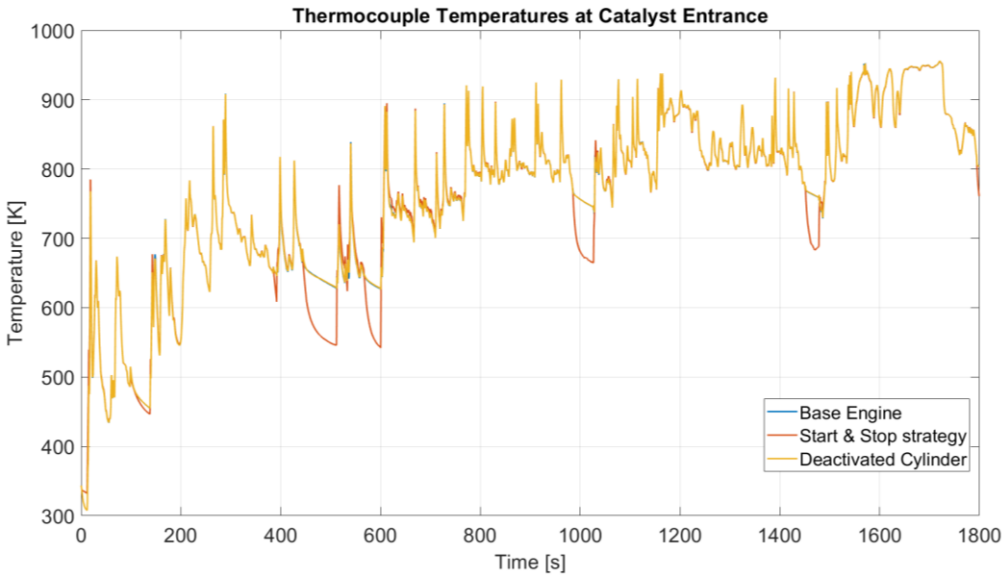

Figure 6.15 Thermocouple readings of a virtual thermocouple placed at the catalyst entrance.

The thermocouple and flow temperature readings do not show the asymptotical behaviour that the catalyst walls have shown in the previous figures because they are characterized by a much faster thermodynamical behaviour, while on the other hand the catalyst walls have a much higher thermal inertia.

Chapter 7 Conclusions

At the end of this master thesis work the main objective of creating a full vehicle simulation model adopting the cosimulation strategy has been reached.

The work began by initially undergoing a validation analysis between the virtual simulation engine model implemented in the GasDyn environment with the experimental data supplied by the French manufacturer Renault.

Once it was assessed that the engine model worked correctly, the initial phase was followed from the implementation of a very basic longitudinal vehicle dynamics simulation model which was used for testing the correctness of the cosimulation environment through simple driving cycles. It was at first a feed forward logic in which the engine block received as input the engine speed, coming from the kinematic chain of the wheels and the gearbox, and the throttle opening from the driver, linked through an exponential relationship that put into communication the throttle pedal with the throttle body angle. Once this strategy was deemed unsuccessful, a feedback logic was instead preferred, in which the engine control unit was able to translate the requests from the driver in to a torque demand given to the engine, which was fulfilled by operating on the internal controllers implemented directly inside the GasDyn software, i.e. the throttle PI, the intercooler temperature control and the wastegate valve controller.

Once it was assessed that the vehicle model coupled with the engine model was working and outputting truthful results, a full WLTP cycle simulation was launched, in order to have baseline results to compare with different engine strategies.

The two proposed evolutions in terms of engine strategies have been the Start & Stop one, and the Deactivated Cylinder. Both were implemented from a software point of view as blocks inside the ECU of the virtual vehicle, giving the possibility to the user to select either one at the beginning of the simulation, by communicating the selection through the co-simulation blocks to the engine model.

The results have shown that, indeed, the two proposed strategies are able to reduce the vehicle fuel consumption and pollutant emissions, in particular up to a 3% overall reduction for the Deactivated Cylinder one and up to 5% for the Start & Stop strategy. These results confirm how the virtual model can be trusted as a preliminary tool to analyse different modifications to a baseline model which has been previously validated, reducing consistently prototyping and experimental testing duration and costs.

To conclude, the co-simulation approach exhibited in this case of study, even though in a reduced measure, all its possibilities in terms of virtual simulation flexibility, simulating a real vehicle behaviour during real driving conditions found in a homologation testing procedure. On one side, the engine simulation software GasDyn allows to inspect and evaluate all the engine related parameters and phenomena connected to combustion, gas flow, cooling and heating and geometries internal to the engine, while on the other hand the Simulink software is able to give access to the designer to a very wide range of parameters related to a road vehicle, from the tyres performance to the external body shape for aerodynamic penetration, from the placement of the centre of gravity in the vehicle wheelbase to the gearbox ratios which suit best the adopted powertrain.

This approach opens thus the possibility for numerous future developments and is especially suited for vehicles. This is because a road vehicle, and in general any vehicle nowadays, is the result of the combination of different areas in terms of technology, from the electronics of the vehicle management, the internal combustion engine, the cooling of water and/or oil of the engine, the internal and

external aerodynamics, etc. By creating a co-simulation model, the designer is free to analyse and operate on any parameter related to a vehicle to optimize it based on any objective to be achieved.

In particular, future developments of such a cosimulation environment can be the implementation of electrification on pre-existing models, always in the optic of reducing pollutant emissions, implementing evolved engine strategies to improve at best the engine performance, for example by intervening on the spark advance during sudden accelerations to avoid turbolag, implementing another external CFD block to simulate the heat exchange between radiator and ambient, and so on. This is the main strength of co-simulation, combining the extreme flexibility with the virtualization of the research and development process.

Chapter 8 Bibliography

[1] S.-Y. L. J. S. M. E. F. M. M. S. J. A. Mario Picerno, “Co-Simulation of Multi-Domain Engine and its Integrated Control for Transient Driving Cycles,” *IFAC-PapersOnLine,* vol. 53, no. 2, pp. 13982-13987, 2020.

[2] E. L. Commision, Regulation (EU) 2017/1151 "Deevlopement of new Euro 5 and Euro 6 limits for loght duty vehicles", Bruxelles, 2020.

[3] A. M. H. S. E. E. T. H. N. I. H. I. M. Tutuianu, Developement of a World-wide Worldwide harmonized Light duty driving Test Cycle (WLTC) - Technical report GRPE-68-03, 2014.

[4] A. M. N. Z. J. P. G. Fontaras, The difference between reported and real-world CO2 emissions: how much improvement can be expected by WLTP introduction?, Transportation Research Procedia, 2017.

[5] E. a. D. K. Mujkic, “Dieselgate: How hubris and bad leadership caused the biggest scandal in automotive history,” *Public Integrity,* vol. 21, no. 4, pp. 365-377., 2019.

[6] G. Ferrari, Internal combustion engines, Bologna: Esculapio, 2016.

[7] S. P. E. L. G. Ebbesen, “Engine downsizing and electric hybridization under consideration of cost and drivability.,” *Oil & Gas Science and Technology–Revue d’IFP Energies nouvelles,* pp. 109-116, 2013.

[8] J. W. G. e. a. Turner, “Ultra Boost for Economy: Extending the Limits of Extreme Engine Downsizing.,” *SAE International Journal of Engines,* 2014.

[9] D. M. D. S. G. Mastrangelo, “Extreme downsizing by the two-cylinder gasoline engine from Fiat,” *MTZ Worldw ,* p. 4–11, 2011.

[10] T. e. a. Lake, “Turbocharging concepts for downsized DI gasoline engines,” SAE Technical Paper, 2004.

[11] R. J. D. O. W. Wakeman, “Closed loop turbocharger control with transient wastegate functions,” SAE Technical Paper, 1986.

[12] H. e. a. Tang, “A review of the application of variable geometry turbines to the downsized gasoline engine.,” *International Journal of Engine Research,* vol. 16, no. 6, pp. 810-825, 2015.

[13] E. S. Y. L. S. L. D. B. a. B. S. W. Lee, “Overview of Electric Turbocharger and Supercharger for Downsized Internal Combustion Engines,” *IEEE Transactions on Transportation Electrification,* vol. 3, no. 1, pp. 36-47, 2017.

[14] H. Hong, “Review and analysis of variable valve timing strategies - eight ways to approach.,” *Journal of Automobile Engineering,* p. 1179–1200, 2004.

[15] P. V. P. J. S. T. Chih Wu, “Performance analysis and optimization of a supercharged Miller cycle Otto engine,” *Applied Thermal Engineering,* 2003.

[16] Exothermia, *GasDyn Theory Manual,* 2020.

[17] Exothermia, *GasDyn User Guide,* 2020.

[18] R. Rajamani, Vehicle Dynamics and Control, Boston: Springer, 2014.

[19] Mathworks, *SImulink user guide and documentation,* 2021.

[20] S. B. A. C. B. P. F. R. A. Z. N. Bachschmid, Fondamenti di meccanica teorica e applicata, Milano: McGraw - Hill education, 2015.